ASSESSING RIVER ICE BREAKUP DATE, COASTAL TUNDRA VEGETATION AND CLIMATE DIVISIONS IN THE CONTEXT OF ALASKA CLIMATE VARIABILITY

By

Peter A. Bieniek

RECOMMENDED: Donald A. Walker

Xiangdong Zhang

Nicole Mölders

Uma K Bhatt

Advisory Committee Chair

Nicole Mölders

Chair, Department of Atmospheric Sciences

APPROVED: Paul W Layer

Dean, College of Natural Science and Mathematics

Lawrence K Duffy

Dean of the Graduate School

July 16, 2012

Date

ASSESSING RIVER ICE BREAKUP DATE, COASTAL TUNDRA VEGETATION AND CLIMATE DIVISIONS IN THE CONTEXT OF ALASKA CLIMATE VARIABILITY

A

DISSERTATION

Presented to the Faculty

of the University of Alaska Fairbanks

in Partial Fulfillment of the Requirements

for the Degree of

DOCTOR OF PHILOSOPHY

By

Peter A. Bieniek, B.S., M.S.

Fairbanks, Alaska

August 2012

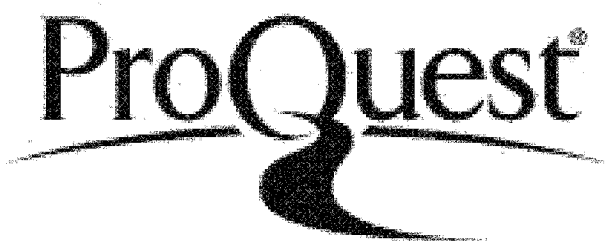

ProQuest LLC
789 East Eisenhower Parkway
P.O. Box 1346
Ann Arbor, MI 48106-1346

Abstract

In Alaska, there exists a substantial knowledge gap of key climate drivers and filling these gaps is vital since life and the economy are inexorably linked with climate in the state. This thesis identifies and investigates three topics that advance the understanding of Alaska climate variability: the role of large-scale climate in Interior river ice breakup, the link between climate and arctic tundra vegetation, and climate divisions based on objective methods.

River ice breakup in the Yukon-Kuskoswim watershed is occurring earlier by 1.3 days decade^{-1} 1948-2008 and displays large year-to-year variability. April-May Interior Alaska air temperatures are the best predictor of river ice breakup and were linked to El Niño Southern Oscillation (ENSO). During the warm phase of ENSO, fewer storms track into the Gulf of Alaska during Boreal Spring, resulting in reduced April-May cloudiness over Alaska, increased solar insolation at the land surface, warmer air temperatures and consequently earlier breakup.

Northern Alaska tundra vegetation productivity has increased 1982-2011, based on the Normalized Difference Vegetation Index (NDVI), a satellite measure of vegetation correlated with above ground biomass. Vegetation productivity was linked to the Beaufort High circulation as well as snowfall, in addition to land surface temperatures and coastal sea ice extent. NDVI has decreased from 1982-2011 over the coastal tundra along the Bering Sea and was correlated with delayed springtime warming due to enhanced coastal sea ice and a delayed snowmelt.

Cluster analysis was applied to 2-meter air temperature data 1977-2010 at meteorological stations to construct climate divisions for Alaska. Stations were grouped together objectively based on similar homogeneous seasonal and annual climate variability and were refined using local expert knowledge to ultimately identify 13 divisions. Correlation analysis using gridded downscaled temperature and precipitation data validated the final division lines and documented that each division has similar a similar annual cycle in temperature and precipitation.

Overall, this work documented substantial links and identified mechanisms joining the large-scale climate to that of Alaska. A better understanding of the role of large-scale climate variability in river ice breakup or tundra greening holds promise for developing seasonal and longer-term forecasts.

Table of Contents

List of Figures

Page

List of Tables

Page

Acknowledgements

I would like to begin by thanking my advisor, Uma Bhatt for the time and effort that she has put in to help me learn to conduct research while at the University of Alaska Fairbanks (UAF). I also thank the members of my committee: Nicole Mölders, Xiangdong Zhang and Skip Walker for their comments and collaboration that have improved my research and their mentorship throughout my time as a PhD student.

I would like to especially thank the coauthors of my three papers for their support of my research. Specifically I would like to thank Larry Rundquist and Scott Lindsay of the Alaska-Pacific River Forecast Center for their help with the breakup and discharge data, their help with interpreting results. Special thanks is owed to Rick Thoman of National Weather Service Fairbanks for helping out throughout my time here at UAF with interpretation of synoptic weather and climate and tracking down hard to find climate data. I also thank Rick Fritcsh, Eric Holloway, John Papineau, James Partain and Gary Hufford of the National Weather Service for their help finalizing the climate divisions. Special thanks are due to David Hill and Stavros Calos of Oregon State University for providing excellent downscaled precipitation and temperature data never before created for Alaska. Heather Angeloff who helped me track down numerous station data sets for Alaska, and for always happy to help no matter what. I would also like to thank Martha Shulski, John Walsh and Chris Daily for advising me on the processes of creating climate divisions for Alaska. I would also like to thank Josefino Comiso, Howard Epstein, Wendy Ermold, Mike Steele, Jorge Pinzon, and Compton Tucker for gracious use of their various data sets and technical support. To Martha Raynolds I

especially owe deep gratitude for the invaluable GIS analysis knowledge she has given me that has aided my research and analysis.

I owe special thanks to the faculty, staff and students of the Department of Atmospheric Sciences (DAS) at UAF, the Geophysical Institute and the International Arctic Research Center. Specifically, I would like to thank Rich Collins, Igor Polyakov, Javier Fochesatto, David Atkinson, Cathy Cahill, Gerhard Kramm, Ken Sassen and Vladimir Alexeev for many great conversations and advice over the years. I would like to thank my MS advisor Gerd Wendler for giving me my initial chance to go to graduate school in Alaska at UAF. Special gratitude is owed also to Barbara Day for helping out with all of my paperwork since I first applied to UAF in 2005. I also owe countless thanks to many students and alumni of DAS/UAF for their collaboration, support and friendship. Particularly, I thank Debasish Pai Mazumder, Oceana Francis, Patrick Cobb, Jeanie Talbot, Oliver Dammann, Jiang Zhu, John Mayfield, Julie Malingowski, Brentha Thurairajah, Mitali Patil, Soumik Basu, Huy and Trang Tran, Stefanie Bourne, Pavan Kankanala, Zhao Li, Rawshan Muna, Colin Murray, Ramaswamy Tiruchirpalli, Manbharat Singh Dhadly James Campbell, Becky Legatt, Cece Borries, Greg Deemer, Ted Fathauer, Vinay Kayetha, Rick Lader, Derek Starkenburg, Anna Liljedahl, Paula Moreira, Tod Fortun, Dea Huff, Taryn Lopez, Agatha Light, and Dee Leelasakultum for your support during my time as a DAS student. In addition, I thank Don Bahls of the Arctic Region Supercomputing Center for your help with running scripts/models on the supercomputers. I also thank Brent Lofgren of the Great Lakes Environmental Research Laboratory for getting me started in research and programming.

I would like to acknowledge the many sources of funding that made this thesis possible and have allowed me to be paid to conduct research while going to school for free. The exact funding sources that supported each project are acknowledged in each chapter. The work in this thesis was partially funded by: NOAA grant NA06OAR4600179, National Science Foundation awards ARC-0652838, ARC-051180, ARC-0902175, NASA grant NNG6NEA00A, a UAF graduate fellowship, and the UAF Geophysical Institute.

Finally, I would like to thank the many teachers, professors and mentors that have guided me along my education journey and to which I owe the achievement of this PhD. I especially extend my thanks to the faculty and staff of the Detroit Waldorf School, Lakeview High School and Valparaiso University. At long last, I thank my family, friends, and parents, Cynthia and Christian Bieniek, in Michigan for their great support on my long academic journey. This PhD was a team effort and I could not have achieved it successfully without the kind support of all of the people acknowledged here.

Chapter 1 Introduction

1.1 Motivation

From the economy to subsistence, nearly every aspect of life in Alaska is intimately tied to weather and climate (Lovecraft and Eicken 2011). Alaska's high latitude location, vast geographic extent and complex terrain (see Figure 1.1) result in a region marked by an equally complex and varied climate. The climate of Alaska is experiencing change with trends in seasonal temperatures and precipitation observed throughout the year (ACIA 2005). Due to its generally Arctic location, climate change in Alaska is also enhanced due to the effects of polar amplification (e.g. Bekryaev et al. 2010; Serreze and Barry 2011). There exist many critical knowledge gaps of the fundamental characteristics and processes that control the regional climate of Alaska. Because of the impact of climate on life in this region it is important to understand how climate variability and change function.

While Alaska is remote, there is significant international economic interest in Alaska due to mineral, oil, gas and maritime resources. The characteristics of the seasonal climate impacts all of these industries as these activities are often seasonal and weather dependent and frequently require lengthy travel to remote sites making the Alaska economy especially vulnerable to climate variability and change (ACIA 2005; AAG 2010; Lovecraft and Eicken 2011). As a result, many sectors of industry are major stakeholders in weather and climate issues. Alaska Native peoples are also vulnerable to climate variability and change in many ways due to their dependence on the land and rivers for subsistence and transportation (ACIA 2005; Bell et al. 2010; Lovecraft and

Eicken 2011). As a result, it is imperative to understand the mechanisms of climate change in Alaska to identify and plan for impacts on industry and society. Understanding the drivers of climate can also be applied to enhance seasonal climate forecasting for Alaska. Improvements in seasonal forecasting would benefit the transportation/oil/gas industry since for example, managers would better know when ice roads are available to reach remote oil/gas exploration sites.

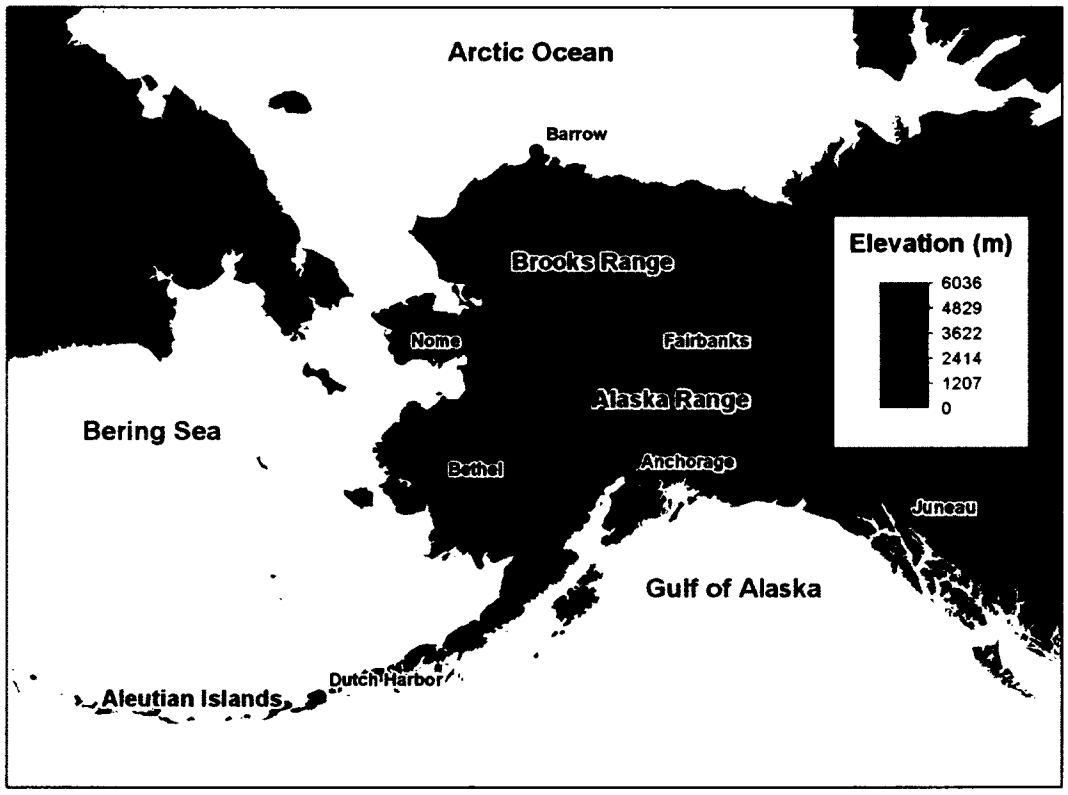

Figure 1.1 Topography of Alaska. Terrain height is shaded and is in units of meters. Major cities and towns, physical features and main water bodies are labeled.

The purpose of this study is to help begin to fill some of these gaps in knowledge of the fundamental, physical mechanisms that drive and characterize the climate of Alaska, while drawing links to the biological and human components of the earth system. This thesis will assess three major topics in the context of climate variability and change in Alaska: river ice breakup date, coastal tundra vegetation change, and climate divisions. Each of these addresses a specific problem in a specific sector of Alaska regional climate while providing an assessment of the whole.

River ice breakup date has great implications for travel in regions of Alaska with few roads. Breakup helps show the linkages between the large-scale climate, teleconnections and the regional climate. These linkages can then be applied to enhance forecasts of spring breakup in the future. Evaluating coastal tundra vegetation change creates a picture of how climate processes at multiple scales, sea ice, and land surface changes are interacting to result in change in Alaska. Finally, climate divisions are of high practical value as they highlight the regions of homogeneous climate variability. These regions can aid climate stakeholders and decision makers in managing data, focusing regional research needs and numerous other economical and social applications.

1.2 Climate characteristics of Alaska

The climate of Alaska is characterized by a wide variety of climate types (Shulski and Wendler 2007). Alaska is bounded by oceans on three sides and has extensive mountain ranges (Figure 1.1). Climatological land and sea surface temperature and sea level pressure (SLP) for the winter (Dec-Feb) and summer (Jun-Aug) are shown in Figure

1.2. The Aleutian Low is a prominent climatological feature in the atmospheric circulation during the winter and is centered south of the Aleutian Islands (Figure 1.2a). The Aleutian Low represents the average of many storms (low pressure systems or cyclones) tracking over the Aleutian Islands into the Gulf of Alaska or Bering Sea (Rodionov et al. 2007; Zhu et al. 2007). Many storms track into the Gulf of Alaska from the west and south and tend to linger and collect there as the coastal mountains to the north and east tend to block their progress further eastward resulting in a "graveyard" of North Pacific storms in this region (Mesquita et al. 2010). Average winter surface temperatures tend to be below 0°C throughout the region. The winter Arctic Ocean and Bering Sea are generally ice covered, but sea surface temperatures in the Gulf of Alaska are well above 0°C. These relatively warm sea surface temperatures, proximal ice cover, and the position of the Aleutian Low have a strong influence on the climates of each region of the state. During summer (Figure 1.2b) the ice edge is located in the Arctic Ocean and land temperatures are all above 0°C on average. The primary circulation feature in summer is the Beaufort High centered over the Arctic Ocean and the subtropical high to the south of Alaska.

The seasonal climate of each region of the state is linked to their terrain and proximity to the coasts (Shulski and Wendler 2007). The southeast and central coastal region along the Gulf of Alaska south of the Alaska Range includes the cities of Juneau, Anchorage and Dutch Harbor. The Gulf of Alaska and North Pacific generally do not have sea ice during the winter and as a result the neighboring coasts are exposed to relatively warm sea surface temperatures. Therefore, this region has a relatively moist,

mild, maritime climate throughout the year and receives the highest precipitation amounts in the state but also has a small annual temperature range and low variability.

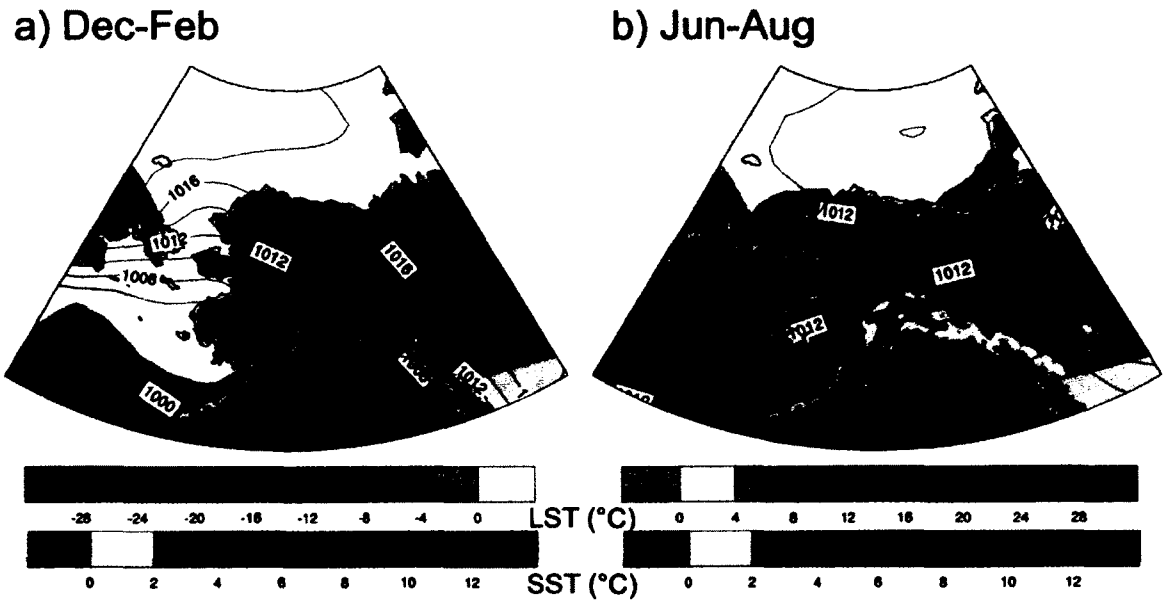

Figure 1.2 Long-term average (1982-2011) land surface (LST, upper color bar, °C) and sea surface temperature (SST, lower color bar, °C), sea ice extent (shaded white), and mean sea level pressure (2hPa contour interval) in winter (a) and summer (b). Land surface temperatures were derived from the Advanced Very High Resolution Radiometer data set (Comiso 2003). The SLP climatology was calculated from the National Centers for Environmental Prediction/National Center for Atmospheric Research Reanalysis 1 (Kalnay et al. 1996). Sea ice and SST seasonal averages were calculated from the Hurrel SST climatology data set (Hurrell et al. 2008).

The Interior region north of the Alaska Range includes the city of Fairbanks. The Alaska Range is a natural barrier between the maritime climates to the south and consequently the Interior has a continental climate type with much drier conditions than the southern coastal regions and experiences far greater extremes in temperature. The

warm dry conditions of summer make the Interior susceptible to wildfires in summer (Bieniek 2007).

The west coast along the Bering Sea that includes the towns of Bethel and Nome, has a seasonal climate that is complicated by the presence of seasonal sea ice in winter and generally ice-free conditions in summer. The seasonal nature of sea ice results in a relatively moderate maritime type climate in summer but a cold continental climate in winter. The west coast region is also susceptible to coastal erosion issues related to Bering Sea storms and sea ice (Rachold et al. 2005).

The northernmost area of the state is bounded to the south by the Brooks Range and to the north by the Arctic Ocean and includes the city of Barrow. This region experiences cold, Arctic conditions in winter and its summer is especially influenced by variations of sea ice cover. When the ice edge is far from shore the summer can have a more maritime climate, however summers with significant amounts of ice near shore also occur.

The climate of Alaska is particularly impacted by pronounced seasonal differences. Alaska experiences substantial changes in seasonal solar insolation during the year that ranges from none in winter to 24 hours in summer. The greatest extremes in daylight occur in the region north of the Arctic Circle. Each region also has seasonal snow cover that can last throughout the winter, but most are usually snow free in summer. These many factors all have different and complex impacts on the mechanisms that drive and characterize the climate of Alaska.

Climate change has been noted throughout Alaska. Warming seasonal and annual temperatures have been observed throughout the region, with the greatest warming having occurred in winter and mixed trends in precipitation throughout the year (ACIA 2005). The impacts of a warming Alaska climate are many and varied. Many landscape changes have been attributed to climate change and have been observed throughout Alaska and the Arctic. Changes have been noted such as permafrost thawing and coastal erosion and are known to impact the way of life for many people that reside in Alaska and the Arctic (Hinzman et al. 2005). But what links global climate to change and climate variability in Alaska? Major climate teleconnections are known to impact the climate in numerous ways throughout the year. The El Niño Southern Oscillation, the Pacific Decadal Oscillation (Mantua et al. 1997), and the Arctic Oscillation (Thompson and Wallace 1998) have been documented as the primary drivers of Alaka climate. The known impacts on Alaska of each of each of the major teleconnections will be discussed individually in the subsequent sections along with their associated patterns.

1.2.1 Ocean climate drivers

The El Niño Southern Oscillation (ENSO) has been identified as a major driver of the climate of Alaska throughout the year (Niebauer 1988; Barnston and He 1996; Papineau 2001). The positive phase of ENSO, called El Niño, is characterized by warmer than normal sea surface temperatures in the eastern equatorial Pacific and has been shown to result in warmer than average temperatures throughout the state, especially in winter (Niebauer 1988; Papineau 2001). Winter precipitation variability has also been linked with ENSO through the atmospheric circulation pattern named the Pacific North

America (PNA) pattern (L'Heureux et al. 2004). El Niño conditions also tend to result in warm and dry summer conditions in the Interior, which can result in increased wildfire activity (Hess et al. 2001). ENSO has also been shown to have some predictive skill for seasonal temperature and precipitation in portions of Alaska (Barnston and He 1996). A major reason that Alaska is extensively impacted by ENSO is due to the relationship between ENSO and the Pacific North American (PNA) Pattern. The PNA originates as a Rossby Wave response to the anomalous warming and cooling of the equatorial Pacific due to ENSO (Horel and Wallace 1981). These Rossby Waves propagate northward directly towards Alaska and seems to play a considerable role in how ENSO impacts the region.

Also associated with ENSO, and a major driver of the decadal climate of Alaska, is the Pacific Decadal Oscillation (PDO). The PDO is a leading mode of variability of Sea Surface Temperatures (SSTs) in the North Pacific (Mantua et al. 1997) and has been argued to be a midlatitude oceanic response to ENSO (Newman et al. 2003). A noteworthy increase in temperatures throughout Alaska in the late 1970s has been linked to a major shift in the phase of the PDO with warmer seasonal average temperatures occurring in conjunction with the warm phase of the PDO (Hartmann and Wendler 2005). Shifts in the strength and position of the Aleutian Low have been linked with the PDO due its influence on the North Pacific storm tracks (Rodionov et al. 2007). The PDO has also been shown to have a changing influence on surfaced based temperature inversions throughout Alaska with time (Bourne et al. 2010).

1.2.2 Atmospheric climate drivers

The Arctic Oscillation (AO) is a leading mode of sea level pressure variability in the northern hemisphere, which impacts the large-scale circulation (Thompson and Wallace 1998). The AO impacts the atmospheric circulation about Alaska and it tends to amplify the change in average temperatures when ENSO and the AO are of the same sign and moderate the effect of ENSO when of opposite sign (Bond and Harrison 2006). Decreased summer precipitation has also been linked with the negative phase of the AO (L'Heureux et al. 2004).

Other atmospheric circulation related teleconnections have been linked with seasonal temperature and precipitation in Alaska. The West Pacific Pattern/North Pacific Oscillation is another noteworthy mode of atmospheric variability in the North Pacific and is broadly defined as a difference in SLP between Alaska and Hawaii that influences storm tracks (Walker and Bliss 1932). During its positive phase, it has been shown to increase warm air advection into the region during the winter (Linkin and Nigam 2008).

1.3 Project overview and objectives

Much is generally known about the impacts of teleconnections on seasonal temperature and precipitation in Alaska. However, the basic physical mechanisms that explain how many of these teleconnections drive the climate of Alaska remain poorly understood. Elucidating these mechanisms is necessary in order to better understand climate variability and change in Alaska. This thesis will focus on the statistical analysis of numerous observation data sets to:

1. Understand the role of climate in the timing of river ice breakup
2. Determine mechanisms driving change in coastal tundra vegetation
3. Identify the distribution of regional climate variability

Each of these three assessments addresses a specific need in Alaska. Together they broadly help fill the gaps in knowledge of the controls of climate variability by either identifying basic mechanisms that relate the large-scale climate to the climate of Alaska, or improving the fundamental knowledge of the distribution of climate variability throughout the region.

1.3.1 River ice breakup

Due to the lack of roads, travel often depends on the rivers in Alaska. The occurrence of river ice breakup results in difficult or impossible travel. Additionally, severe river ice breakup conditions can result in flooding along the rivers, causing damage to villages. Because of its impacts, breakup date is monitored throughout Alaska by observers, and many locations have lengthy records often dating back to the early 20th century as at Nenana, AK (Figure 1.3). Visual inspection of Figure 1.3 highlights many different trends and low frequency variability in the record that possibly indicates a role of climate in breakup. Identifying the climate drivers of the timing of river ice breakup can be applied to improve forecasts of breakup and to better understand the drivers of climate variability in springtime Alaska. In chapter 3 the mechanism that relates the large-scale climate and breakup date in Alaska is developed through statistical analysis of observational data. This project was completed through collaboration with forecasters

from the Alaska-Pacific River Forecast Center (APRFC) with the goal of promptly improving the APRFC breakup forecasts. This climate analysis revealed a plausible mechanism by which the positive phase of ENSO leads to warmer spring temperatures in Alaska through a southward shift of the storm tracks and an associated reduction of cloud cover over Alaska.

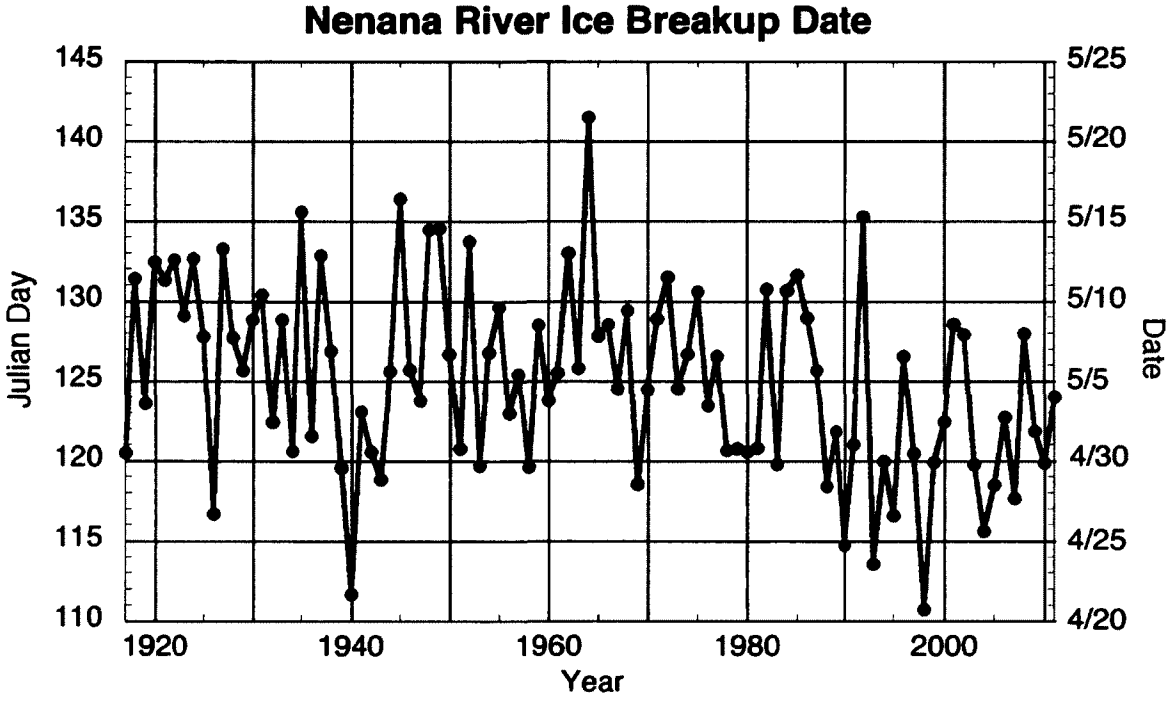

Figure 1.3 River ice breakup date observations at Nenana, AK for 1917-2011 (available online: http://www.nenanaakiceclassic.com/). Many different trends and low frequency variability can be visually observed in this time series. Breakup makes travel impossible on rivers and can endanger life and property when it causes flooding. How is river ice breakup date in Alaska related to climate?

1.3.2 Coastal tundra vegetation

The satellite derived Normalized Difference Vegetation Index (NDVI) is an indicator of plant productivity and is correlated with aboveground biomass (Raynolds et al. 2011). Coastal tundra vegetation is changing throughout the Arctic as observed using NDVI. NDVI has generally been increasing throughout the Arctic, while summer sea ice has declined during the satellite record (Figure 1.4). The northern coastal tundra regions along the Beaufort and Chukchi Seas have experienced increased NDVI and southwest Alaska tundra along the Bering Sea has seen decreased NDVI. These changes have been linked with the decline in summer sea ice and warming summer temperatures (Bhatt et al. 2010). Better understanding the relationship between climate and NDVI is valuable as it further demonstrates how the large-scale is linked to the summer climate of Alaska and changes the landscape. The climate-NDVI relationship also highlights the complex mechanism by which global climate change is acting on Alaska. This project was conducted through multidisciplinary collaboration with plant ecologists, remote sensing experts and climate scientists to understand the role of climate in Alaska tundra changes and variability.

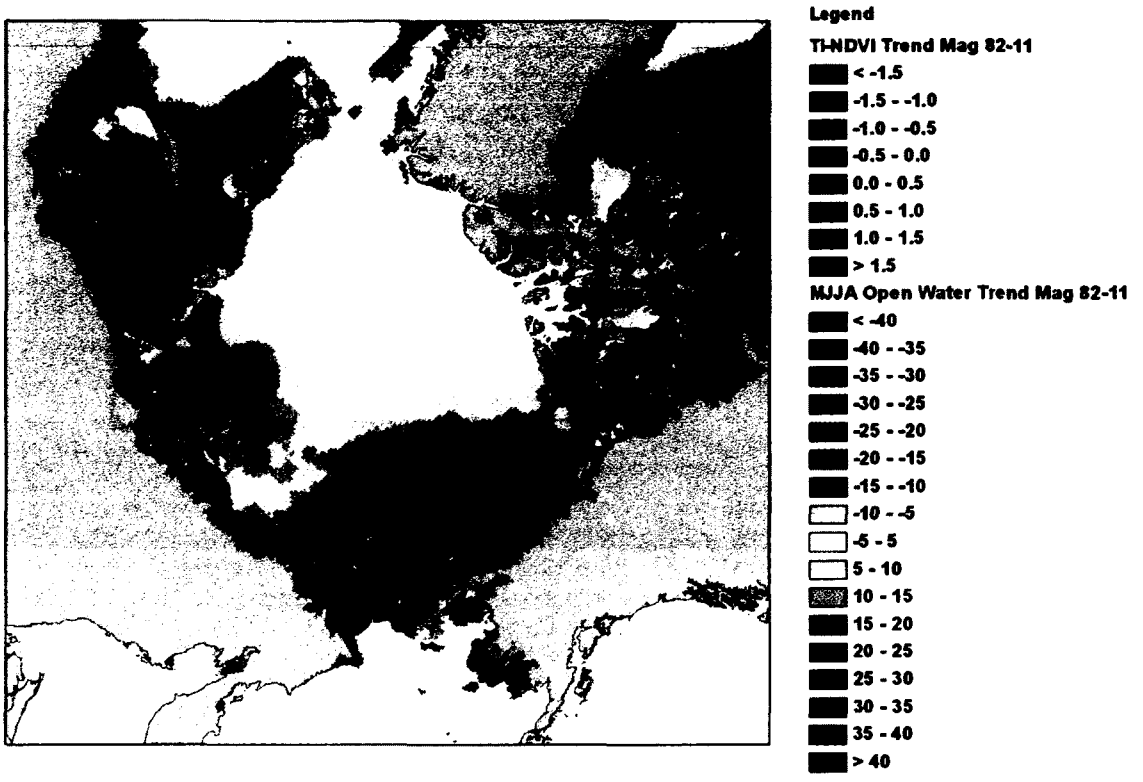

Figure 1.4. Time Integrated NDVI and May-Aug open water total magnitude change for 1982-2011. NDVI trends were derived from the GIMMS3g NDVI data set (Pinzon et al. 2012) and open water trends from the Special Sensor Microwave Imager sea ice data set (Comiso and Nishio 2008). The TI-NDVI trend (sum of the biweekly NDVI during the growing season) is unitless and the open water trend is in percent concentration. NDVI and summer open water are increasing throughout much of the Arctic, however NDVI is decreasing in some areas, notably southwest Alaska. How is the NDVI in Alaska coastal tundra regions related to climate?

1.3.3 Climate divisions

Understanding how climate variability is distributed throughout Alaska is critical for conducting seasonal forecasts and numerous climate research applications. The discussion in section 1.2 showed that various, broad climate regions have been identified in Alaska, however only limited analysis has been conducted to objectively delineate these regions. Climate divisions classify regions by homogeneous climate variability and can be used to help fill this need. Previously, Alaska climate regions and divisions have been loosely based on river drainage basins and/or terrain without extensive objective analysis of station data (Figure 1.5). In this project, described in chapter 4, climate divisions were developed for Alaska using cluster analysis of station data. This method objectively groups the stations into clusters with similar climatic variability. This type of statistical analysis has only recently become possible since it requires relatively long and complete station records. The final boundaries and interpretation was aided through collaboration with National Weather Service forecasters from offices throughout Alaska and other climate experts.

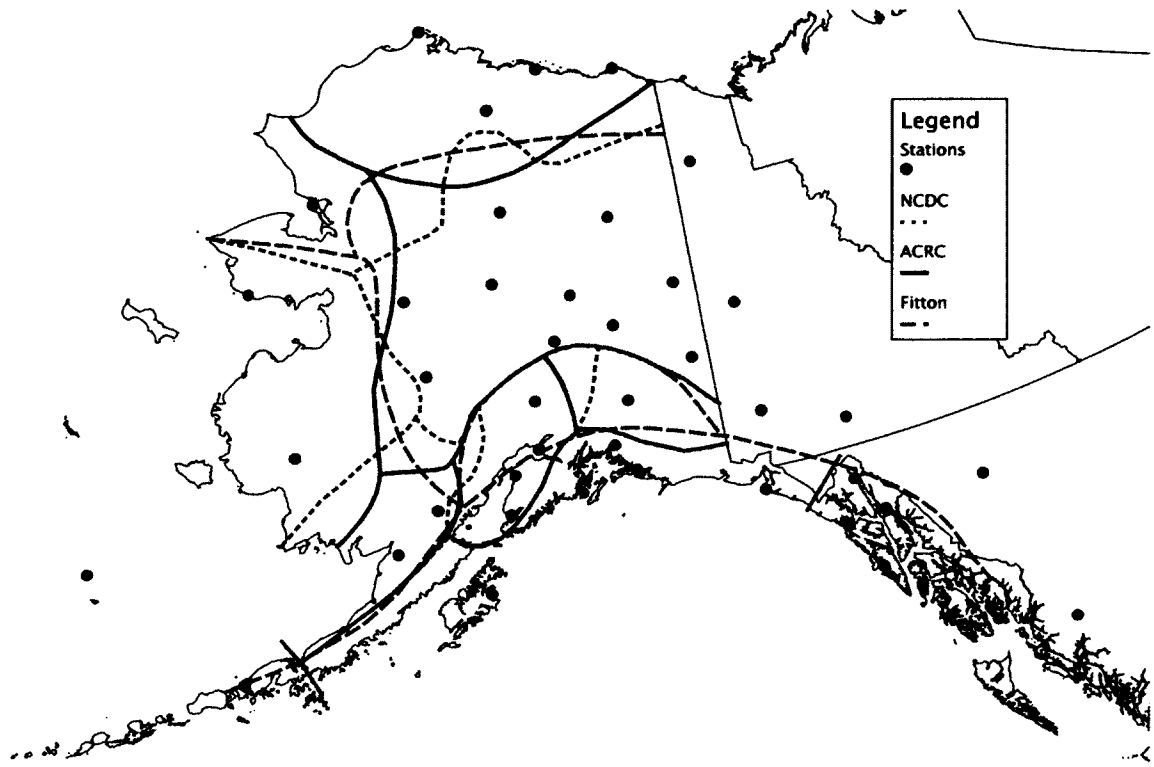

Figure 1.5. Historical Alaska climate divisions. The original Fitton (1930) climate division boundaries are shown as red dashed lines, the boundaries currently used by the National Climate Data Center (Searby 1968) are shown as green dashed lines and those currently used by the Alaska Climate Research Center (Shulski and Wendler 2007) as solid blue lines. The locations of the current primary weather observation stations are shown as red dots. All of the historical divisions were based on drainage basins and/or terrain boundaries. There is great need to objectively identify climate divisions to advance research and seasonal climate forecasting applications.

1.4 Summary

The climate has a prominent role in the economy and daily life in Alaska. With the noteworthy emergence of observed climate change it is vital to understand the mechanisms by which the climate of Alaska functions. This can then be applied in numerous ways to benefit the stakeholders of weather and climate. Each of these projects addresses this in a different way. Climate divisions are necessary to understand the regional nature of climate variability, which is critical for evaluating and predicting seasonal climate. Identifying the key climate mechanisms that drive river ice breakup date can be applied to forecasting breakup date itself. Linking the timing of breakup to the large-scale climate enhances predictability because the slowly oceans are inherently more predictable than local processes. Improved river ice breakup forecasts are highly valuable for transportation. Finally, understanding the role of climate in coastal tundra vegetation and its associated changes highlights the role of climate in the landscape of Alaska. Together each of these research outcomes helps to improve our understanding of the climate of Alaska.

References

AAG, 2010: Alaska's climate change strategy: addressing impacts in Alaska. Paper submitted by the Adaptation Advisory Group to the Alaska Climate Change Sub-cabinet, State of Alaska, January 27, State of Alaska.

ACIA, 2005: *Arctic climate impact assessment.* Cambridge University Press, 1042 pp.

Barnston, A. G., and Y. X. He, 1996: Skill of canonical correlation analysis forecasts of 3-month mean surface climate in Hawaii and Alaska. *J Climate*, **9**, 2579-2605.

Bekryaev, R. V., I. V. Polyakov, and V. A. Alexeev, 2010: Role of Polar Amplification in Long-Term Surface Air Temperature Variations and Modern Arctic Warming. *J Climate*, **23**, 3888-3906.

Bell, J., M. Brubaker, K. Graves, and J. Berner, 2010: Climate change and mental health: uncertainty and vulnerability for Alaska natives. *CCH Bulletin*, No. 3, April 15, 2010.

Bhatt, U. S., and Coauthors, 2010: Circumpolar Arctic Tundra Vegetation Change Is Linked to Sea Ice Decline. *Earth Interact*, **14**, doi:10.1175/2010E1315.1.

Bieniek, P. A., 2007: Climate and predictability of Alaska wildfires. Thesis (M.S.), University of Alaska Fairbanks, 84 pp.

Bond, N. A., and D. E. Harrison, 2006: ENSO's effect on Alaska during opposite phases of the Arctic Oscillation. *Int J Climatol*, **26**, 1821-1841.

Bourne, S. M., U. S. Bhatt, J. Zhang, and R. Thoman, 2010: Surface-based temperature inversions in Alaska from a climate perspective. *Atmos Res*, **95**, 353-366.

Comiso, J. C., 2003: Warming trends in the Arctic from clear sky satellite observations. *J Climate*, **16**, 3498-3510.

Comiso, J. C., and F. Nishio, 2008: Trends in sea ice cover using enhanced and compatible AMSR-E, SSM/I, and SMMR data. *J Geophys Res*, 113, C02S07, doi:10.1029/2007JC004257.

Fitton, E. M., 1930: The climates of Alaska. *Mon Weather Rev*, p. 85-103.

Hartmann, B., and G. Wendler, 2005: The significance of the 1976 Pacific climate shift in the climatology of Alaska. *J Climate*, **18**, 4824-4839.

Hess, J. C., C. A. Scott, G. L. Hufford, and M. D. Fleming, 2001: El Nino and its impact on fire weather conditions in Alaska. *Int J Wildland Fire*, **10**, 1-13.

Hinzman, L. D., and Coauthors, 2005: Evidence and implications of recent climate change in northern Alaska and other arctic regions. *Climatic Change*, **72,** 251-298.

Horel, J. D., and J. M. Wallace, 1981: Planetary-Scale Atmospheric Phenomena Associated with the Southern Oscillation. *Mon Weather Rev*, **109,** 813-829.

Hurrell, J. W., J. J. Hack, D. Shea, J. M. Caron, and J. Rosinski, 2008: A new sea surface temperature and sea ice boundary dataset for the Community Atmosphere Model. *J Climate*, **21,** 5145-5153.

Kalnay, E., and Coauthors, 1996: The NCEP/NCAR 40-year reanalysis project. *B Am Meteorol Soc*, **77,** 437-471.

L'Heureux, M. L., M. E. Mann, B. I. Cook, B. E. Gleason, and R. S. Vose, 2004: Atmospheric circulation influences on seasonal precipitation patterns in Alaska during the latter 20th century. *J Geophys Res-Atmos*, **109,** doi:10.1029/2003JD003845.

Linkin, M. E., and S. Nigam, 2008: The north pacific oscillation-west Pacific teleconnection pattern: Mature-phase structure and winter impacts. *J Climate*, **21,** 1979-1997.

Lovecraft, A. L., and H. Eicken, 2011: *North by 2020 : perspectives on Alaska's changing social-ecological systems.* University of Alaska Press, 736 pp.

Mantua, N. J., S. R. Hare, Y. Zhang, J. M. Wallace, and R. C. Francis, 1997: A Pacific interdecadal climate oscillation with impacts on salmon production. *B Am Meteorol Soc*, **78,** 1069-1079.

Mesquita, M. D. S., D. E. Atkinson, and K. I. Hodges, 2010: Characteristics and Variability of Storm Tracks in the North Pacific, Bering Sea, and Alaska. *J Climate*, **23,** 294-311.

Newman, M., G. P. Compo, and M. A. Alexander, 2003: ENSO-forced variability of the Pacific decadal oscillation. *J Climate*, **16,** 3853-3857.

Niebauer, H. J., 1988: Effect of El Nino Southern Oscillation and North Pacific Weather Patterns on Interannual Variability in the Subarctic Bering Sea. *J Geophys Res-Oceans*, **93,** 5051-5068.

Papineau, J. M., 2001: Wintertime temperature anomalies in Alaska correlated with ENSO and PDO. *Int J Climatol*, **21,** 1577-1592.

Pinzon, J. E. and Coauthors, 2012: Revised, continuously updated GIMMS3g (AVHRR NDVI) data from 1982 onward. (in prep.) *Remote Sensing*.

Rachold, V., F. E. Are, D. E. Atkinson, G. Cherkashov, and S. M. Solomon, 2005: Arctic coastal dynamics (ACD): an introduction. *Geo-Mar Lett*, **25,** 63-68.

Raynolds, M. K., D. A. Walker, H. E. Epstein, J. E. Pinzon, and C. J. Tucker, 2011: A new estimate of tundra-biome phytomass from trans-Arctic field data and AVHRR NDVI. *Remote Sensing Letters*, **3,** 403-411.

Rodionov, S. N., N. A. Bond, and J. E. Overland, 2007: The Aleutian Low, storm tracks, and winter climate variability in the Bering Sea. *Deep-Sea Research Part II-Topical Studies in Oceanography*, **54,** 2560-2577.

Searby, H. W., 1968: Climates of the states: Alaska, ESSA, Climatology of the United States. No. 60-49, U.S. Government Printing Office, 23 pp.

Serreze, M. C., and R. G. Barry, 2011: Processes and impacts of Arctic amplification: A research synthesis. *Global Planet Change*, **77,** 85-96.

Shulski, M., and G. Wendler, 2007: *The climate of Alaska.* University of Alaska Press, 216 pp.

Thompson, D. W. J., and J. M. Wallace, 1998: The Arctic Oscillation signature in the wintertime geopotential height and temperature fields. *Geophys Res Lett*, **25,** 1297-1300.

Walker, G. T., and E. W. Bliss, 1932: World weather V. *Mem Roy Meteor Soc*, **4,** 53-84.

Zhu, X. J., J. L. K. Sun, Z. Y. Liu, Q. Y. Liu, and J. E. Martin, 2007: A synoptic analysis of the interannual variability of winter cyclone activity in the Aleutian low region. *J Climate*, **20,** 1523-1538.

Chapter 2 Large-Scale Climate Controls of Interior Alaska River Ice Breakup[1]

Abstract

Frozen rivers in the Arctic serve as critical highways because of the lack of roads; therefore, it is important to understand the key mechanisms that control the timing of river ice breakup. The relationships between springtime Interior Alaska river ice breakup date and the large-scale climate are investigated for the Yukon, Tanana, Kuskokwim, and Chena Rivers for the 1949–2008 period. The most important climate factor that determines breakup is April–May surface air temperatures (SATs). Breakup tends to occur earlier when Alaska April–May SATs and river flow are above normal. Spring SATs are influenced by storms approaching the state from the Gulf of Alaska, which are part of large-scale climate anomalies that compare favorably with ENSO. During the warm phase of ENSO fewer storms travel into the Gulf of Alaska during the spring, resulting in a decrease of cloud cover over Alaska, which increases surface solar insolation. This results in warmer-than-average springtime SATs and an earlier breakup date. The opposite holds true for the cold phase of ENSO. Increased wintertime precipitation over Alaska has a secondary impact on earlier breakup by increasing spring river discharge. Improved springtime Alaska temperature predictions would enhance the ability to forecast the timing of river ice breakup.

---

[1]Bieniek, P., U. Bhatt, L. Rundquist, S. Lindsey, X. Zhang, and R. Thoman, 2011: Large-scale climate controls of Interior Alaska river ice breakup. *J. Climate*, **240**, 286–297.

2.1 Introduction

Because Alaska lacks roads in rural areas, rivers serve as critical highways—on ice in winter and on water in summer—but are impassable during breakup. In winter, rivers are used as ice roads to reach remote sites for oil and gas exploration and mining operations, as well as to reach the next village. The timing of ice-free conditions, which is dictated largely by the onset of breakup, signals the end of transportation on the ice and the ice roads. The breakup of river ice can also lead to ice jams and flooding in spring (Beltaos 2008) and occurs when broken ice stops moving, piles up, and restricts the flow of a river.

The date of river ice breakup (hereafter breakup) depends on a combination of river discharge and melting river ice; hence, breakup is the result of a balance between multiple forces. Breakup is initiated when the downstream forces of frictional river drag on the ice plus the forces associated with the momentum of moving ice from upstream overcomes the strength of the decaying stationary ice to resist movement. On the Yukon River at Dawson City, Canada, breakup is controlled by runoff from snowmelt at higher elevations and river flow characteristics (Carmack and Alford 1985). The exact date of breakup is somewhat subjective and tends to be defined as the passage of a breakup front at a given location, but the actual definition varies from observer to observer. The breakup date is most difficult to define in years when sufficient ice decay occurs prior to a significant increase in river flow so that the ice begins to move along the length of the river without any significant ice run from upstream. Despite the seemingly vague definition of breakup, our results show that breakup is a robust measure in Alaska as

multiple sites are highly correlated with one another.

The breakup date potentially integrates multiple climate parameters on both spatial and temporal scales into a single representative value. River parameters such as ice thickness have been used as proxies of the corresponding winter climate in the midlatitudes (Beltaos and Prowse 2002). Variability in ice conditions on Lake Baikal in Russia has been shown to be sensitive to multiple modes of climate variability across numerous seasons (Todd and Mackay 2003). Breakup trends on rivers and lakes throughout the Northern Hemisphere appear to be linked with observed climate variability (Magnuson et al. 2000). Anomalies in breakup on major rivers in Siberia and Canada have also been linked with the Pacific decadal oscillation (PDO; Pavelsky and Smith 2004), while ice jam activity has been linked with El Niño on the Yukon River (Jasek 1999). Since breakup integrates climate conditions spanning multiple seasons, it can also provide general information about the climate of Alaska and how it may relate to the large-scale climate.

The climate of Alaska has been linked with the large-scale climate in the Pacific sector. The El Niño–Southern Oscillation (ENSO) plays a major role in controlling temperature throughout Alaska and winter air temperatures tend to be warmer on average during warm (El Niño) events (Papineau 2001). In addition, the positive phase of the North Pacific Oscillation/West Pacific Pattern (NPO/WP) is characterized by increased storminess near Alaska that increases warm air advection into Alaska during the winter (Linkin and Nigam 2008).

While previous studies have primarily focused on the winter season, this work also explores climate and hydrological anomalies in spring. Through breakup we investigate the relationship between the large-scale (i.e., global or hemispheric scale) and local climate, toward the eventual goal of improving breakup forecasts. The novel aspects of our paper include the following: investigating the role of climate in Alaska breakup, identifying key climate–breakup physical linkages for Alaska, and proposing a plausible physical mechanism relating winter/spring local and large-scale climate processes for Alaska.

2.2 Data and methods

2.2.1 Meteorological data

Station data of monthly average temperature and accumulated liquid precipitation from 1948 to 2008 were provided by the Alaska Climate Research Center (available online at http://climate.gi.alaska.edu/) for the first-order stations located throughout Alaska (Fig. 2.1). The analysis was augmented with daily station observations, which include maximum and minimum daily temperature, sunrise to sunset average sky cover, and accumulated liquid precipitation for 1948–2008. The National Climatic Data Center provided the daily data (available online at http://www.ncdc.noaa.gov/oa/ncdc.html). The chosen stations have relatively long records of high-quality continuous observations since they are professionally operated and maintained by the National Weather Service and the Federal Aviation Administration. The stations are all located at relatively low elevations and represent various climate types ranging from Arctic for Barrow, Alaska, to

continental in Interior Alaska, to coastal in western and southern Alaska (Shulski and Wendler 2007).

To investigate the relationship with the large-scale climate, standard gridded climate data were employed. Over the land, monthly average surface air temperature (SAT) from the University of East Anglia Climate Research Unit (CRU) TS3.0 dataset was used (available online at http://www.cru.uea.ac.uk/cru/data/). This data interpolates global station data to a 0.5° x 0.5° grid over land only for 1901–2006 (Mitchell and Jones 2005). Over the oceans, monthly average sea surface temperature (SST) data from the National Oceanographic and Atmospheric Administration (NOAA) extended reconstructed SST data version 3 (see online at http://www.esrl.noaa.gov/psd/) were used. The SST data are provided on a 2° x 2° grid spanning 1854–2009 and incorporates satellite data after 1985 (Smith et al. 2008).

Data representing the atmospheric circulation were provided by the National Centers for Environmental Prediction–National Center for Atmospheric Research (NCEP–NCAR) reanalysis 1 (see online at http://www.esrl.noaa.gov/psd/). Variables investigated include monthly mean sea level pressure (SLP) and 500-hPa geopotential height (500-hPa height). The NCEP–NCAR reanalysis 1 assimilates observations using a weather forecast model and is provided on a 2.5° x 2.5° grid spanning 1948–2008 (Kalnay et al. 1996).

The storm track data are based on the tracking algorithm of Zhang et al. (2004) and span 1948–2008. The tracking algorithm searches gridded 6-hourly SLP data to determine points of minimum pressure and then flags these as candidate cyclone (storm)

centers. The candidate centers were then tracked through time and the individual storms were identified by a tracking criterion of minimum lifetime. Individual storms were identified and tracked in the Northern Hemisphere north of 30°N and were constructed from the NCEP–NCAR reanalysis.

Climate indices were used to complement the analysis. The Niño-3 index was obtained from the Earth System Research Laboratory Physical Science Division (see online at http://www.esrl.noaa.gov/psd/) and spans 1871–2008. The Pacific–North American (PNA) index was obtained from the Climate Prediction Center (see online at http://www.cpc.noaa.gov/) and covers 1950–2008.

2.2.2 Hydrological data

Monthly average river discharge was provided by the U.S. Geological Survey (USGS), which maintains flow gauges on the rivers in Alaska (Fig. 2.1) where the breakup date is measured. Only a few flow gauges were collocated with the breakup observation locations, so proximal gauges on the same rivers were selected for the period 1948–2008.

Breakup date data were provided by the Alaska Pacific River Forecast Center (see online at http://aprfc.arh.noaa.gov/data/breakup.php) for the three locations (Fig. 2.1) on the Yukon, Tanana, and Kuskokwim Rivers in interior and western Alaska. The three breakup sites were chosen because of their location along major rivers, location in Interior Alaska, and their superior data quality relative to the other sites (only a few missing years). Bethel was initially selected to compare with the interior locations but it

was significantly correlated with the interior sites; hence, it was grouped with the interior stations. Winter river ice thickness measurements contained temporal inconsistencies and extensive periods of missing data so they could not be used.

The term breakup refers to the time when a breakup front (i.e., the interface between the stationary and moving ice) reaches the location of the observer, which can be somewhat subjective. Despite the subjectivity involved in breakup observations, the three locations (Fig. 2.2a) all tend to have the same sign anomalies each year, which is evident from visual inspection of Fig. 2.2a. They display significant correlations ranging from 0.70 Dawson City and Bethel, to 0.80 between Bethel and Nenana, and 0.80 between Nenana and Dawson City. The average breakup (Fig. 2.2b) is employed in this study because of the covariability between measurement sites.

Breakup typically occurs in early May, beginning in upstream reaches and then moving downstream toward the coast. Bethel has the latest breakup date and Nenana the earliest (Table 2.1) with a standard deviation at each station of about 1 week. The extreme latest breakup date observed was 3 June 1964 at Bethel while the earliest was at Nenana on 24 April 1998. All three sites have a significant decreasing trend with breakup occurring 1.3 days earlier per decade.

2.2.3 Analysis methods

Standard statistical techniques for climate analysis were employed in this study to investigate the relationships between the various climate and hydro-climate parameters. Pearson correlation coefficients were calculated on linearly detrended (least squares

method) time series since trends can be quite large in the Arctic. Linear regression coefficients were calculated using the least squares method. The correlation and regression analyses yielded similar results so only the regression analysis is presented. For ease of discussion, results were scaled by a factor of -1 as needed to reflect anomalies corresponding with early breakup. The statistical significance of correlations and regressions was assessed using a two-tailed t test at the 95% or greater level. Composite analysis was constructed by combining events larger than one standard deviation. As our datasets all have different record lengths, the analysis was conducted on the common period of 1948–2008.

Seasonal average analyses are presented in the paper for the sake of brevity. Winter in Alaska is a time of minimal solar radiation and snow cover, whereas in spring solar insolation leads to significant daytime heating. Snow however, remains on the ground until at least April for many areas of Alaska and controls the radiative properties of the surface because of its high albedo relative to bare ground. By grouping months with similar physical processes we defined winter as December–March (DJFM) and spring as April–May (AM).

2.3 Results

2.3.1 Local controls of breakup

Station temperature was regressed on breakup (Fig. 2.3a) and indicated that breakup tends to occur 1 day earlier (later) when average AM temperatures are 0.2°–0.3°C warmer (cooler) in interior/western and northern Alaska. In southern Alaska the

relationship between station temperature and breakup is weaker but still statistically significant. Springtime (AM) discharge regressed on breakup (Fig. 2.3b) suggests that breakup tends to occur earlier when river discharge is higher. Conversely breakup tends to occur later when river discharge is lower. The notable exception is the Chena River, which is a relatively small river. River discharge was normalized for all stations (excluding the Chena River) and then averaged to construct an interior river discharge time series. Regressions of DJFM precipitation on the AM-average-normalized river discharge (Fig. 2.3c) indicate that increased DJFM precipitation in interior and northern Alaska is associated with above-average AM discharge. However, wintertime (DJFM) temperature and precipitation were weakly related with breakup, with only a few stations having significant regression coefficients (not shown). When AM station temperature was regressed on the normalized spring discharge (Fig. 2.3d) it was found that increased spring discharge is related to warmer spring temperatures throughout Alaska.

In summary, warmer AM temperatures melt the snowpack, increase river discharge, and degrade the river ice leading to earlier thermal and mechanical forcing that breaks up river ice cover. Conversely, cooler AM temperatures maintain the snowpack, reduce river discharge, and maintain the river ice leading to later breakup. While breakup is related to runoff from the melting snowpack, winter precipitation was only weakly related to breakup. In conclusion, this suggests that AM surface air temperatures are the most important climate variable that determines breakup.

2.3.2 Large-scale controls of breakup

Winter (DJFM) and spring (AM) gridded climate data were regressed on breakup to investigate large-scale climate variability patterns particularly during the winter that could be exploited for breakup forecasting.

Regressions of wintertime (DJFM) surface temperatures (SAT over land and SST over oceans) on breakup (Fig. 2.4a) display significant negative values in the midlatitude Pacific and significant positive values along coastal North America and in the eastern equatorial Pacific. This DJFM regression pattern (Fig. 2.4a) in the Pacific compares favorably with the ENSO signal (Parker et al. 2007) and shows that during the positive phase of ENSO breakup is earlier than normal. The absence of significant regressions between breakup and DJFM SAT over Alaska is consistent with the analysis of local station data (section 2.3.1) where also no significant coefficients were found in winter. Breakup was only weakly correlated with the DJFM Niño-3 index (not shown); however, composite analysis of DJFM SSTs (not shown) revealed that while the positive phase of ENSO tends to occur with early breakup, the negative phase is only weakly related to late breakup. This suggests a nonlinear relationship where the warm phase of ENSO has a larger impact than the cool phase in controlling breakup.

Winter (DJFM) SLP regressed on breakup (Fig. 2.4b) displays an area of significant negative coefficients in the eastern midlatitude Pacific, which suggests enhanced southerly flow into Alaska during earlier breakup. The regressions of 500-hPa height on breakup (Fig. 2.4c) display a pattern extending from the tropics with a high–low–high–low pattern that compares favorably with the positive phase of the PNA

pattern. As the PNA is considered to be an atmospheric response to ENSO forcing (Horel and Wallace 1981), it is reasonable to conclude that the PNA-like regression pattern (Figs. 2.4b,c) is the atmospheric response to the ENSO structure (Fig. 2.4a). In summary, local winter conditions in Alaska have a minimal direct impact on breakup, however, there may be an indirect relationship since the winter SST and circulation anomaly patterns persist into spring.

Regressions of springtime (AM) temperature on breakup (Fig. 2.4d) are similar to those during winter (see Fig. 2.4a). The notable difference between DJFM and AM is that in AM there are significant positive regressions over all of Alaska. As a result of the high degree of similarity of the SST patterns in the Pacific between Figs. 2.4a,d and the slow speed of ocean processes, Pacific spring and winter SST patterns are likely linked through seasonal anomaly development in the ocean. This is supported by the large pattern correlation (0.77) between the winter and spring regression patterns (Figs. 2.4a,d) over the ocean.

Regressions of spring SLP and 500-hPa height on breakup (Figs. 2.4e,f) display patterns that are similar to those during winter, except the magnitudes of spring regressions are generally larger and shifted westward. The correlation between the AM PNA index and breakup was -0.47 (95% level significance), consistent with an earlier breakup during the positive phase of the PNA. In summary, breakup is impacted by ENSO- and PNA-related climate anomalies in the Pacific that begin to develop in DJFM and persist into AM.

2.3.3 Local to large-scale connection

Thus far, our results have shown that breakup is most closely linked with local AM temperature and with ENSO-related climate anomalies on the large scale. Regression and composite analysis of storm tracks, with breakup and climate variables, are used to investigate a physical mechanism linking the local and large-scale climate anomalies. Alaska is situated north of the major storm track in the Pacific (Klein 1957; Zhang et al. 2004; Mesquita et al. 2010) and storms primarily impact the state through the Gulf of Alaska with a secondary track through the Bering Sea for storms of more western origin (Klein 1957; Rodionov et al. 2007; Mesquita et al. 2010). In this analysis we investigated the relationship between breakup, storms approaching Alaska, and the large-scale climate. Storms entering the Gulf of Alaska (GOA; 55°–62°N, 137°–158°W, see box in Fig. 2.7a) and Bering Sea (Bering; 55°–70°N, 163°W–180°, see box in Fig. 2.6) were counted for DJFM and AM. The time series for the regional storm counts are shown in Fig. 2.5, with a 5-yr smoothing that highlights the decadal to multidecadal variability. The observed station data and gridded data were regressed on the GOA and Bering storm counts for DJFM and AM to evaluate their relationships.

During the winter (DJFM) only the Bering storm count had a significant relationship with accumulated precipitation in Interior Alaska at the seasonal scale (Fig. 2.6). More storms approaching Alaska from the Bering in DJFM results in increased DJFM precipitation, while, less storms approaching Alaska from the Bering in DJFM results in reduced DJFM precipitation. This finding is consistent with the self-organized map analysis of Cassano and Cassano (2009), which found that low pressure in the

Bering Sea results in increased precipitation over the Yukon basin. Storms that approach Alaska through the Bering allow more moisture penetration and precipitation in Interior Alaska, since the topographic barriers are significantly smaller than for storms that approach from the Gulf of Alaska. GOA storms deposit most of their precipitation on the windward side of the Alaska range (Mock et al. 1998). Since breakup has a weak relationship with DJFM precipitation and AM river discharge is primarily controlled by AM temperatures, the role of precipitation from DJFM Bering storms is concluded to be of minor importance.

Gulf of Alaska storms play a prominent role during the spring and station temperature regressed on AM GOA counts (Fig. 2.7a) indicated that fewer storms occurring in the Gulf of Alaska resulted in warmer surface air temperatures and earlier breakup. Conversely, more storms entering the Gulf of Alaska resulted in cooler surface air temperatures and later breakup. In contrast, during winter GOA storms warm Interior Alaska from adiabatic warming from downslope southerly flow over the Alaska range. Bering storms did not have a significant relationship with temperature in the spring. Spring SST/SAT, SLP, and 500-hPa height regressions on AM GOA storm counts (Figs. 2.7b–d) display patterns that compare favorably with the corresponding panels shown in Figs. 2.4d–f for breakup. The frequency of storms occurring in the Gulf of Alaska during spring is linked to similar large-scale climate patterns as breakup, suggesting that GOA storms are a key control of breakup variability through their influence on temperature in Interior Alaska.

The results have shown that spring (AM) Gulf of Alaska storm counts are

correlated with breakup and spring station temperature and all of these variables are related to similar large-scale climate patterns. Next we investigated how Gulf of Alaska (GOA) storms in spring (AM) control the local conditions (i.e., AM temperature) that lead to breakup.

Composites of accumulated thawing degree-days (the sum of temperatures above 0°C), accumulated sunrise to sunset cloud fraction, and accumulated precipitation were computed in relation to breakup date using the Fairbanks, Alaska, meteorological station data. Fairbanks was selected for this analysis as it had consistently high correlations with breakup and best illustrates the impact of GOA storms on the interior. Composite years for early breakup (1951, 1953, 1958, 1961, 1969, 1979, 1990, 1993, and 1998) and late breakup (1952, 1962, 1964, 1972, 1982, 1985, 1986, 1987, 1992, 2002, and 2006) were identified. The days in the composite were keyed to breakup and included 30 days before and 5 days after breakup, with breakup occurring on day 0. This was done to analyze the local weather conditions leading up to breakup and to facilitate a comparison with GOA storms.

Composites of maximum and minimum air temperatures for late and early breakup (Figs. 2.8a,b) indicate that temperatures tend to be warmer when breakup is earlier. Earlier breakup occurs when there is decreased cloud cover, reduced precipitation, and decreased numbers of storms occurring in the Gulf of Alaska (Figs. 2.8c–e). During spring, when solar radiation heats the surface, decreased cloud cover and precipitation help to raise surface air temperatures by increasing net solar radiation at the surface and is consistent with an earlier breakup. Conversely, more GOA storms,

increased cloudiness, and enhanced precipitation lead to a later breakup by reducing the amount of solar radiation reaching the surface.

A detailed analysis of the relationship between storms in the Gulf of Alaska and Pacific SSTs during DJFM and AM is beyond the scope of this study; however, published literature can provide insight on this topic. Using climate models and observations, Seager et al. (2010) found that there is a southward shift in the Pacific storm track during positive ENSO events. This is consistent with our findings that when storm counts decrease in the Gulf of Alaska there is an increased storm count into a box just to the south (not shown).

2.3.4 Low-frequency breakup signal

Visual inspection of the smoothed (5-yr running mean) breakup time series (Fig. 2.2b) suggests the presence of decadal variability, which accounts for 29% of the variance. This hypothesis was confirmed and quantified using singular spectrum, wavelet, and harmonic analysis on the unsmoothed breakup time series (not shown). The wavelet analysis also suggested that the decadal signal changes in frequency in the late 1980s. Closer examination of the low-frequency line in Fig. 2.2b indicated that there was a shift to earlier breakup between the mid-1980s to the mid-1990s. It has been noted that a shift in the leading mode of SST variability in the North Pacific in the early 1990s (Bond et al. 2003) from a PDO-like pattern to the North Pacific gyre oscillation (NPGO) pattern (Di Lorenzo et al. 2008) has occurred. The regression patterns of DJFM Pacific SSTs on breakup before and after 1989 are consistent with the empirical orthogonal

function (EOF) analysis from Bond et al. (2003) and Di Lorenzo et al. (2008), which showed a shift from the first to the second mode in Pacific SST variability (not shown). In addition, Bourne et al. (2010) found that surface-based temperature inversion parameters in Alaska were more strongly correlated with the PDO before 1989 than afterward. While a shift to earlier breakup was observed from the 1980s to 1990s, the storm counts (see Fig. 2.5) do not display a corresponding shift. While a physical mechanism linking the changes in breakup to North Pacific SST variability is unknown, there is some indication that the change to lower-frequency variability in breakup since 1989 reflects the concurrent shift noted in the North Pacific.

2.4 Conclusions

A summary of the key processes that relate breakup to the large-scale climate is shown schematically in Fig. 2.9. Breakup is primarily controlled by local spring surface air temperatures and river discharge. Additionally, river discharge is strongly influenced by surface air temperatures, with warmer temperatures leading to higher discharge due to runoff from the melting snowpack. Winter precipitation, despite providing the snowpack, influences breakup to a lesser extent since spring temperatures control the rate and timing of melt. Breakup is linked to ENSO-related climate anomalies that persist from winter into spring, suggesting that breakup may have some degree of predictability prior to the spring.

The overall climate–breakup mechanism (Fig. 2.9) can be summarized as follows: during El Niño in spring (AM), fewer storms occur in the Gulf of Alaska reducing

cloudiness, warming air temperatures, and leading to earlier interior river ice breakup. Although weaker than the influence of El Niño, during La Niña in spring (AM) more storms occur in the Gulf of Alaska increasing cloudiness, cooling temperatures, and resulting in later breakup.

The findings of this study expand on those of Papineau (2001), which linked winter temperatures in Alaska with ENSO. Our study indicated that ENSO-related climate anomalies influence Alaska springtime temperatures as well as the timing of breakup. Breakup was also found to contain a low-frequency climate signal when smoothed and a shift to earlier breakup after the 1980s was revealed that might reflect the shift in Pacific variability documented in 1989. This study shows that breakup in Alaska is sensitive to large-scale, low-frequency climate variability in the Pacific. The winter Pacific SST anomaly patterns, which persist into spring, may be potentially exploited to develop seasonal forecasts of springtime temperatures in Alaska. Consequently, seasonal predictions of spring temperatures in Alaska would help forecast river breakup date, breakup severity, and breakup-related flooding.

Acknowledgements

This work benefited from discussions with D. Dammann and E. Carmack. This research was supported with funds from the NOAA "Social Vulnerability to Climate Change and Extreme Weather of Alaskan Coastal Communities" Grant NA06OAR4600179. P. Bieniek was partially supported by funds from a University of Alaska Fairbanks graduate fellowship and the Geophysical Institute. Material presented here is based upon work supported in part by the National Science Foundation under Award ARC-0652838 through the International Arctic Research Center. We highly appreciate the fine work of B. Moore who prepared Fig. 2.1. We thank the three anonymous reviewers for their insightful comments that substantially improved this manuscript. Plots have been prepared using the open source software packages NCL (available online at http://www.ncl.ucar.edu) and GrADS (available online at http://www.iges.org/grads/).

References

Beltaos, S., 2008: Progress in the study and management of river ice jams. *Cold Reg. Sci. Technol.*, **51**, 2–19.

Beltaos, S., and T. D. Prowse, 2002: Climatic control of river-ice hydrology: A review. *Hydrol. Processes*, **16**, 805–822.

Bond, N. A., J. E. Overland, M. Spillane, and P. Stabeno, 2003: Recent shifts in the state of the North Pacific. *Geophys. Res. Lett.*, **30**, 2183, doi:10.1029/2003GL018597.

Bourne, S. M., U. S. Bhatt, J. Zhang, and R. Thoman, 2010: Surface-based temperature inversions in Alaska from a climate perspective. *Atmos. Res.*, **95**, 353–366.

Carmack, E. C., and M. E. Alford, 1985: Factors leading to a mild break-up of the Yukon River near Fort Selkirk: 1985. National Water Research Institute Tech. Rep. 85-01, 12 pp.

Cassano, E. N., and J. J. Cassano, 2009: Synoptic forcing of precipitation in the Mackenzie and Yukon River basins. *Int. J. Climatol.*, **30**, 658–674, doi:10.1002/joc.1926.

Di Lorenzo, E., and Coauthors, 2008: North Pacific Gyre Oscillation links ocean climate and ecosystem change. *Geophys. Res. Lett.*, **35**, L08607, doi:10.1029/2007GL032838.

Horel, J. D., and J. M. Wallace, 1981: Planetary-scale atmospheric phenomena associated with the Southern Oscillation. *Mon. Wea. Rev.*, **109**, 813–829.

Jasek, M. J., 1999: 1998 break-up and flood on the Yukon River at Dawson—Did El Niño and climate change play a role? *Ice in Surface Waters*, H. T. Shen, Ed., Balkema, 761–768.

Kalnay, E., and Coauthors, 1996: The NCEP/NCAR 40-Year Reanalysis Project. *Bull. Amer. Meteor. Soc.*, **77**, 437–471.

Klein, W. H., 1957: Principal tracks and mean frequencies of cyclones and anticyclones in the Northern Hemisphere. U.S. Weather Bureau, 53 pp.

Linkin, M. E., and S. Nigam, 2008: The North Pacific Oscillation–West Pacific teleconnection pattern: Mature-phase structure and winter impacts. *J. Climate*, **21**, 1979–1997.

Magnuson, J. J., and Coauthors, 2000: Historical trends in lake and river ice cover in the Northern Hemisphere. *Science*, **289**, 1743–1746.

Mesquita, M. D. S., D. E. Atkinson, and K. I. Hodges, 2010: Characteristics and variability of storm tracks in the North Pacific, Bering Sea, and Alaska. *J. Climate*, **23**, 294–311.

Mitchell, T. D., and P. D. Jones, 2005: An improved method of constructing a database of monthly climate observations and associated high-resolution grids. *Int. J. Climatol.*, **25**, 693–712.

Mock, C. J., P. J. Bartlein, and P. M. Anderson, 1998: Atmospheric circulation patterns and spatial climatic variations in Beringia. *Int. J. Climatol.*, **18**, 1085–1104.

Papineau, J. M., 2001: Wintertime temperature anomalies in Alaska correlated with ENSO and PDO. *Int. J. Climatol.*, **21**, 1577– 1592.

Parker, D., C. Folland, A. Scaife, J. Knight, A. Colman, P. Baines, and B. W. Dong, 2007: Decadal to multidecadal variability and the climate change background. *J. Geophys. Res.*, **112**, D18115, doi:10.1029/2007JD008411.

Pavelsky, T. M., and L. C. Smith, 2004: Spatial and temporal patterns in Arctic river ice breakup observed with MODIS and AVHRR time series. *Remote Sens. Environ.*, **93**, 328–338.

Rodionov, S. N., N. A. Bond, and J. E. Overland, 2007: The Aleutian low, storm tracks, and winter climate variability in the Bering Sea. *Deep-Sea Res. II*, **54**, 2560–2577.

Seager, R., N. Naik, M. Ting, M. A. Cane, N. Harnik, and Y. Kushnir, 2010: Adjustment of the atmospheric circulation to tropical Pacific SST anomalies: Variability of transient eddy propagation in the Pacific–North America sector. *Quart. J. Roy. Meteor. Soc.*, **136**, 277–296, doi:10.1002/qj.588.

Shulski, M., and G. Wendler, 2007: *The Climate of Alaska*. University of Alaska Press, 214 pp.

Smith, T. M., R. W. Reynolds, T. C. Peterson, and J. Lawrimore, 2008: Improvements to NOAA's historical merged land– ocean surface temperature analysis (1880–2006). *J. Climate*, **21**, 2283–2296.

Todd, M. C., and A. W. Mackay, 2003: Large-scale climatic controls on Lake Baikal ice cover. *J. Climate*, **16**, 3186– 3199.

Zhang, X. D., J. E. Walsh, J. Zhang, U. S. Bhatt, and M. Ikeda, 2004: Climatology and interannual variability of arctic cyclone activity: 1948–2002. *J. Climate*, **17**, 2300–2317.

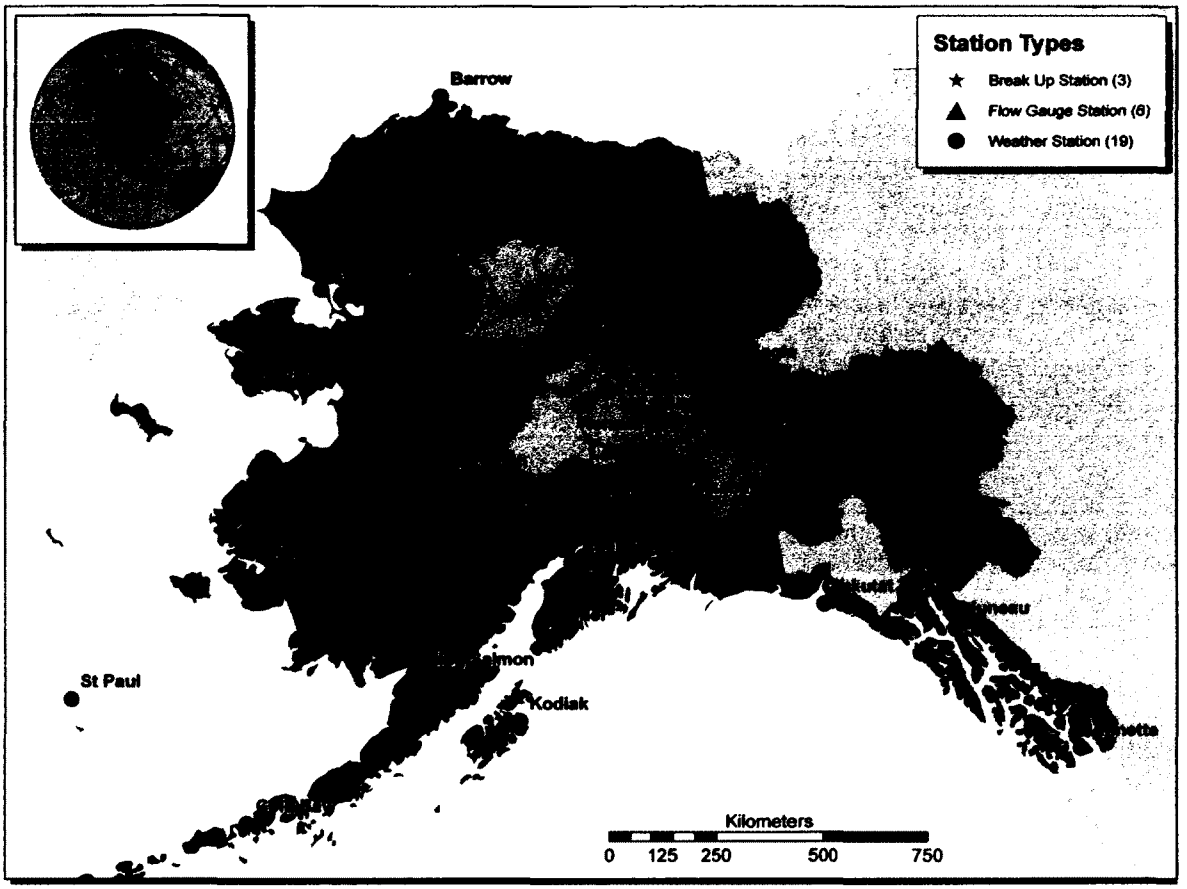

Figure 2.1. Map of Alaska identifying locations of river breakup (gold stars), river discharge (blue triangles), and first-order climate station (red circles) data. River drainage basins are located in western and Interior Alaska.

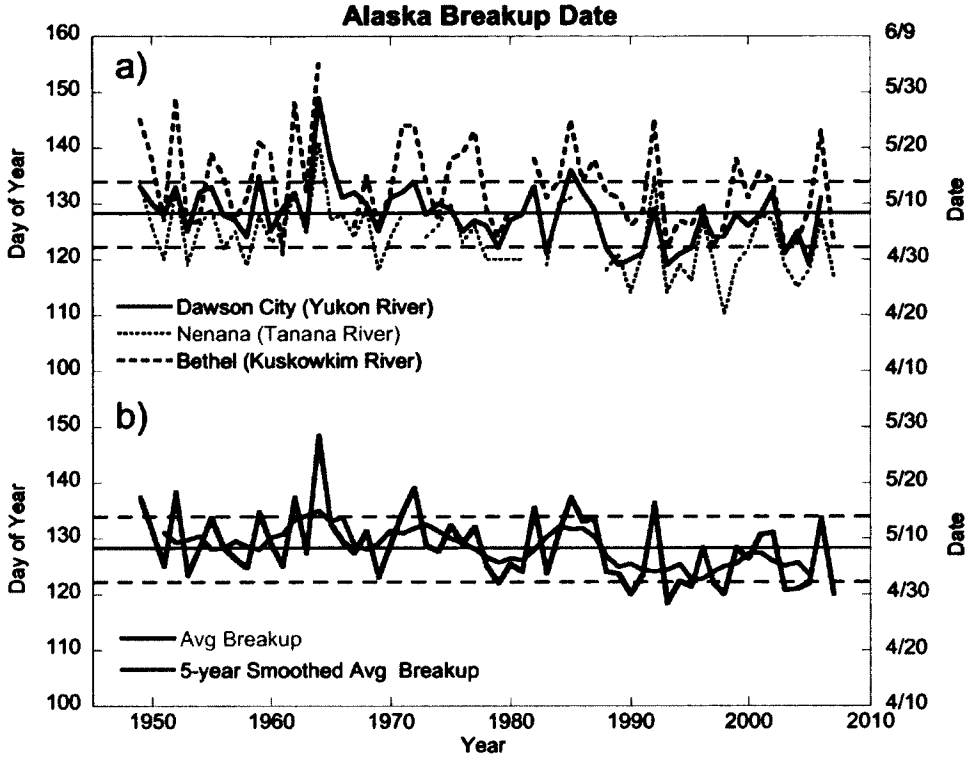

Figure 2.2. (a) Breakup date time series for Dawson City (Yukon River), Nenana (Tanana River), and Bethel (Kuskokwim River) are shown as a solid, gray dotted, and black dashed lines, respectively. (b) The gray line shows the 3-station average, while the 5-yr running mean of the station average is shown in black. The horizontal solid and dashed lines show the mean and standard deviation of the average breakup, respectively. Averaging the stations was justified since they were significantly correlated (>0.70).

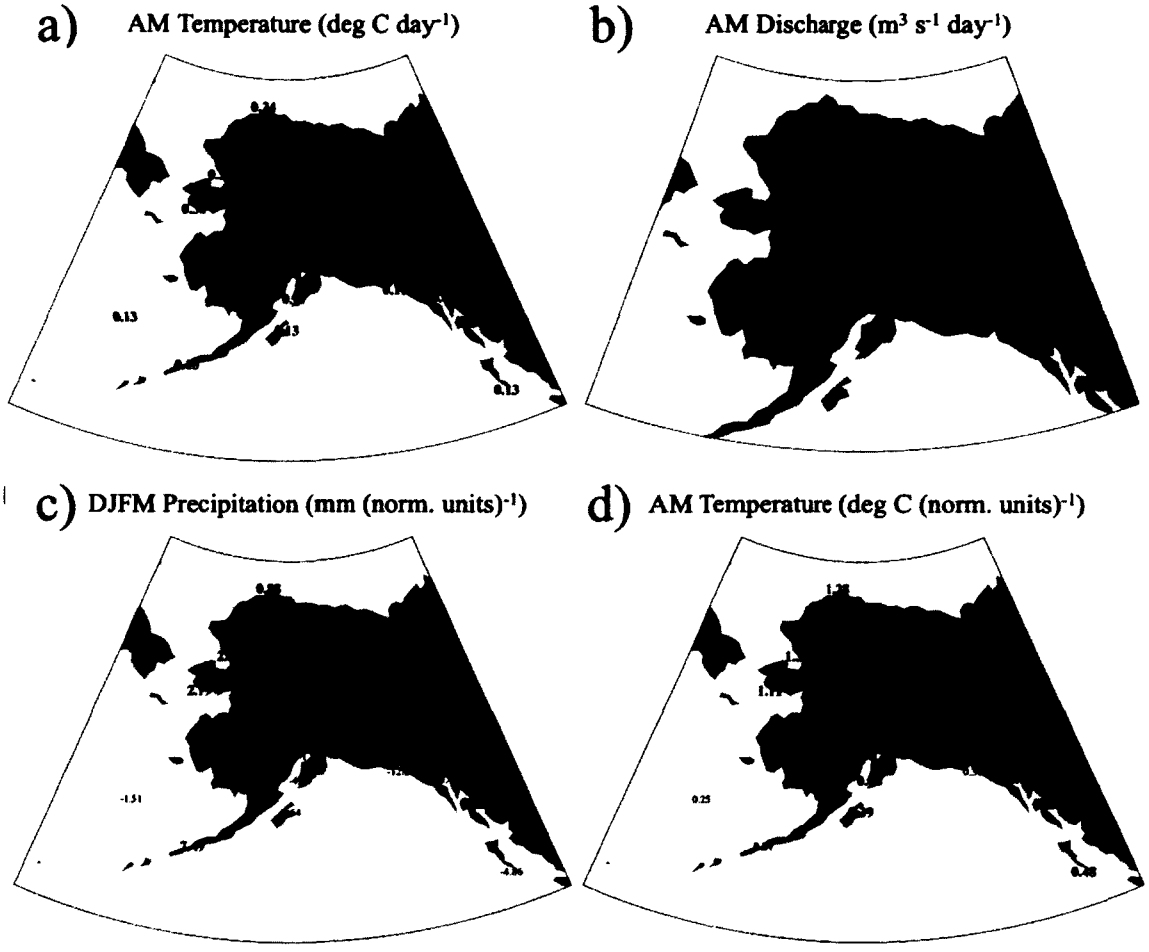

Figure 2.3. Linear regression coefficients of (a) AM temperature, (b) AM river discharge on breakup date, (c) DJFM precipitation, and (d) AM temperature on AM normalized river discharge. Note that (a) and (b) have been scaled by -1. Regressions significant at the 95% or greater level are shown in bold. Breakup tends to occur earlier (later) when temperatures are warmer (cooler) and river discharge is higher (lower). Higher (lower) AM discharge occurs with increased (decreased) DJFM precipitation.

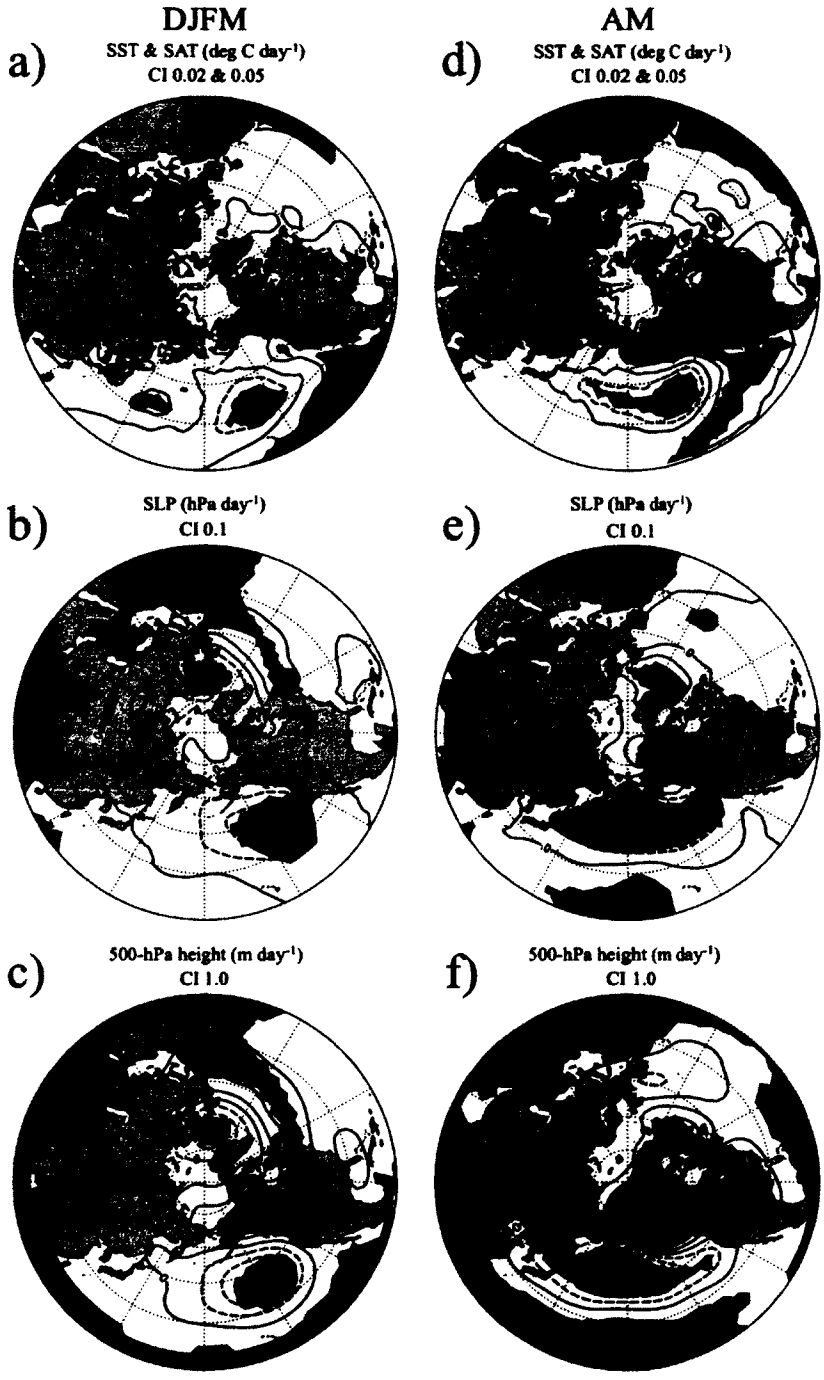

Figure 2.4. Linear regression coefficients of DJFM (a) SST/SAT, (b) SLP, (c) 500-hPa height, and AM (d) SST/SAT, (e) SLP, (f) 500-hPa height on breakup. Note that (a)–(f) have been scaled by -1. Contour intervals (CI) are shown under the titles. Positive (negative) regressions significant at the 95% or greater level are shaded red (blue). DJFM and AM SAT/SST pattern resemble ENSO-related climate anomalies in Pacific. The warm phase of ENSO is associated with an earlier breakup.

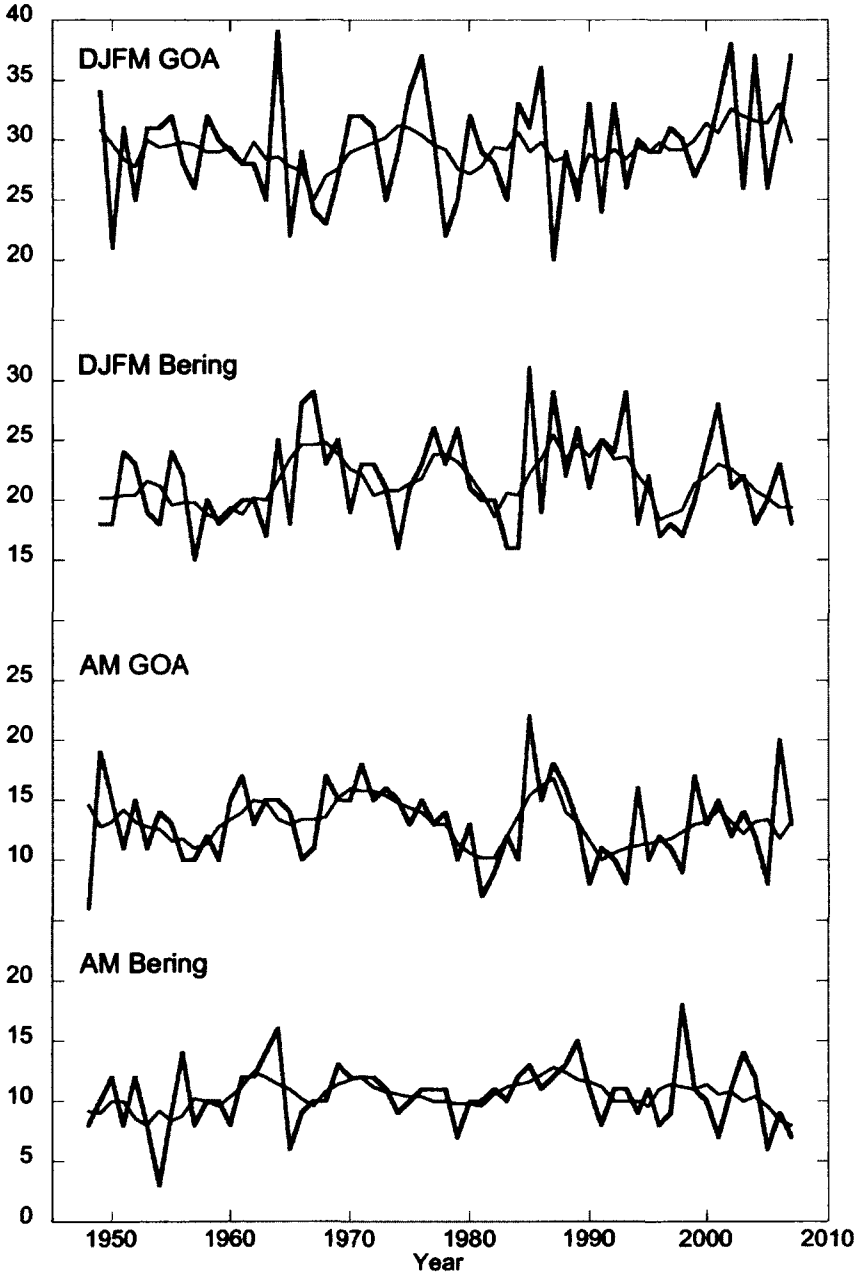

Figure 2.5. Time series of DJFM and AM GOA and Bering Sea storm counts shown by gray lines. Smoothed (5 yr) time series are shown by black lines. The plot limits vary, but the scale is the same for all line plots.

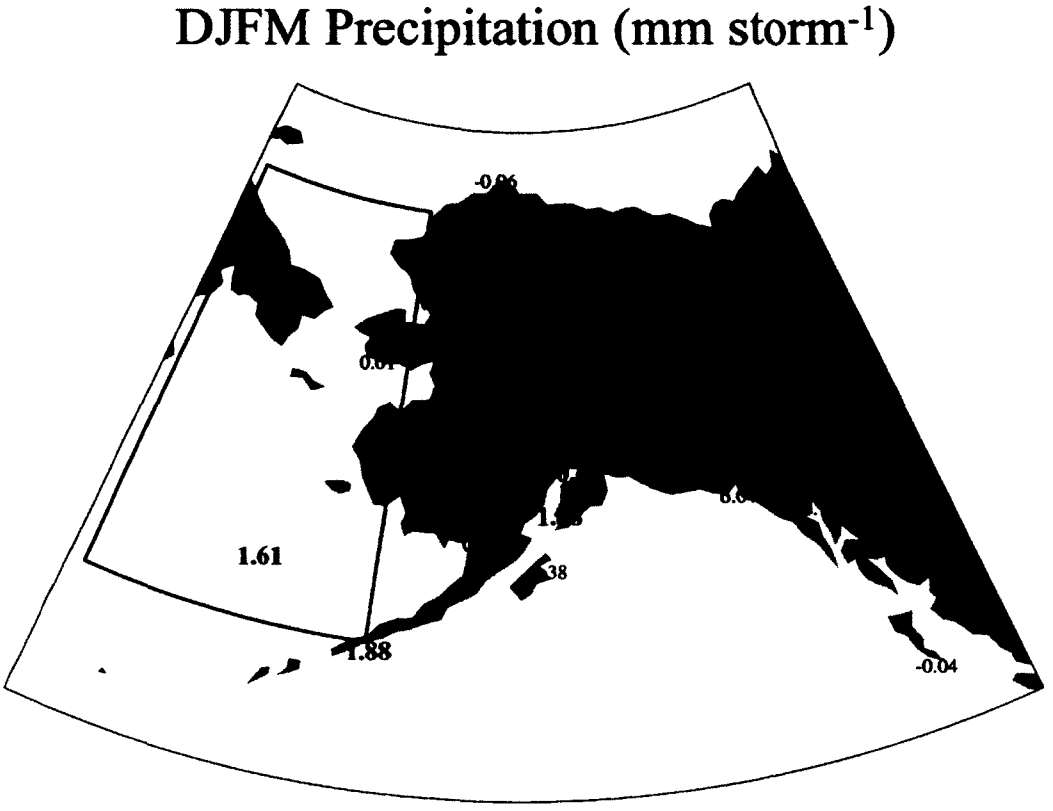

Figure 2.6. Linear regression coefficients of DJFM precipitation on DJFM Bering Sea storm count. Storms that entered the outlined box were included in the storm count. Regressions significant at the 95% or greater level are shown in bold. Increased (decreased) storms result in more (less) precipitation in Interior Alaska in winter.

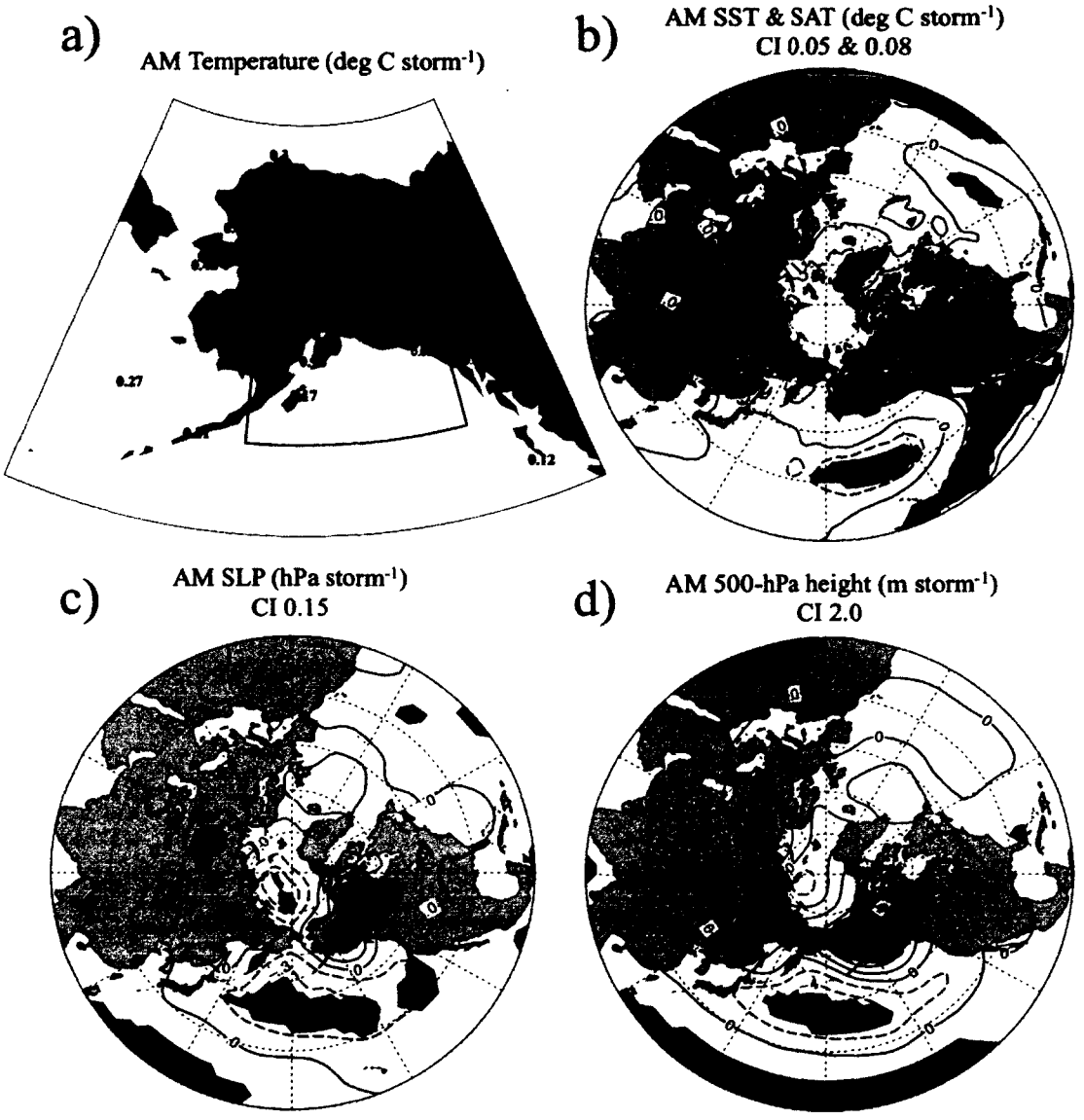

Figure 2.7. Linear regression coefficients of AM (a) station temperature, (b) SST/SAT, (c) SLP, and (d) 500-hPa height on the AM GOA storm count. Note that (a)–(d) have been scaled by -1. Contour intervals shown above plots. In (a), regressions significant at the 95% or greater level are shown in bold. Positive (negative) regressions that are significant at the 95% or greater level are shaded red (blue). Storms that entered the outlined box in (a) were included in the storm count. Increased (decreased) GOA storm counts are associated with the cool (warm) phase of ENSO. Increased (decreased) storm counts result in cooler (warmer) temperature in Alaska.

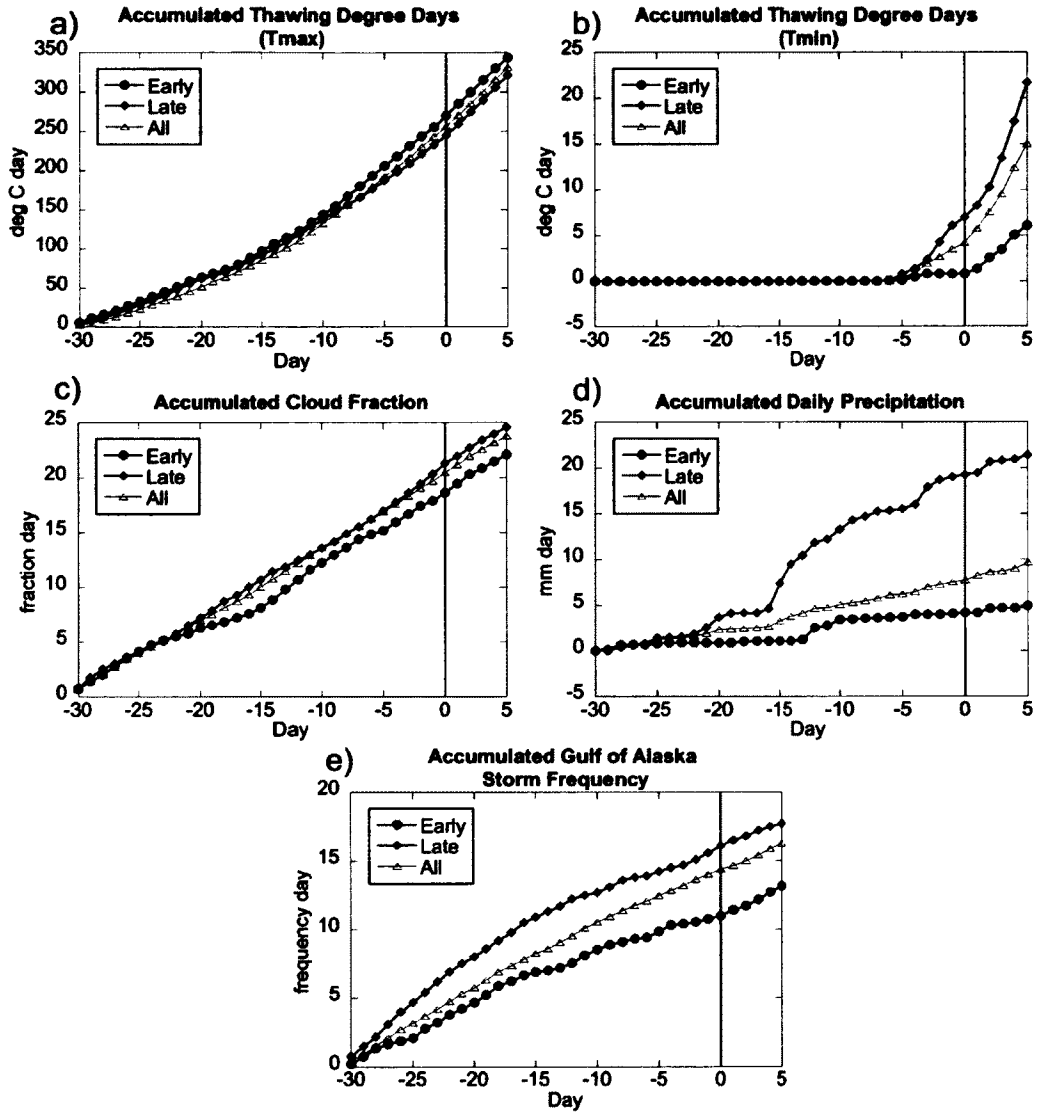

Figure 2.8. Daily average composites for late, early, and average breakup of Fairbanks observed (a) accumulated thawing degree-day based on maximum temperature, (b) accumulated thawing degree-day based on minimum temperature, (c) accumulated cloud fraction, (d) accumulated precipitation, and (e) accumulated GOA daily storm count. The window starts 30 before and ends 5 days after breakup date, which is marked with a vertical line.

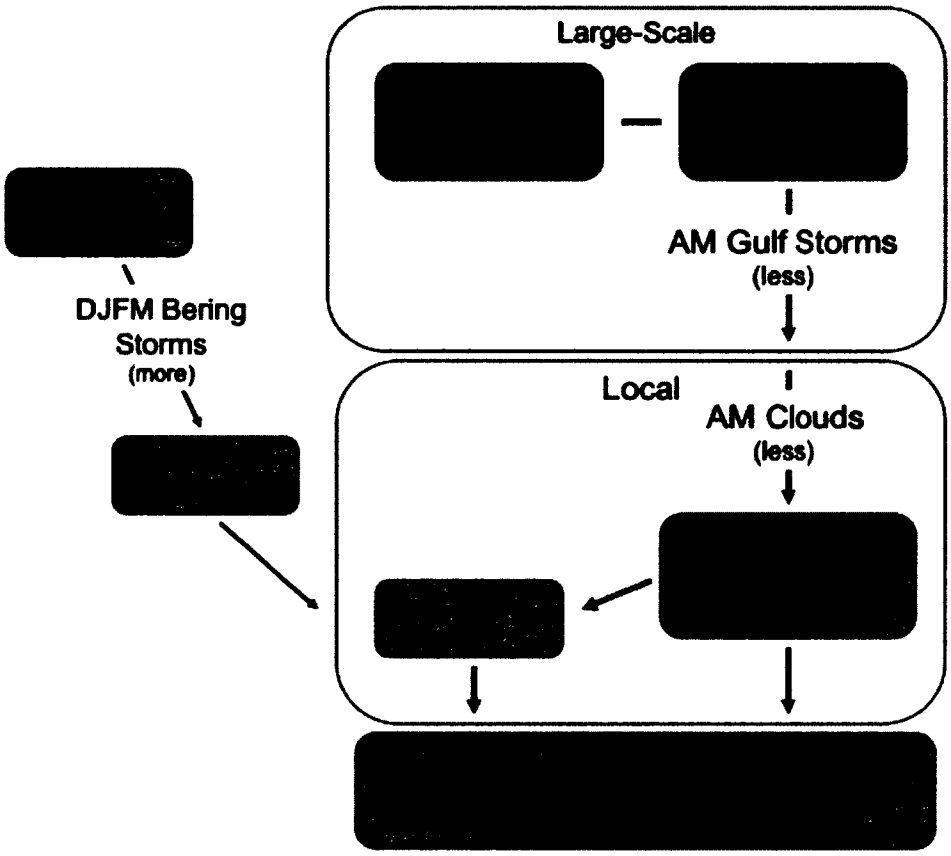

Figure 2.9. Summary of the breakup–climate mechanism highlighted for early breakup. The primary mechanism is outlined within the boxes, with the secondary mechanism shown on the left. DJFM represents the December–March period while AM signifies April–May. Later breakup can be described by opposite sign anomalies.

Table 2.1. Average, standard deviation, record minimum and maximum, and trend for breakup observed at Dawson City, Nenana, Bethel, and the average breakup.

	Dawson	Nenana	Bethel	Avg
Avg (day of year)	128	124	133	128
Std dev (days)	5	6	8	6
Record min (day of year)	119	110	121	118
Record max (day of year)	149	141	155	148
Trend (days per decade)	-1.3	-1.3	-1.3	-1.3

Chapter 3 Alaska Coastal Tundra Vegetation Links to Climate[1]

Abstract

Changes in the seasonal climate in arctic coastal regions of Alaska have been documented during the satellite record and are linked to tundra vegetation productivity. The Arctic Normalized Difference Vegetation Index (NDVI) data set (a measure of vegetation photosynthetic capacity) has been used to document coherent temporal relationships between near-coastal sea ice, summer tundra land surface temperatures, and vegetation productivity throughout the Arctic. In the tundra of northern Alaska, significant increases have been documented in seasonal maximum (max) NDVI along the Beaufort and Chukchi Sea coasts. In contrast, maxNDVI over coastal tundra areas in southwest Alaska along the Bering Sea has declined. Increasing land surface temperatures have been documented in the Chukchi, Beaufort and Bering Sea tundra regions during the summer, but temperatures have declined in midsummer. The purpose of this study is to identify the climate system components that are linked to Alaska coastal tundra NDVI changes on seasonal and sub-seasonal time scales.

Three coastal tundra domains were evaluated based on the Treshnikov divisions and they are named the East Bering, East Chukchi, and Beaufort, in reference to the adjacent seas. In the Beaufort and East Chukchi regions, the strength of the Beaufort High was correlated with NDVI, however the sign of the relationship changes from month to month in summer indicating a complex relationship. The maxNDVI is above

[1]Bieniek P., U. Bhatt, D. Walker, M. Raynolds, J. Comiso, H. Epstein, J. Pinzon, C. Tucker, R. Thoman, H. Trang, N. Mölders, W. Ermold, J. Zhang, and M. Steele, 2012: Alaska coastal tundra vegetation links to climate. *Earth Interact.*, in preparation for submission.

average when the June Beaufort High (BH) is stronger, however, a weaker BH in July is also linked with increased TI-NDVI (time-integrated over the season). This suggests that a stronger BH, which suppresses cloudiness and increases solar insolation, may drive warming in June. Trends in wind speeds suggest that the changes in temperature are also linked with changes in the local sea breeze circulation, and stronger winds along the coast are correlated with warmer temperatures over land. The decline in the July BH may be, in part, enhanced due to a weakening of the sea breeze circulation that occurs from land surface cooling that reduces the land-sea contrast. The cooling over land may be the result of increased convection and increased cloud cover, which reduces solar insolation.

Increased NDVI has been documented in the early part of the season in the Beaufort and Chukchi regions and is consistent with earlier snowmelt. The decline of NDVI in the East Bering region is consistent with later snowmelt due to late season snowfall that delays the onset of the growing season. The delay in snowmelt may be linked to an increase in occurrences of the positive phase of the West Pacific Pattern. Winter snow water equivalent in the East Bering tundra region is positively correlated with maxNDVI, where reduced maxNDVI tends to occur with reduced winter snowfall.

3.1 Introduction

Vegetation throughout Alaska and the Arctic is experiencing changes that have been to linked climate change and variability (Jia et al. 2003; Bhatt et al. 2010). Many climatic changes have been documented in Alaska and the Arctic summer during the satellite record and longer time scales, most notably increasing surface air temperatures and a decline in sea ice (ACIA 2005). These climatic changes are especially pronounced in the Arctic due to the role of polar amplification (Bekryaev et al. 2010; Serreze and Barry 2011). The satellite derived Normalized Difference Vegetation Index (NDVI) data set (Pinzon et al. 2012) has been extensively used as a measure of vegetation productivity and is correlated with the amount of aboveground biomass in the Arctic (Raynolds et al. 2011). Changes in Alaska arctic coastal tundra seasonal maximum NDVI (Figure 3.1) have been documented over the satellite record; primarily greening (increasing NDVI) along the Beaufort and Chukchi Sea coasts (Jia et al. 2003) and browning (decreasing NDVI) in southwest Alaska along the Bering Sea coast (Verbyla 2008; Bhatt et al. 2010).

The greening trend in the northern portion of Alaska has been attributed to an increase in shrubs (Sturm et al. 2001; Tape et al. 2006) and this region is experiencing an increased growing season length (Jia et al. 2003). The browning trend in southwest Alaska in the inland boreal forest regions has been attributed to increased drought stress and insect infestation (Parent and Verbyla 2010). In Alaska, the climate has also been linked with outbreaks of spruce beetles (Sherriff et al. 2011) and also years with extensive area burned by wildfires (Hess et al. 2001; Duffy et al. 2005), which can reduce and/or alter the vegetation primarily in the boreal forest region (Goetz et al. 2005).

Alaska is experiencing widespread changes in vegetation that have also been documented throughout the pan-Arctic. Increasing (greening) trends in NDVI have been observed throughout much of the pan-Arctic and Alaska coastal tundra (Figure 3.1a,b) during the satellite record (Jia et al. 2003; Goetz et al. 2005; Bhatt et al. 2010). It is suggested that temperature (Walker et al. 2003) and sea ice (Bhatt et al. 2010) are linked to the increase in coastal tundra NDVI in the pan-Arctic. In this study, we investigate the seasonality of trends and variability of NDVI and climate parameters to better understand how the climate is linked to the observed changes and variations of NDVI in the coastal tundra regions of Alaska.

The Arctic tundra biome is controlled by the cool summer air mass associated with the location of the sea ice (Yurtsev 1994; Epstein et al. 2004). Changes in sea ice distribution in summer have occurred in conjunction with changes in the nearby atmospheric temperatures (Bhatt et al. 2008; Lawrence et al. 2008). While precipitation amounts are small in the Arctic, tundra plants are primarily temperature limited, as the soils tend to be moist due to the permafrost layer limiting the runoff of water. The air is also moist due to the moisture available from the adjacent Arctic Ocean, especially when it is ice-free. With the decline in sea ice, summer temperatures are not as constrained by the cold, high albedo surface of ice and can more readily increase with solar insolation. The goal of this study is to understand the climate processes of trends and variability that impact vegetation productivity in Alaska.

This study builds on the previous studies of Alaska coastal tundra NDVI change by documenting the sub-seasonal trends. The Beaufort High and a sea breeze circulation

are shown to possibly play a role in climate and NDVI change in the coastal tundra regions of northern Alaska. A hypothesis is also presented showing that increased vegetative productivity in northern Alaska may have a feedback on climate by impacting the atmospheric circulation. Links between NDVI and the timing of spring snowmelt were also identified. Most importantly, climate-NDVI linkages are shown to change from month-to-month over the season.

3.2 Data and methods

The Normalized Difference Vegetation Index is defined as NDVI = (NIR – VIS)/(NIR + VIS), where NIR is surface reflectance of near infrared radiation and VIS is the reflectance of visible radiation (Deering 1978; Tucker 1979). The NDVI represents the fraction of photosynthetically active radiation that is absorbed by the plant canopy and ranges from zero (no vegetation activity) to one and is unitless. The amount of radiation absorbed primarily depends on the physical properties of the vegetation including the species, the vertical and horizontal structure, phenological stage, and the physiological condition. The NDVI data set used in this study is the GIMMS3g NDVI data set, which is derived from the wavelength bands retrieved from the Advanced Very High Resolution Radiometer (AVHRR) sensors 1982-2011 (Pinzon et al. 2012). The maximum NDVI (maxNDVI) is the highest summer NDVI value, representing seasonal peak values. The unitless time-integrated NDVI (TI-NDVI) is the sum of biweekly values above zero from April to September. TI-NDVI incorporates the length of the growing season and phenological variations and better represents gross primary production than

maxNDVI (Tucker and Sellers 1986). In addition, TI-NDVI was found to be more strongly correlated than maxNDVI to climate parameters such as spring sea ice cover and tundra land surface temperatures (Bhatt et al. 2010).

Weekly sea ice concentration from Special Sensor Microwave Imager (SSM/I) data (Comiso and Nishio 2008) and AVHRR radiometric surface temperature from 1982 to 2011 were used in this analysis. The area average sea ice concentration was calculated within a 100km buffer of the coast of each tundra region. The AVHRR surface temperature data have been enhanced through more effective cloud masking techniques and calibration through the utilization of in situ surface temperature data (Comiso 2003). Monthly AVHRR land surface temperatures were used to calculate the summer warmth index (SWI), which is the sum of May-Sep monthly average land surface temperatures greater than 0°C, while weekly and monthly temperature data were used to examine seasonality of changes and variability.

Weekly ocean heat content data was calculated from the Pan-Arctic Ice-Ocean Modeling and Assimilation System (PIOMAS) data set (Steele et al. 2011) for 1988-2011. The amount is a vertical integration from the surface to 100m depth or the bottom if shallower. The heat content was calculated by the density of the ocean times a fixed ocean heat capacity of 4218 J/kg/°C times the ocean temperature minus 2°C. The data was then area averaged within a 100km buffer of the coast of each tundra region.

Snow cover data were obtained from the Moderate Imaging Spectrometer (MODIS) Terra Satellite for 2000-2011 at the National Snow and Ice Data Center (NSIDC; available online at http://nsidc.org). The MODIS snow cover data are an 8-day

composite and are provided on a 5km grid (Hall et al. 2006). SSM/I derived snow water equivalent (SWE) data were also obtained from NSIDC and are available at a monthly resolution on a 25km Equal-Area Scalable Earth (EASE)-grid for the period 1987-2007 (Armstrong et al. 2007). To enhance the relatively short records of the satellite derived snow data, station snow data records were also analyzed at the few available stations located in the coastal tundra regions of Alaska (Figure 3.1d). Daily and monthly snow depth, temperature, and precipitation were obtained from the National Climatic Data Center for Bethel, Kotzebue, and Barrow for 1982-2011, Kuparuk for 1983-2011 and Umiat for 1982-2001. Additional station cloud cover data was obtained for Barrow, Kotzebue and Bethel from the Integrated Surface Data (ISD; available online at: http://www.ncdc.noaa.gov/oa/climate/isd/index.php) for 1982-2011.

The NDVI, MODIS snow and SWE data were subdivided in this analysis by their proximity to oceans. The regions used in this analysis follow those utilized in Bhatt et al. (2010), which were based on the ocean regions outlined by Treshnikov (1985) and floristic provinces modified by Walker et al. (2005). The tundra domains employed in this study will be referred to as East Bering, East Chukchi and Beaufort and represent the areas of coastal tundra regions as well as nearby ocean domains (Figure 3.1d).

Gridded reanalysis data were analyzed to investigate the links between tundra and the atmospheric circulation. Gridded monthly and 6-hourly mean sea level pressure (MSLP), surface air temperature (SAT) and 10m winds were obtained from the Climate Forecast System Reanalysis (CFSR; available online at: http://cfs.ncep.noaa.gov/cfsr/) for 1982-2009 (Saha et al. 2006). The CFSR data are available at various spatial resolutions

and the MSLP were obtained at 0.5 degree, and the SAT and 10m winds were obtained at T382 (~38km) resolution. Storm track information is based on the NCEP/NCAR Reanalysis MSLP 2.5 (Kalnay et al. 1996) degree data analyzed using a cyclone-tracking algorithm developed by Zhang et al. (2004) for 1982-2011. The storm track algorithm provides the location, and central pressure of each storm throughout its lifecycle.

3.3 Results

3.3.1 Beaufort and East Chukchi

The Beaufort and East Chukchi coastal tundra regions are bounded to the south by the Brooks Range and to the north by the Arctic Ocean (Figure 3.1d). Both regions are located almost entirely within the Arctic climate division of Alaska (Bieniek et al. 2012) with the exception of the southern extent of the East Chukchi tundra region, which is located in the west coast climate division. These two regions exhibit broadly similar seasonal climate variability throughout the year so they are discussed in parallel in this section. Climatologically, these regions receive very little precipitation throughout the year and experience 24 hours of sunlight in summer and complete darkness in winter (Shulski and Wendler 2007).

Increasing or greening trends in both TI-NDVI and maxNDVI are evident throughout the Beaufort and Chukchi regions (Figure 3.1a,b). Time series over the full tundra domains of both regions also display increased NDVI (Figure 3.2a,c) over the satellite record. The increase in NDVI has occurred in conjunction with decreased summer sea ice or increased open water and increased SWI (Figure 3.2b,d). However,

mixed spatial trends in SWI are present, especially in the Beaufort region (Figure 3.1c). When weekly sea ice, temperature and NDVI trends were evaluated, intra-seasonal differences in the trends are evident. Sea ice in the Beaufort Sea (Figure 3.3a) has a trend towards more open water throughout the summer with the largest trends during the transition times indicating earlier breakup and later freeze up. Weekly land surface temperature trends (Figure 3.3b) display warming at the beginning and end of summer, but are cooling during midsummer. Similar trends of reduced Arctic warming and even cooling in summer have been noted in some recent studies (e.g. Manabe et al. 2011). NDVI trends are positive throughout the growing season (Figure 3.3c) and the largest trends have occurred in midsummer, concurrent with the cooling land surface temperatures. This appears inconsistent with positive correlations between TI-NDVI and surface temperature, however plants do not necessarily immediately respond to climate anomalies and changes and the vegetation may in fact slowly respond over many years. Cooling temperatures are also in contrast to the overall warming trends in SWI and a hypothesis explaining this set of relationships will be explored later in this section. In the Chukchi tundra region, sea ice is declining throughout the summer (Figure 3.4a), and the largest declines have occurred in early summer and fall. Weekly surface temperatures (Figure 3.4b) are warming during early and late summer, but are cooling in midsummer similar to the Beaufort region. NDVI is increasing more modestly throughout the summer season in the Chukchi (Figure 3.4c) than the Beaufort (Figure 3.3c) and May-June NDVI is declining.

The declining trend in sea ice within 100km of the Beaufort and East Chukchi coastal regions has occurred in conjunction with an increase in total column ocean heat content over the period 1988-2011 (Figure 3.5a,b). Increased ocean heat content in this region has been recently documented and has been attributed several factors, including discharge from the Mackenzie River (Wood et al. 2012).

To understand the relationship between the timing of greenup and senescence and TI-NDVI and maxNDVI, the biweekly NDVI data set was interpolated to daily data using the phenology curve fitting procedure developed by Jonsson and Eklundh (2002). Unfortunately the biweekly data at the start and end of the growing season were nearly identical from year to year so it was not possible identify any discernable change in greenup or senescence timing. Therefore we must rely on the combination of the limited spatial extent of the station data in Alaska and limited temporal range of the satellite data to evaluate the trends of growing season length and snow parameters.

Snow depth and timing of melt impact vegetation. The timing of melt determines when plants may begin to photosynthesize and grow, while snow depth can influence the amount of soil moisture available for the plants in the Arctic summer. A trend towards earlier snowmelt was found when the first snow free date was evaluated within the Beaufort and Chukchi tundra regions (Figure 3.6). The long-term station records of snow depth indicate trends to earlier snowmelt across the region with the exception of Barrow. Barrow has been experiencing later snowmelt since 2005 with an increase in late season snowfall (not shown), which has changed the sign of the overall trend. MODIS also exhibits a trend to earlier snow melt in the Beaufort and Chukchi tundra regions during

its relatively short record (2000-2011). This is consistent with the findings of Stone et al. (2002), who found earlier snow melt at stations and in satellite derived data across northern Alaska. Trends to earlier river ice breakup (which is related to snowmelt) have been observed throughout Interior Alaska and the onset of breakup was found to be linked to spring temperatures and the large-scale climate (Bieniek et al. 2011), so the warmer spring temperatures documented in the Beaufort and East Chukchi regions may be driving earlier snow melt in these regions.

While not significantly correlated with NDVI, this region has also experienced increasing winter snow depth and snow water equivalent trends (Liston and Hiemstra 2011; Muskett 2012), which is consistent with the notion of increased snowfall resulting from declining sea ice (Higgins and Cassano 2011; Liu et al. 2012a). While this appears contrary to the earlier snow melt date documented above, Bieniek et al. (2011) showed that, for Interior Alaska, the depth of snow was not as important as the spring temperatures for the onset of the melt season. Therefore, when spring snow depth increases, snowmelt may still occur earlier when spring temperatures are warmer than normal. The exact mechanism driving the changes in timing of snowmelt in northern Alaska is a worthy research topic that is beyond the scope of this study.

TI-NDVI for both regions is significantly, negatively correlated (time series were first linearly detrended) with station snowmelt at all stations in the region (Table 3.1), suggesting that when snowmelt is earlier, NDVI is greater since vegetation is able to begin photosynthesis earlier. This result is further supported by the high negative correlation between early season NDVI and snowmelt date. The early season trend of

increased NDVI, particularly in the Beaufort region (Figure 3.3c), is also consistent with a more efficient growing season due to earlier snowmelt

Increasing NDVI has also been linked with increased summer warmth (Walker et al. 2003), therefore changes in the summer atmospheric circulation should play a role in the increasing summer temperatures observed in the Beaufort and East Chukchi regions. The Beaufort High is a major climatological feature over the Beaufort Sea in summer (Overland 2009; Serreze and Barrett 2011) and typically extends over northern Alaska in summer (see contours in Figure 3.7a). Climatologically, the Beaufort High is strongest in June (Figure 3.7b) and then weakens by August (Figure 3.7d). The spatial trends in MSLP show a strengthening Beaufort High for the summer season and in all months except July (Figure 3.7c). In June (Figure 3.7b) the MSLP is increasing throughout all of Alaska, while July and August (Figure 3.7c-d) have decreasing MSLP over land in Alaska. The Beaufort High trends were also captured when area average MSLP in a box bounding the Beaufort High region (Figure 3.8) was analyzed. In July (Figure 3.8b), the regional MSLP is decreasing or rather the high is weakening while it is strengthening in the other months of the summer (Figure 3.8a,c). These intra-seasonal differences in trends in the atmospheric circulation highlight the seasonal nature of climate variability and change in this region.

High pressure during the summer is usually correlated with clear sky conditions, which can result in warm temperatures at the surface in Alaska especially outside of winter (Bieniek et al. 2011). Increased cloud cover consistent with a weakened Beaufort High in July could be a plausible explanation for the midsummer decline in temperatures

observed in Figures 3.3b and 3.4b. Observed cloud cover at Barrow and Kotzebue (Figure 3.9a-b) show that both stations climatologically receive their greatest amount of seasonal cloud cover during the period April through October. At Barrow, the peak increase in cloudiness is occurring March and October, preceding and concurrent with the times of year when the sea ice concentration has declined the most in June and October respectively (compare Figures 3.3a and 3.4a with Figure 3.9a). Barrow monthly station cloudiness was negatively correlated with the concurrent monthly MSLP of the Beaufort High and the highest correlation occurs in July (Table 3.2). Therefore, the July Beaufort High is linked with cloudiness at Barrow. This linkage suggests that the increase in July cloudiness at Barrow could be related to the weakened Beaufort High. The increase in cloudiness could also be a result of increased open water and the subsequent increased moisture availability, which is consistent with observed reduction of temperatures in July. Recent work supports this notion, Liu et al. (2012b) documented that MODIS cloud cover has increased over the Arctic Ocean in areas where sea ice has declined.

The Beaufort High is also significantly correlated with TI-NDVI and maxNDVI in both the Beaufort and Chukchi tundra regions (Table 3.2). These correlations however switch sign between June and July. In June, a stronger Beaufort High is linked with higher maxNDVI. Stronger high pressure reduces cloudiness and is consistent with the negative correlations between cloudiness at Barrow and the Beaufort High. Reduced cloudiness results in increased solar insolation, warmer land surface temperatures, and increased plant growth as manifest by the increased maxNDVI. The July Beaufort High is negatively correlated with TI-NDVI in both regions and appears to be perplexing as

higher pressure is generally thought to be linked with warmer temperatures and increased plant growth as found in June. However, the state of vegetation is integrated over the climate conditions over many years, therefore a rapid response in NDVI to changes in temperature may not be expected. Possible links between the Beaufort High, temperature, and NDVI will be discussed further later in this section.

The summer climate of the northern coastal regions of the Beaufort and East Chukchi regions is strongly influenced by the position of the Arctic frontal boundary, which marks the boundary between cold air mass of the Arctic Ocean and the relatively warmer air mass of Interior Alaska (Conover 1960). These regions consistently experience sea breezes in summer (Moritz 1977; Walsh 1977; Kozo 1979). Sea breezes are the result of the land-sea temperature contrast. The air over the land, warmed due to solar heating of the surface, rises and the relatively cooler air over the ocean moves in underneath resulting in wind blowing from the water towards the land. These sea breezes have a great influence on the spatial patterns of temperatures during the warm season in this region (Haugen and Brown 1980; Kozo 1982a) due to their control the position of the Arctic Frontal boundary. Temperatures farther inland near the Brooks Range tend to be more influenced by the amount of cloudiness than the sea breeze since as the sea breeze usually does not extend so far inland from the coast (Zhang et al. 1996). The strength of the sea breeze of the Beaufort region has also been shown to be related to the ambient synoptic flow and was found to occur even when the large-scale flow is counter to the direction of the sea breeze circulation (Kozo 1982b). Many of these previous studies have suggested that changes in the position, strength or extent of the sea breeze in this region

can greatly impact summer temperatures and, moreover, that the sea breeze is itself linked to the distribution of land-sea temperatures.

A trend to increasing winds has been documented near the coast over the Beaufort Sea in the summer months since 1979 (Stegall and Zhang 2012). Correlation analysis of the winds with respect to land surface temperatures and NDVI revealed a maximum in correlation with the areas of increasing wind speed trends (not shown). Stronger winds near the coast occur when the temperatures over land are increased. This is consistent with a strengthened sea breeze when the land surface is warmer. Changes in the position of the sea breeze, and Beaufort High appear to both be complimentary and interacting to result in change of the climate of the Beaufort and East Chukchi regions which allows for the overall increase in SWI and NDVI.

Curiously, decreasing temperatures were noted in Figures 3.3b and 3.4b in late June and July. Trend analysis based on a 15-year moving window since 1982 based on the weekly land surface temperature showed that a switch to declining midsummer temperatures has started to occur within the last part of the record (not shown). Analysis of the station temperature observations (not shown) display a similar declining trend in daily maximum temperatures, which are often linked to daytime solar heating, cloudiness, daytime convection, and the sea breeze circulation (which is at its maximum strength during the day). A declining trend was not found in minimum temperatures, which are not linked with the sea breeze circulation, solar insolation, and convection.

The decline in midsummer land surface and daily maximum temperatures also coincides with the declining July trends in the Beaufort High strength. Several possible

hypotheses may explain this phenomenon. Since the sea breeze is strongly linked with the land-sea temperature contrast, strong positive temperature anomalies over land may be driving a deeper penetration of the sea breeze in July and would result in the cooling of land-surface temperatures. Changes in the temperature anomalies over the now increasingly ice free Beaufort Sea also likely play a role in position and strength of the sea breeze.

Another possible hypothesis may be partially due to the plants themselves. An increase in vegetation results in increased evapotranspiration, which enhances the amount of moisture available in the lower atmosphere, and when coupled with warmer surface temperatures, the atmospheric response could be an increase in convection. Increased convection would have the effect of cooling the land surface through increased precipitation and cloudiness blocking solar insulation. As surface temperatures are warming in June and cooling in July, this mechanism may initiate in June, but the maxNDVI does not occur until July so convection is delayed until July when more surface moisture is available for convection. Cooling of the land surface temperatures would have the effect of reducing the sea breeze circulation (the land-sea temperature contrast would be reduced), which forms part of the subsidence supporting the Beaufort High, resulting in the observed reduction in sea level pressure in this region. A general circulation model (GCM) experiment showed that when Arctic tundra vegetation related albedo is increased the response is increased convection and cloud cover, which reduces surface temperatures in the region (Pai Mazumder and Mölders 2009). Increased vegetation was also found to modify the atmospheric pressure fields through the albedo-

convection-cloudiness mechanism that appears to support such a hypothesis. Modification of the sea breeze circulation can also result from changes in the spatial distribution of temperatures of the Arctic Ocean. The observed changes in sea ice and ocean heat content may also play an important role in the changes of the local circulation that is impacting the climate and so NDVI of the Beaufort and East Chukchi tundra regions.

3.3.2 East Bering

The East Bering tundra region is located entirely within Alaska's west coast climate division (Bieniek et al. 2012). This region experiences more precipitation and also warmer temperatures in summer than the Beaufort and Chukchi regions (Shulski and Wendler 2007). This region is also located in close proximity to the Bering Sea storm tracks and Aleutian Low, but these are almost absent in summer (Rodionov et al. 2007; Mesquita et al. 2010).

The Bering Sea is generally free of sea ice in summer (Figure 3.10b), however sea ice is declining in May and October (Figure 3.11a). In contrast to the Beaufort and East Chukchi regions is that the spring sea ice concentration is increasing (Figure 3.11a) and there is an overall decline in ocean heat content (Figure 3.5c). NDVI in the East Bering coastal tundra region is declining while summer temperatures are warming (Figure 3.10). Similar to the Beaufort and East Chukchi regions, temperatures are increasing in early and late summer, but are declining in midsummer (Figure 3.11b). The decline in NDVI is greatest in the beginning of the season (Figure 3.11c). These conflicting trends suggest

that a different mechanism is driving the change in NDVI in the East Bering than in northern Alaska.

Local expert knowledge from Native Alaskan elders in the East Bering region has suggested that changes in the characteristics of snow cover, including reduced snow depth and snow water equivalent are occurring (e.g. Fienup-Riordan and Rearden 2012). Declines in snow depth and snow water equivalent may lead to decreased moisture available for the vegetation and may thus drive the declines in NDVI in the East Bering tundra region. Alaska Native elders have indicated that the timing of the berry harvest is occurring earlier within their memory and that the harvest is less plentiful when the winter snow depth is reduced (Fienup-Riordan and Rearden 2012). Overall there appears to be a link between vegetation and the winter snow regime in the East Bering region.

The snow cover melts on average in early May in the East Bering region. There is a trend towards later snowmelt at Bethel (1982-2011) and in the MODIS (2000-2011) snow cover data (Figure 3.6). Close inspection of the spatial MODIS snowmelt date trends shows that the recent declining trend was mixed over the region and snow is even melting earlier over the Seward Peninsula. Early season May-June average maxNDVI and TI-NDVI are both significantly correlated with melt date and total season maxNDVI is reduced when snowmelt occurs later (Table 3.1). Therefore, since snowmelt is a factor in determining the onset of the growing season, the longer snow duration acts to reduce TI-NDVI. The trend to later snowmelt is likely playing an important role in the NDVI browning in this region, especially the declining NDVI in the early season.

The West Pacific (WP) Pattern is a mode of atmospheric variability in the Pacific that influences the strength of a trough or low pressure in the atmospheric circulation centered over the Bering Sea (Wallace and Gutzler 1981). Increased sea ice in the eastern Bering Sea region has been linked with the positive phase of the West Pacific (WP) Pattern (Matthewman and Magnusdottir 2011). The positive phase of the WP represents a strengthening of the low pressure over the Bering Sea region. Low pressure, while advecting moisture from the Pacific, also brings clouds that reduce temperatures and increase precipitation in the spring in Alaska (Bieniek et al. 2011). More frequent positive phases of the WP pattern since the 1980s (Linkin and Nigam 2008) may be driving the increases in spring sea ice and the trend to later snow melt in the East Bering region. Bieniek et al. 2011 had previously found a trend to earlier river ice breakup date on the Kuskokwim River at Bethel (which is located within the southern portion of the region) and locations throughout the state. Bieniek et al. (2011) showed that early breakup date is tied in part to both an earlier snowmelt and a reduction in the number of storms tracking into the Gulf of Alaska. The trend to delayed snowmelt due to late season snowfall in the East Bering region is consistent with increased cloud cover, precipitation and reduced temperatures brought about by low pressure over the Bering Sea enhanced by the WP. Therefore, while other regions of Alaska (i.e. Beaufort and East Chukchi) are experiencing earlier snowmelt, possibly due to a reduction in Gulf of Alaska storms (i.e. Bieniek et al. 2011), the spring climate of the East Bering region may also be influenced by the WP related increase in low pressure over the Bering Sea resulting in a delayed onset of the summer.

End of winter snow water equivalent (SWE) based on the remotely sensed SSM/I sensor has declined over its period of record (1987-2007) in the central portion of the Bering region (Figure 3.12). This decline agrees with the Bethel station snow depth when calculated over the same period as the SSM/I SWE, however Bethel (Figure 3.12b) is experiencing a trend to slightly increased snow later in the season over a longer record. Care must be taken when examining trends due to the inherent large interannual-decadal-multidecadal variability in the Arctic (Polyakov et al. 2012). The increase in spring snow depth at Bethel is also consistent with the later snowmelt being observed. In northern Alaska, while only weakly correlated with NDVI, SWE is increasing.

Monthly area average SWE was separated into two regions for further analysis: the Seward Peninsula, were spring SWE has increased, and the East Bering lowlands including the Yukon Delta (excluding the mountains in the southern portion of the region). SWE peaks in February-March with an average amount in the range of 45-50mm on the Seward Peninsula (Figure 3.13b) and around 40mm in the East Bering lowlands (Figure 3.13a). Climatologically, SWE starts increasing from September until February-March and then the amount quickly decreases in April and May until the start of the growing season. SWE displays decreasing trends throughout much of the winter season with declines in all months except for February-March. The maxNDVI is significantly correlated (0.45) with January and February SWE in the East Bering lowlands. This suggests that less midwinter snow depth is linked to reduced maxNDVI in summer. The trend towards reduced maxNDVI is consistent with reduced snow depth in fall and winter in the Bering region. Reduced winter snow can result in less water available for plants;

this coupled with the warm summer temperatures will stress the plants and hinder their productivity. The reduced late winter SWE appears to result from the reduction in snow in the autumn, as it appears to be propagating forward and plays a role in the reduced SWE later in the season. However, caution needs to be used when interpreting SWE as it is an integrative quantity of the preceding months and more robust winter precipitation data at higher temporal and spatial scales, when made available, may be needed in future to finalize any conclusions concerning the role of winter snow depth and NDVI.

While located geographically much further away from the Beaufort High than the Beaufort and Chukchi zones, the strength of the Jul-Aug Beaufort High is significantly correlated with the Bering TI-NDVI and Bethel June cloudiness (Table 3.2). An increased Beaufort High results in reduced TI-NDVI in this region and increased cloud cover. This highlights two possibilities: the large geographic area over which the Beaufort High exerts its influence in Alaska during summer, or that a completely separate process impacting both may be at work.

3.4 Conclusions

NDVI in the Beaufort and East Chukchi tundra regions in northern Alaska is increasing (greening) and in contrast declining (browning) in the East Bering tundra region in southwest Alaska. The intra-seasonal trends in the Beaufort region indicate an overall increase in NDVI while the East Chukchi was more varied with a slight decline earlier in the season. In the East Bering, NDVI is declining throughout the growing season with the greatest declines early in the season. The summaries of the climate

drivers of NDVI in the three Alaska coastal tundra regions are shown in Figure 3.14. The early season trends in all three regions were significantly linked with the timing of snowmelt in the respective region. An earlier snowmelt as in the Beaufort and East Chukchi regions coincides with increased TI-NDVI. The trend towards a delayed melt in the East Bering region may largely explain the decline in TI-NDVI in that region. The delay in snowmelt may be coupled with an increasing occurrence of the positive phase of the West Pacific (WP) Pattern, which has been previously linked with increased sea ice concentration over the eastern Bering Sea. The TI-NDVI decline in the Bering region is also linked with reduced winter and spring SWE.

The increases in TI-NDVI and maxNDVI in northern Alaska were also linked with the changes in temperature. The Beaufort High was found to play an important role in NDVI because of its control of cloud cover and temperatures in the Beaufort and Chukchi regions. An increased Beaufort High in June is linked with increased temperatures and vegetation productivity. This relationship is plausible since the strengthened Beaufort High reduces cloudiness, especially inland from the coast, allowing for increased solar insolation and surface warming. There is also an indication that changes in the local sea breeze may be linked with the temperature trends in the Beaufort and East Chukchi regions as there is a trend to increased winds near the Beaufort Sea coast (Stegall and Zhang 2012). The Beaufort High is negatively correlated with TI-NDVI in July when there are declining trends in temperatures in late June and July in this region. Several possible explanations exist for this relationship and these trends, one being a feedback between the increased vegetation and the atmosphere.

Increased vegetation has been found to increase convection and cloudiness resulting in land surface cooling in the Arctic based on a GCM study that imposed increased surface albedoes in the Arctic (Pai Mazumder and Mölders 2009). This process can change the atmospheric pressure fields, which could be playing a role in this case. Such a relationship implies that a complex climate process relating winter snowmelt, and the summer atmospheric circulation are resulting in NDVI change in northern Alaska.

The results of this study demonstrate that the linkages between satellite observed NDVI and climate are complex and vary sub-seasonally. NDVI is unique in that it represents plants that respond to climate over the course of many years adding to the complexity and even the possibility that the plants themselves may impact the course of changes in the climate system. Such a coupled feedback may be at work in the Arctic. Higher spatial and temporal resolution NDVI time series, as well as model studies, will be necessary to fully diagnose linkages between the landscape and the greater atmosphere-climate system.

Acknowledgements

The authors would like to thank Jim Overland, Ann Fienup-Riordan, Alice Reardon, Matthew Sturm, Torre Jorgenson, and the members of the Calista Elders Council for their fruitful discussion that have improved this research. This study was supported by funds from NSF grants ARC-051180, ARC-0902175, and NASA grant NNG6NEA00A.

References

ACIA, 2005: *Arctic climate impact assessment.* Cambridge University Press, 1042 pp.

Armstrong, R. L., M. J. Brodzik, K. Knowles, and M. Savoie, 2007: *Global Monthly EASE-Grid Snow Water Equivalent Climatology.* Boulder, Colorado USA: National Snow and Ice Data Center. Digital media.

Bekryaev, R. V., I. V. Polyakov, and V. A. Alexeev, 2010: Role of polar amplification in long-term surface air temperature variations and modern Arctic warming. *J Climate*, **23,** 3888-3906.

Bhatt, U. S., M. A. Alexander, C. Deser, J. E.Walsh, J. S. Miller, M. Timlin, J. D. Scott, and R. Tomas, 2008: *The Atmospheric Response to Realistic Reduced Summer Arctic Sea Ice Anomalies*, in Arctic Sea Ice Decline: Observations, Projections, Mechanisms, and Implications, *Geophys. Monogr. Ser.*, vol. 180, edited by E. T. DeWeaver, C. M. Bitz, and L. B. Tremblay, pp. 91-110, AGU, Washington, D. C.

Bhatt, U. S., and Coauthors, 2010: Circumpolar Arctic tundra vegetation change is linked to sea ice decline. *Earth Interact*, **14,** doi:10.1175/2010E1315.1.

Bieniek, P. A., U. S. Bhatt, L. A. Rundquist, S. D. Lindsey, and X. D. Zhang, 2011: Large-Scale Climate Controls of Interior Alaska River Ice Breakup. *J Climate*, **24,** 286-297.

Bieniek, P., and Coauthors, 2012: Climate divisions for Alaska based on objective methods. *J Appl Meteor Climatol*, doi:10.1175/JAMC-D-11-0168.1, in press.

Comiso, J. C., 2003: Warming trends in the Arctic from clear sky satellite observations. *J Climate*, **16,** 3498-3510.

Comiso, J. C., and F. Nishio, 2008: Trends in the sea ice cover using enhanced and compatible AMSR-E, SSM/I, and SMMR data. *J Geophys Res-Oceans*, **113**, C02S07, doi:10.1029/2007JC004257.

Conover, J. H., 1960: Macro- and microclimatology of the Arctic Slope of Alaska. *U.S. Army Headquarters Quartermaster Research and Engineering Command, Natick, Massachusetts, Technical Report*, EP-139. 65 pp.

Deering, D. W., 1978: *Rangeland reflectance characteristics measured by aircraft and spacecraft sensors*. Ph.D. dissertation, Texas A&M University, 338 pp.

Duffy, P. A., J. E. Walsh, J. M. Graham, D. H. Mann, and T. S. Rupp, 2005: Impacts of large-scale atmospheric-ocean variability on Alaskan fire season severity. *Ecol Appl*, **15,** 1317-1330.

Epstein, H. E., and Coauthors, 2004: The nature of spatial transitions in the Arctic. *J Biogeogr*, **31,** 1917-1933.

Fienup-Riordan, A., and A. Rearden, 2012: *Ellavut Our Yup'ik World and Weather.* University of Washington Press, 354 pp.

Goetz, S. J., A. G. Bunn, G. J. Fiske, and R. A. Houghton, 2005: Satellite-observed photosynthetic trends across boreal North America associated with climate and fire disturbance. *P Natl Acad Sci USA*, **102,** 13521-13525.

Hall, D. K., G. A. Riggs, and V. V. Salomonson, 2006: *MODIS/Terra Snow Cover 8-Day L3 Global 0.05deg CMG V005*, [retrieved March 23, 2012]. Boulder, Colorado USA: National Snow and Ice Data Center. Digital media.

Haugen, R. K., and J. Brown, 1980: Coastal-inland distributions of summer air-temperature and precipitation in northern Alaska. *Arctic Alpine Res*, **12,** 403-412.

Hess, J. C., C. A. Scott, G. L. Hufford, and M. D. Fleming, 2001: El Niño and its impact on fire weather conditions in Alaska. *Int J Wildland Fire*, **10,** 1-13.

Higgins, M., and J. Cassano, 2011: Northern Alaskan land surface response to reduced Arctic sea ice extent. *Clim Dynam*, **38,** 2099-2113.

Jia, G. S. J., H. E. Epstein, and D. A. Walker, 2003: Greening of arctic Alaska, 1981-2001. *Geophys Res Lett*, **30.**

Jonsson, P., and L. Eklundh, 2002: Seasonality extraction by function fitting to time-series of satellite sensor data. *IEEE T Geosci Remote*, **40,** 1824-1832.

Kalnay, E., and Coauthors, 1996: The NCEP/NCAR 40-year reanalysis project. *B Am Meteorol Soc*, **77,** 437-471.

Kozo, T. L., 1979: Evidence for sea breezes on the Alaskan Beaufort Sea coast. *Geophys Res Lett*, **6,** 849-852.

Kozo, T. L., 1982a: An Observational Study of Sea Breezes Along the Alaskan Beaufort Sea Coast .1. *J Appl Meteorol*, **21,** 891-905.

Kozo, T. L., 1982b: A Mathematical-Model of Sea Breezes Along the Alaskan Beaufort Sea Coast .2. *J Appl Meteorol*, **21,** 906-924.

Lawrence, D. M., A. G. Slater, R. A. Tomas, M. M. Holland, and C. Deser, 2008: Accelerated Arctic land warming and permafrost degradation during rapid sea ice loss. *Geophys Res Lett*, **35**.

Linkin, M. E., and S. Nigam, 2008: The north pacific oscillation-west Pacific teleconnection pattern: mature-phase structure and winter impacts. *J Climate*, **21**, 1979-1997.

Liston, G. E., and C. A. Hiemstra, 2011: The changing cryosphere: pan-Arctic snow trends (1979-2009). *J Climate*, **24**, 5691-5712.

Liu, J. P., J. A. Curry, H. J. Wang, M. R. Song, and R. M. Horton, 2012a: Impact of declining Arctic sea ice on winter snowfall. *P Natl Acad Sci USA*, **109**, 4074-4079.

Liu, Y. H., J. R. Key, Z. Y. Liu, X. J. Wang, and S. J. Vavrus, 2012b: A cloudier Arctic expected with diminishing sea ice. *Geophys Res Lett*, **39**.

Manabe, S., J. Ploshay, and N. C. Lau, 2011: Seasonal variation of surface temperature change during the last several decades. *J Climate*, **24**, 3817-3821.

Matthewman, N. J., and G. Magnusdottir, 2011: Observed Interaction between Pacific Sea Ice and the Western Pacific Pattern on Intraseasonal Time Scales. *J Climate*, **24**, 5031-5042.

Mesquita, M. D. S., D. E. Atkinson, and K. I. Hodges, 2010: Characteristics and Variability of Storm Tracks in the North Pacific, Bering Sea, and Alaska. *J Climate*, **23**, 294-311.

Moritz, R. E., 1977: On a possible sea-breeze circulation near Barrow, Alaska. *Arctic Alpine Res*, 9, 427-431.

Muskett, R., 2012: Multi-Satellite and Sensor Derived Trends and Variation of Snow Water Equivalent on the High-Latitudes of the Northern Hemisphere. *International Journal of Geosciences*, **3**, 1-13.

Overland, J. E., 2009: Meteorology of the Beaufort Sea. *J Geophys Res-Oceans*, **114**, C00A07, doi:10.1029/2008JC004861.

Parent, M. B., and D. Verbyla, 2010: The Browning of Alaska's Boreal Forest. *Remote Sensing*, **2**, 2729-2747.

Pai Mazumder, D., and N. Mölders, 2009: Sensitivity of permafrost-vegetation-climate to summer albedo anomalies and increasing carbon dioxide. Report for CISL project 35011030.

Parent, M. B., and D. Verbyla, 2010: The Browning of Alaska's Boreal Forest. *Remote Sensing*, **2,** 2729-2747.

Pinzon, J. E. and Coauthors, 2012: Revised, continuously updated GIMMS3g (AVHRR NDVI) data from 1982 onward. *Remote Sensing* in prep.

Polyakov, I. V., U. S. Bhatt, J. E. Walsh, E. P. Abrahamsen, 2012: Recent oceanic changes in the Arctic in the context of longer term observations, *Ecological Applications*, in press.

Raynolds, M. K., D. A. Walker, H. E. Epstein, J. E. Pinzon, and C. J. Tucker, 2011: A new estimate of tundra-biome phytomass from trans-Arctic field data and AVHRR NDVI. *Remote Sensing Letters*, **3,** 403-411.

Rodionov, S. N., N. A. Bond, and J. E. Overland, 2007: The Aleutian Low, storm tracks, and winter climate variability in the Bering Sea. *Deep-Sea Research Part II-Topical Studies in Oceanography*, **54,** 2560-2577.

Saha, S., and Coauthors, 2006: The NCEP climate forecast system. *J Climate*, **19,** 3483-3517.

Serreze, M. C., and A. P. Barrett, 2011: Characteristics of the Beaufort Sea High. *J Climate*, **24,** 159-182.

Serreze, M. C., and R. G. Barry, 2011: Processes and impacts of Arctic amplification: A research synthesis. *Global Planet Change*, **77,** 85-96.

Sherriff, R. L., E. E. Berg, and A. E. Miller, 2011: Climate variability and spruce beetle (Dendroctonus rufipennis) outbreaks in south-central and southwest Alaska. *Ecology*, **92,** 1459-1470.

Shulski, M., and G. Wendler, 2007: *The climate of Alaska.* University of Alaska Press, 216 pp.

Steele, M., W. Ermold, and J. L. Zhang, 2011: Modeling the formation and fate of the near-surface temperature maximum in the Canadian Basin of the Arctic Ocean. *J Geophys Res-Oceans*, **116**. C11015, doi:10.1029/2010JC006803.

Stegall, S. T., and J. Zhang, 2012: Wind field climatology, changes, and extremes in the Chukchi/Beaufort Seas and Alaska North Slope during 1979-2009. *J Climate*. doi: 10.1175/JCLI-D-11-00532.1, in press.

Stone, R. S., E. G. Dutton, J. M. Harris, and D. Longenecker, 2002: Earlier spring snowmelt in northern Alaska as an indicator of climate change. *J Geophys Res-Atmos*, **107,** doi:10.1029/2000JD000286.

Sturm, M., C. Racine, and K. Tape, 2001: Climate change - Increasing shrub abundance in the Arctic. *Nature*, **411,** 546-547.

Tape, K., M. Sturm, and C. Racine, 2006: The evidence for shrub expansion in Northern Alaska and the Pan-Arctic. *Global Change Biol*, **12,** 686-702.

Treshnikov, A. F., 1985: *Atlas of the Arctic* (in Russian). Administrator of Geodesy and Cartography of the Soviet Ministry, 204 pp.

Tucker, C. J., 1979: Red and photographic infrared linear combinations for monitoring vegetation. *Remote Sensing of Environment*, **8**, 127-150.

Tucker, C. J., and P. J. Sellers, 1986: Satellite remote sensing of primary production. *Int J Remote Sens*, **7**, 1395-1416.

Verbyla, D., 2008: The greening and browning of Alaska based on 1982-2003 satellite data. *Global Ecol Biogeogr*, **17,** 547-555.

Walker, D. A., and Coauthors, 2003: Phytomass, LAI, and NDVI in northern Alaska: Relationships to summer warmth, soil pH, plant functional types, and extrapolation to the circumpolar Arctic. *J Geophys Res-Atmos*, **108.**

Walker, D. A., and Coauthors, 2005: The Circumpolar Arctic vegetation map. *J Veg Sci*, **16,** 267-282.

Wallace, J. M., and D. S. Gutzler, 1981: Teleconnections in the geopotential height field during Northern Hemisphere winter. *Mon Wea Rev,* **109**, 784–812.

Walsh, J. E., 1977: Measurements of the temperature, wind, and moisture distribution across the northern coast of Alaska. *Arctic Alpine Res*, **9,** 175-182.

Wood K. R., J. E. Overland, S. A. Salo, N. A. Bond, B. Williams, and X. Dong, 2012: A preview of the future Arctic emergin in the Beaufort Sea. *Nature Climate Change* submitted.

Yurtsev, B. A., 1994: Floristic Division of the Arctic. *J Veg Sci*, **5,** 765-776.

Zhang, T., T. E. Osterkamp, and K. Stamnes, 1996: Some characteristics of the climate in northern Alaska, USA. *Arctic Alpine Res*, **28,** 509-518.

Zhang, X. D., J. E. Walsh, J. Zhang, U. S. Bhatt, and M. Ikeda, 2004: Climatology and interannual variability of arctic cyclone activity: 1948-2002. *J Climate*, **17,** 2300-2317.

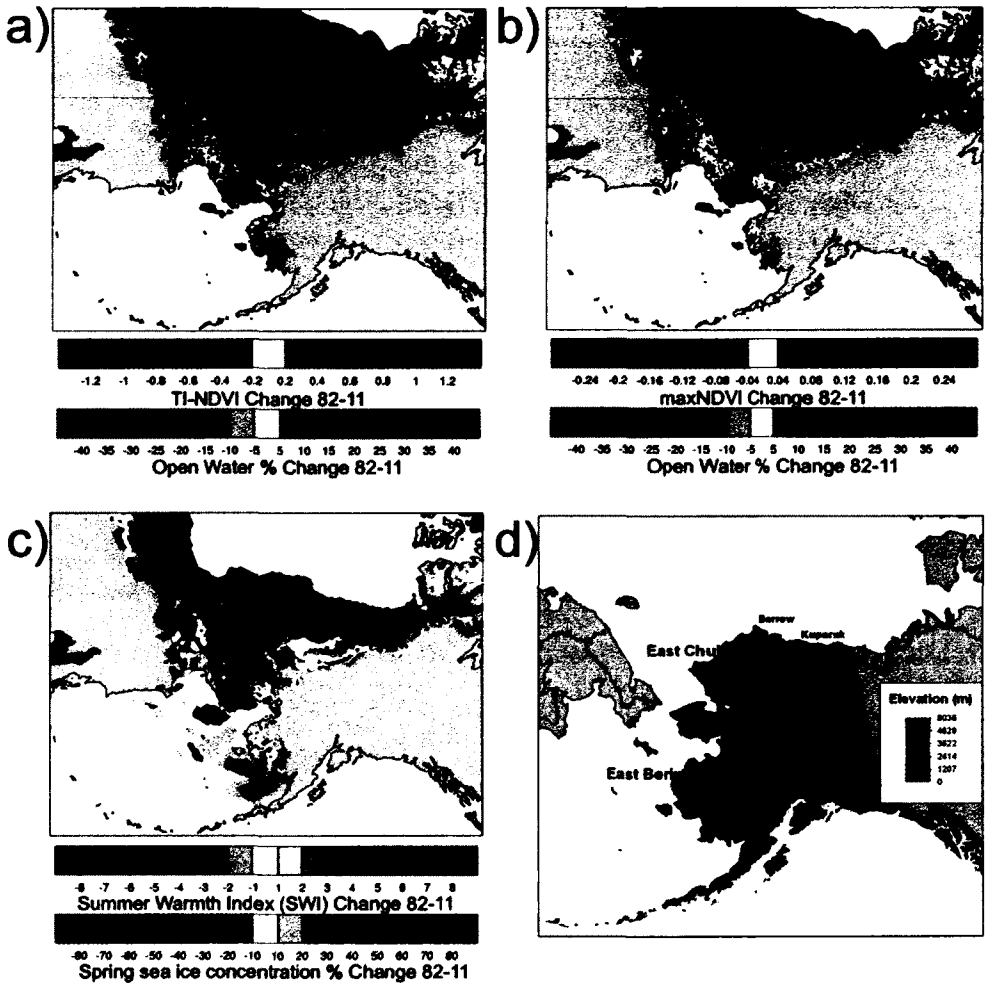

Figure 3.1. Magnitude change from 1982-2011 based on a linear trend of (a) time-integrated NDVI (TI-NDVI) and May-August open water (percent), (b) seasonal maximum NDVI (maxNDVI) and May-August open water (percent), (c) magnitude of change in sea ice break-up (as represented by 50% sea ice concentration) and summer warmth index, topographic features of Alaska and (d) the Treshnikov regions (black lines) along with weather observation stations used in this study. TI-NDVI and maxNDVI increased in the Beaufort and Chukchi regions and decreased in the Bering. SWI increased, except in area of the Beaufort and Bering regions. Sea ice declined in spring and summer. Area average trends have been found to be significant at the 95% or greater level in Alaska for maxNDVI. TI-NDVI, and open water (see Figures 3.2 and 3.10).

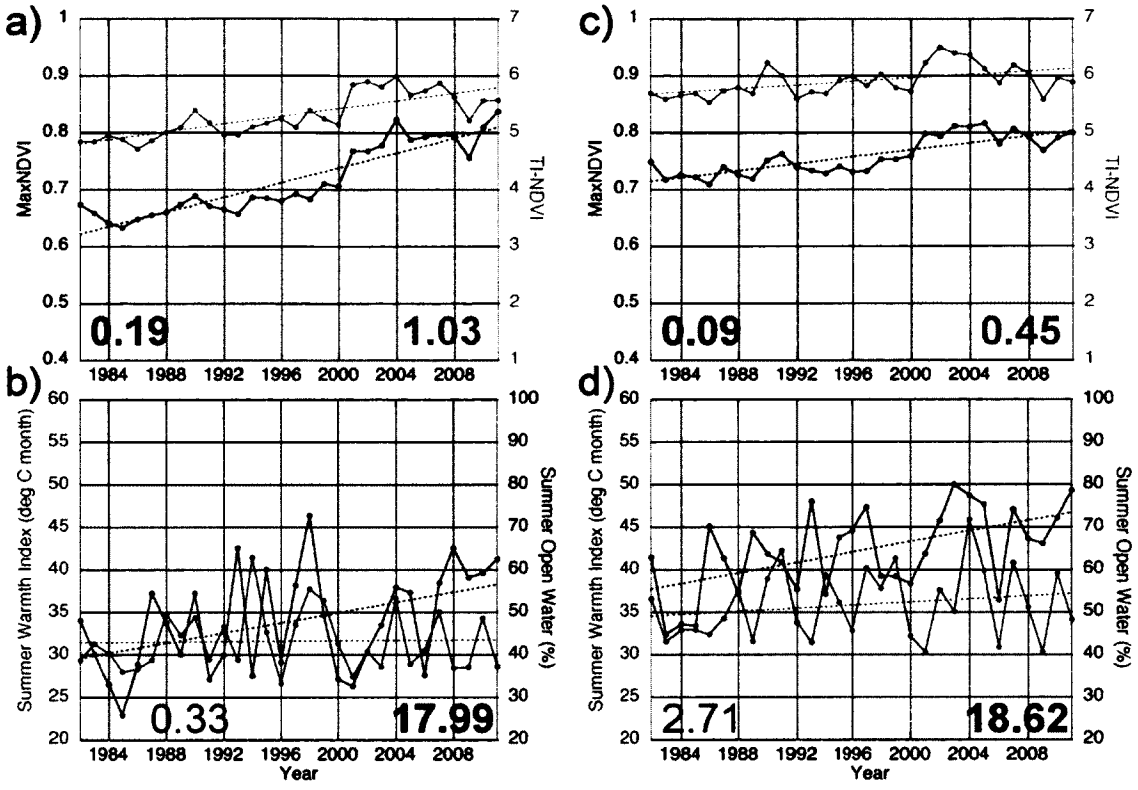

Figure 3.2 Full tundra TI-NDVI and maxNDVI, summer warmth index and 100km open water for Beaufort (a,b) and East Chukchi (c,d) tundra regions. TI-NDVI, maxNDVI, SWI and open water are all increasing in both tundra regions. The magnitude change is based on a linear trend for each variable from 1982 to 2011 and is shown by the colored numbers, where trends significant at the 95% (90%) level greater are bold (italic). The units of the trends are unitless per 30 years for maxNDVI and TI-NDVI, °C month per 30 years for SWI and percent cover per 30 years for open water.

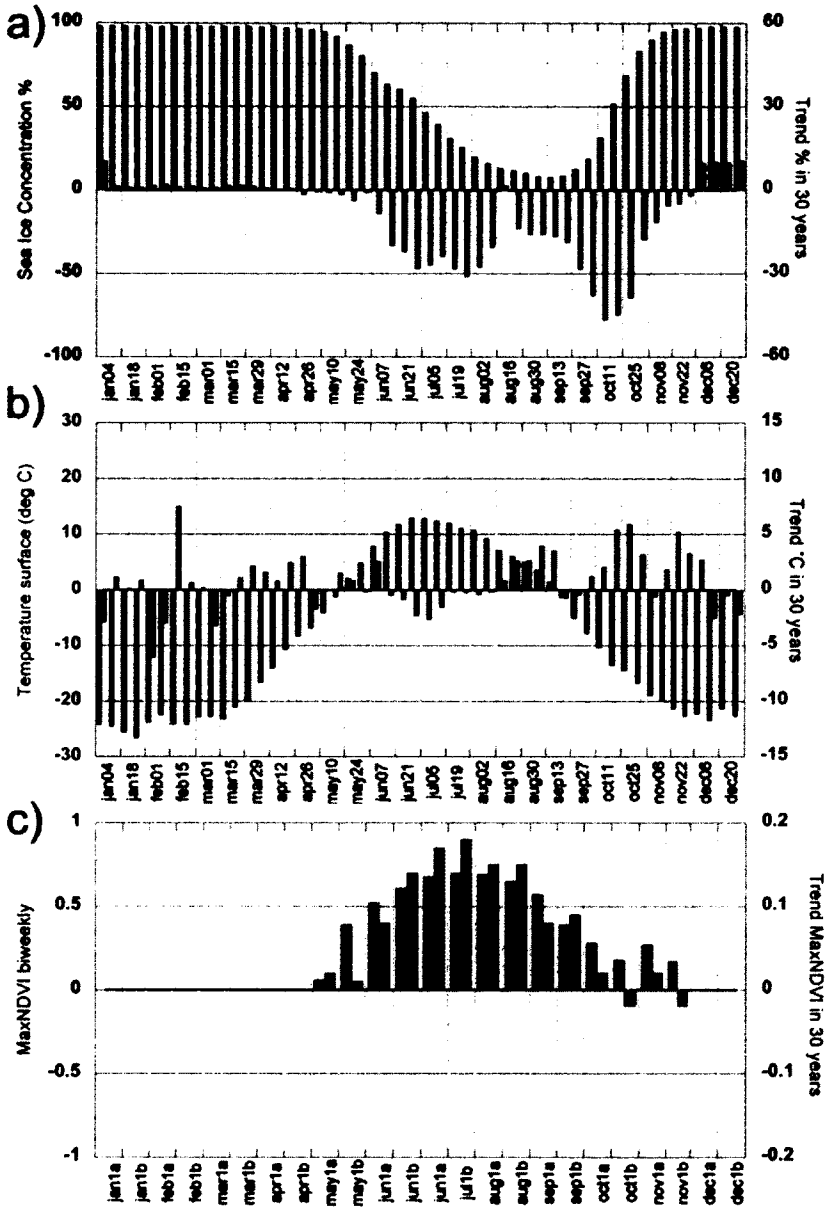

Figure 3.3. Beaufort tundra region long-term mean and weekly magnitude change from 1982-2011 in (a) 100km sea ice concentration, (b) surface temperature and (c) bi-weekly NDVI. Trends are shown in gray. Sea ice is declining most in June and October, with lesser reductions throughout the summer. Surface temperature has mixed trends throughout the year with increasing temperatures in summer in May and August and declines in late June and July. NDVI is increasing throughout the summer with the greatest increases during the peak of the growing season.

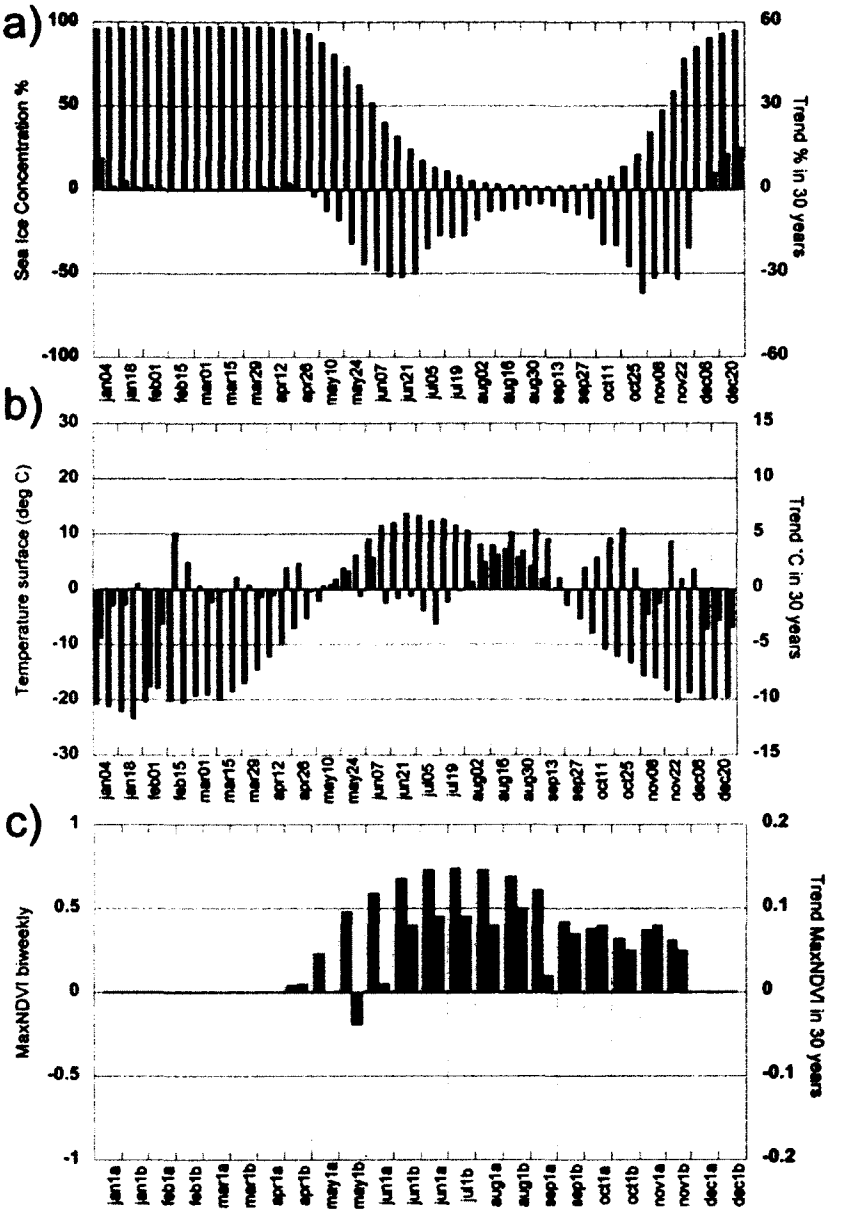

Figure 3.4 East Chukchi tundra region long-term mean and weekly magnitude change from 1982-2011 in (a) 100km sea ice concentration, (b) surface temperature and (c) bi-weekly NDVI. Trends are shown in gray. Sea ice is declining most in early June and late October, with small declines throughout the summer. Surface temperature has mixed trends throughout the year with increasing temperatures in summer in May and August-September and declines in late June and July. NDVI is increasing uniformly from late June until November, small or decreasing trends are occurring in May.

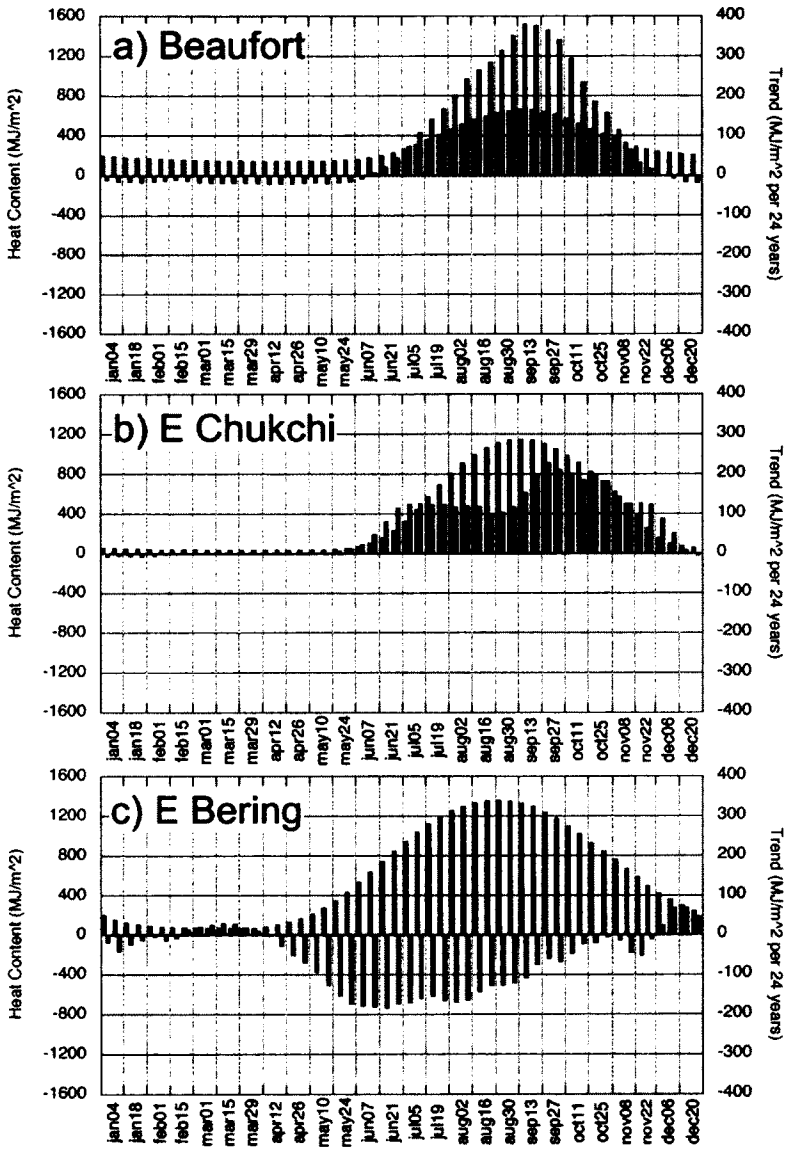

Figure 3.5 Weekly total column ocean heat content climatology and trend magnitude (1988-2011) for the (a) Beaufort, (b) East Chukchi, and (c) East Bering 100km zones. Heat content is increasing in Beaufort and East Chukchi while it is declining in the East Bering. This consistent with the weekly trends in sea ice concentration in each zone.

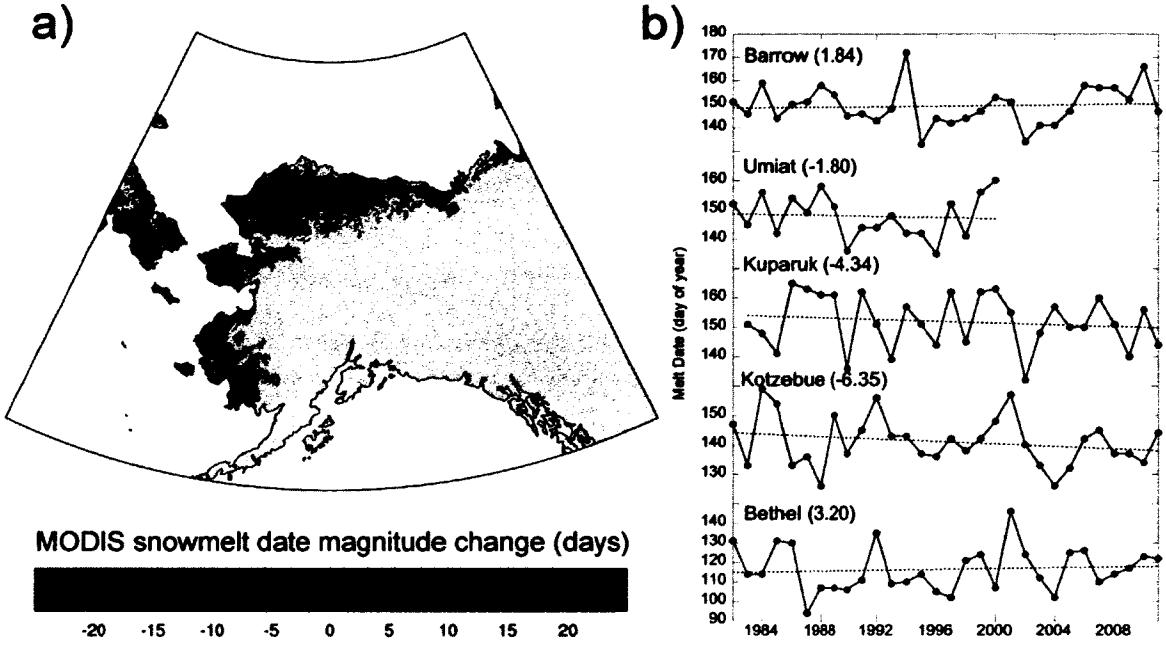

Figure 3.6. Snowmelt date magnitude change in days (2000-2011) derived from the MODIS Terra 8-day snow cover data set (a) and station snowmelt date time series (b). MODIS snowmelt was defined as the 8-day period when snow cover remained less than 5% for the summer. Station snowmelt date is defined as day when snow depth remained less than 2.54cm (1 inch) for the summer. The numbers in parentheses in (b) show the magnitude change (units of days) based on a linear trend for each station for the number of years observed since 1982, where trends significant at the 95% (90%) level greater are bold (italic). Snowmelt is generally occurring earlier across northern Alaska (except Barrow) and occurring generally later in the southwest. Long-term trends at the stations are in agreement with the short-term trends in MODIS.

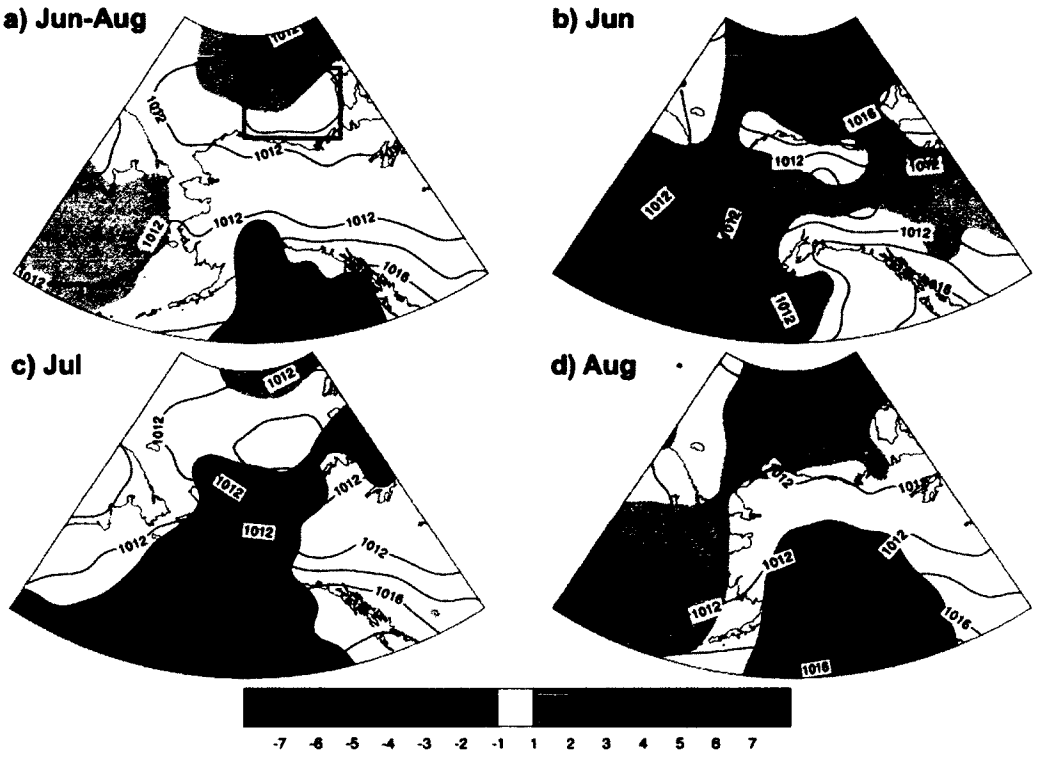

Figure 3.7. Mean sea level pressure climatology (contour) and magnitude change (shaded) over period 1982-2009 for (a) June-August, (b) June, (c) July, and (d) August. Units are hPa. The Beaufort High has been strengthening throughout the summer in all months except in July. The climatological center of the Beaufort High is located in purple box in panel a during Jun-Aug.

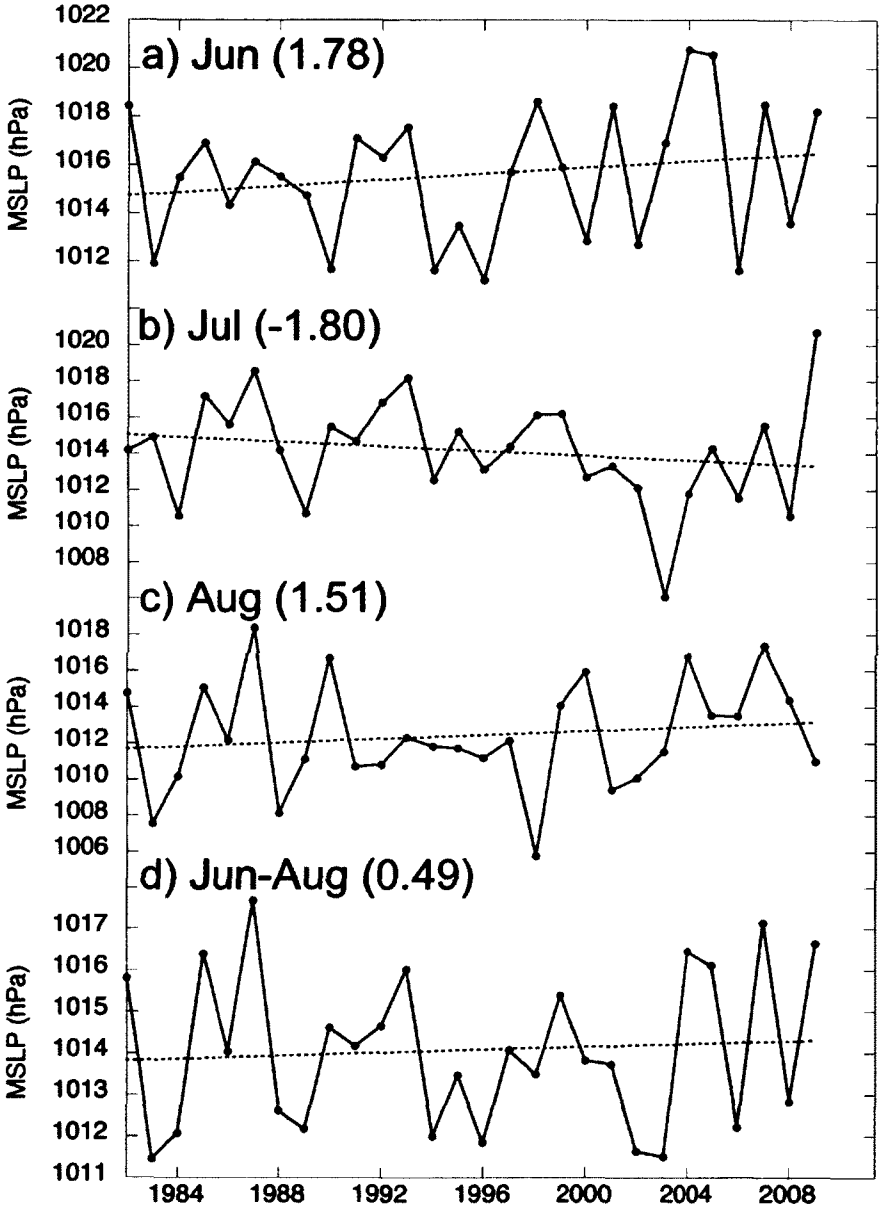

Figure 3.8. Beaufort High (BH) area average mean sea level pressure (MSLP) for (a) June, (b) July, (c) August, and (d) June-August. The box defining the BH is shown in figure 4.6a (160-135°E, 70-76°N). The BH is strengthening in June and August, and weakening in July. The numbers in parentheses show the magnitude change (units of hPa) based on a linear trend for each variable from 1982 to 2009, where trends significant at the 95% (90%) level greater are bold (italic).

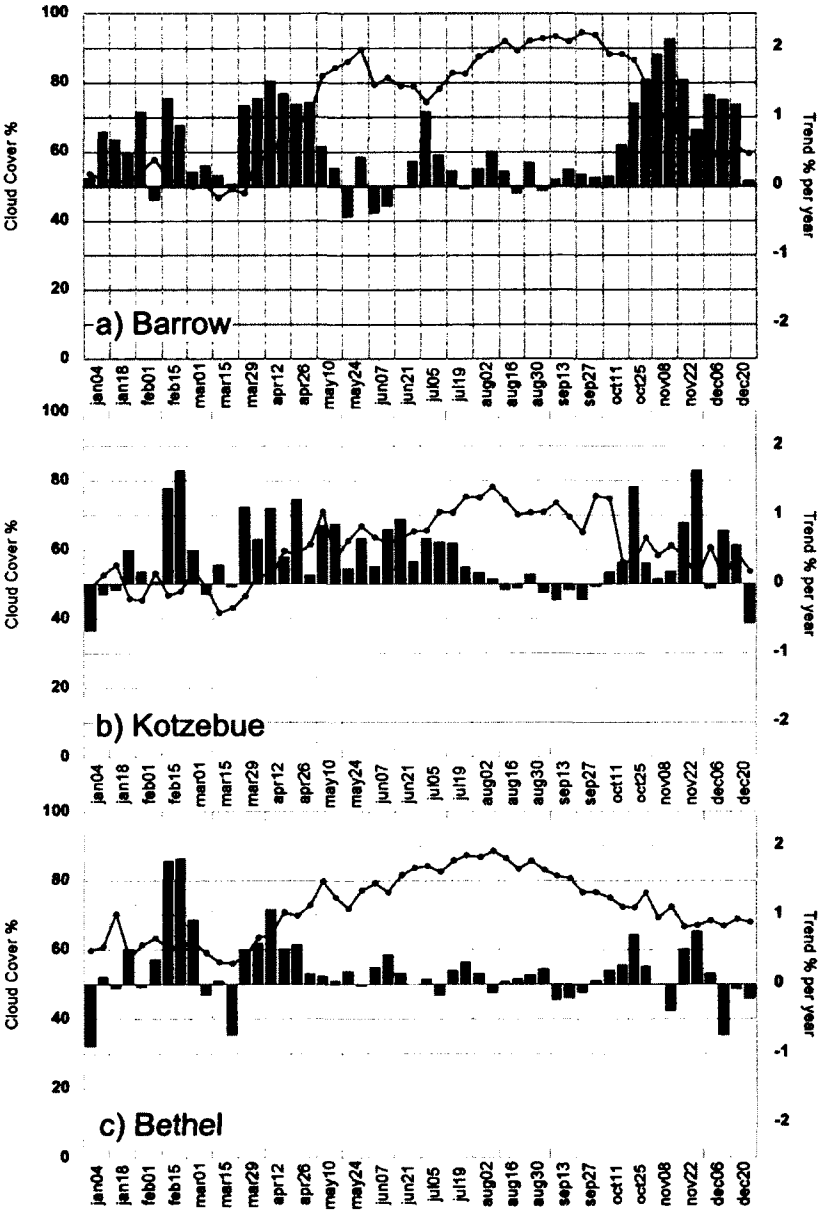

Figure 3.9. Weekly station long-term (1982-2011) average cloudiness percent (blue lines) and trend (gray bars) at (a) Barrow, (b) Kotzebue, and (c) Bethel. All three stations experience their maximum cloudiness in summer. Trends are fairly small in the summer compared with the transition times when the climatological cloudiness is either increasing or decreasing.

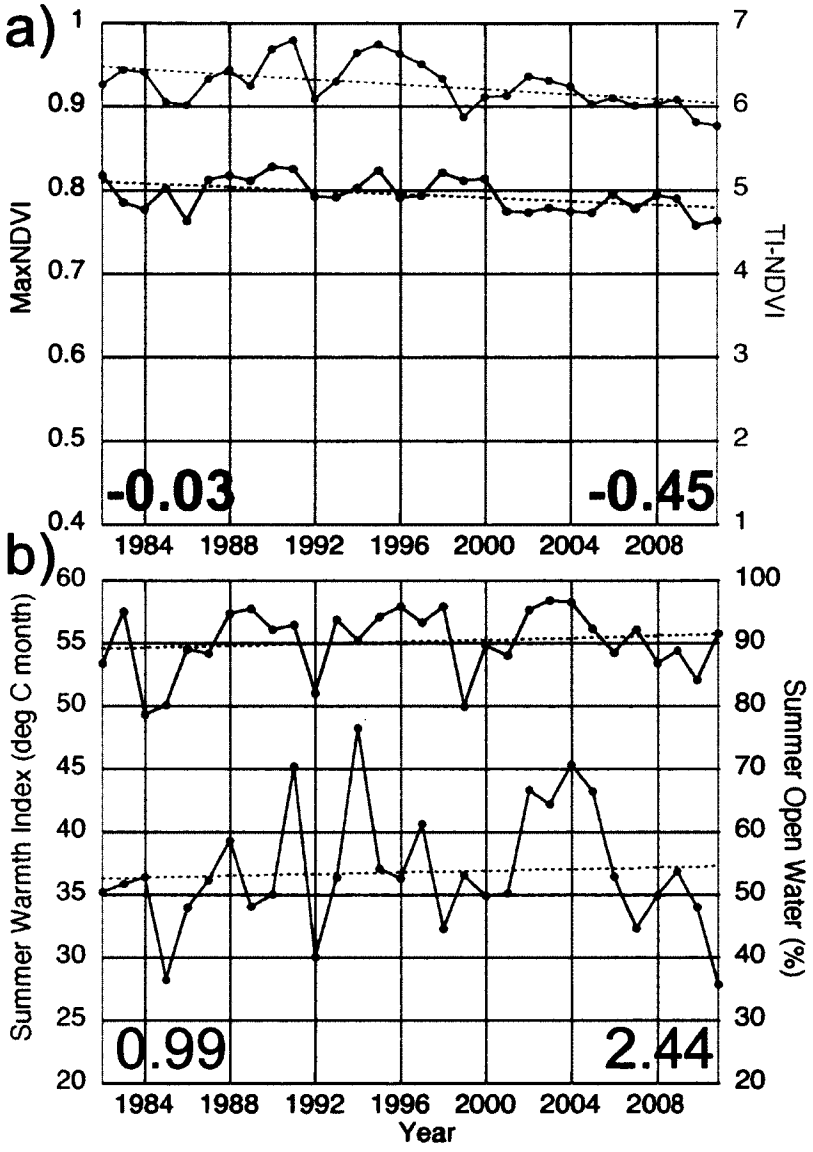

Figure 3.10 Time series for East Bering full tundra (a) TI-NDVI and maxNDVI, (b) summer warmth index and open water. TI-NDVI and maxNDVI are declining, while SWI and open water are all increasing. The magnitude change based on a linear trend for each variable from 1982 to 2011 is shown by the colored numbers, where trends significant at the 95% (90%) level greater are bold (italic). The units of the trends are unitless per 30 years for maxNDVI and TI-NDVI, °C month per 30 years for SWI and % per 30 years for open water.

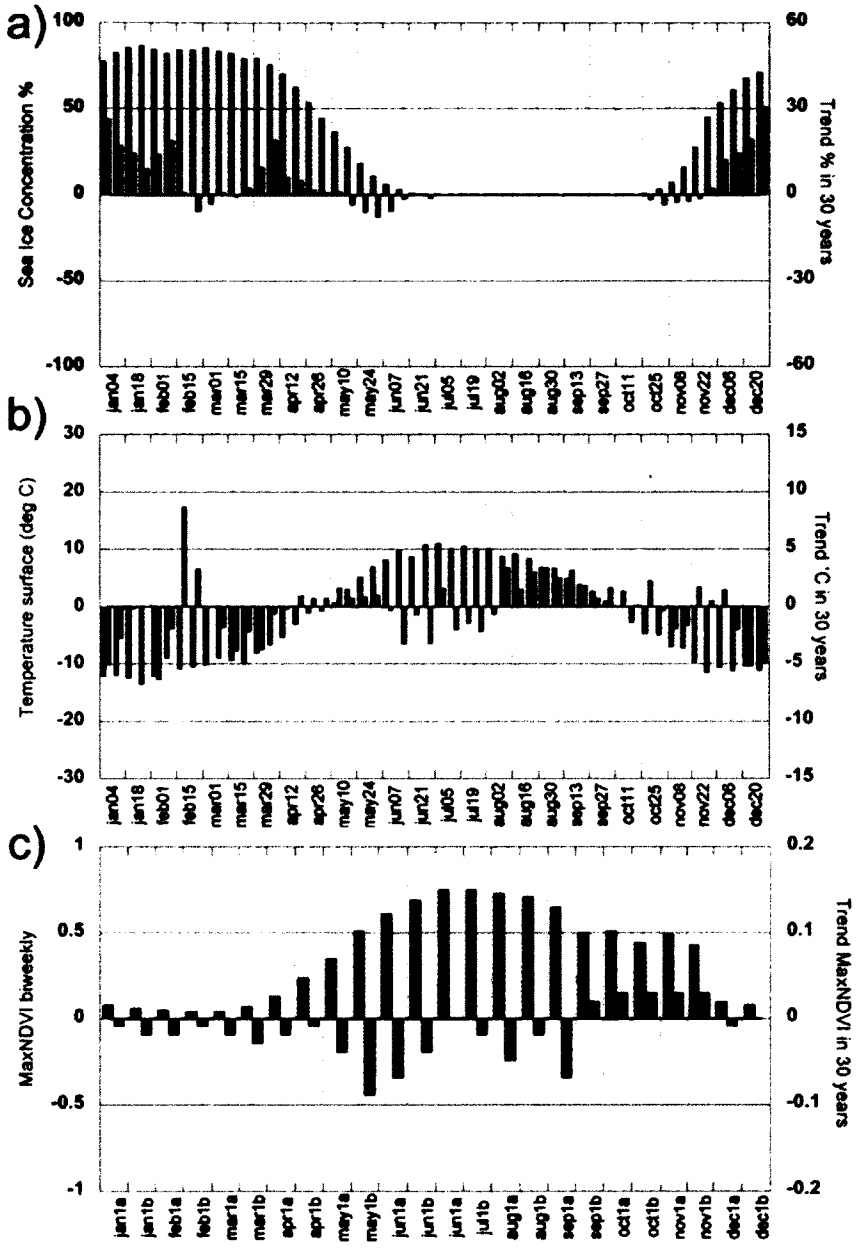

Figure 3.11 East Bering tundra region long-term mean and weekly magnitude change (1982-2011) in (a) 100km sea ice concentration, (b) surface temperature and (c) bi-weekly NDVI. Sea ice is absent in the summer in this region and is slightly decreasing in May and October. Sea ice is increasing periodically in the rest of the year. Temperatures are decreasing in June and July but are increasing in May and August. NDVI is decreasing throughout the summer with increases in the fall. The greatest declines are during the initial growing season.

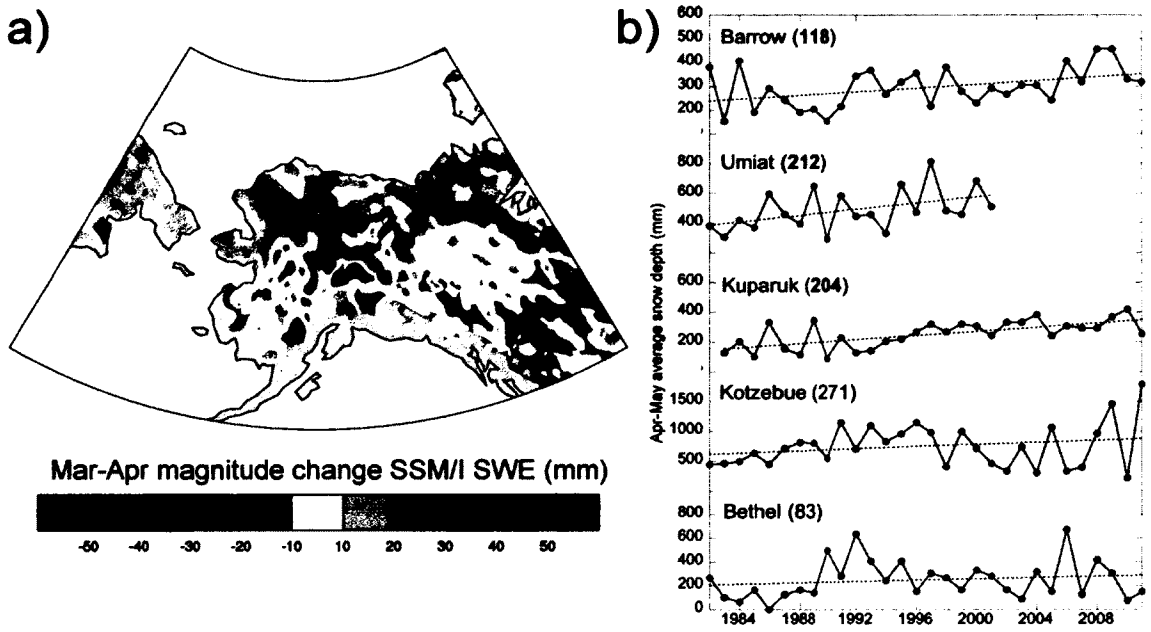

Figure 3.12 March-April (a) SSM/I snow water equivalent (SWE) magnitude change (1987-2007) and (b) station snow depth. SWE is increasing in northern Alaska and decreasing in the southwest. The numbers in parentheses in (b) show the magnitude change (units of mm) based on a linear trend for each station for the number of years observed since 1982, where trends significant at the 95% (90%) level greater are bold (italic). All stations are increasing in average snow depth for 1982-2011. Bethel is decreasing in snow depth during the period of the SSM/I but is increasing in its full record.

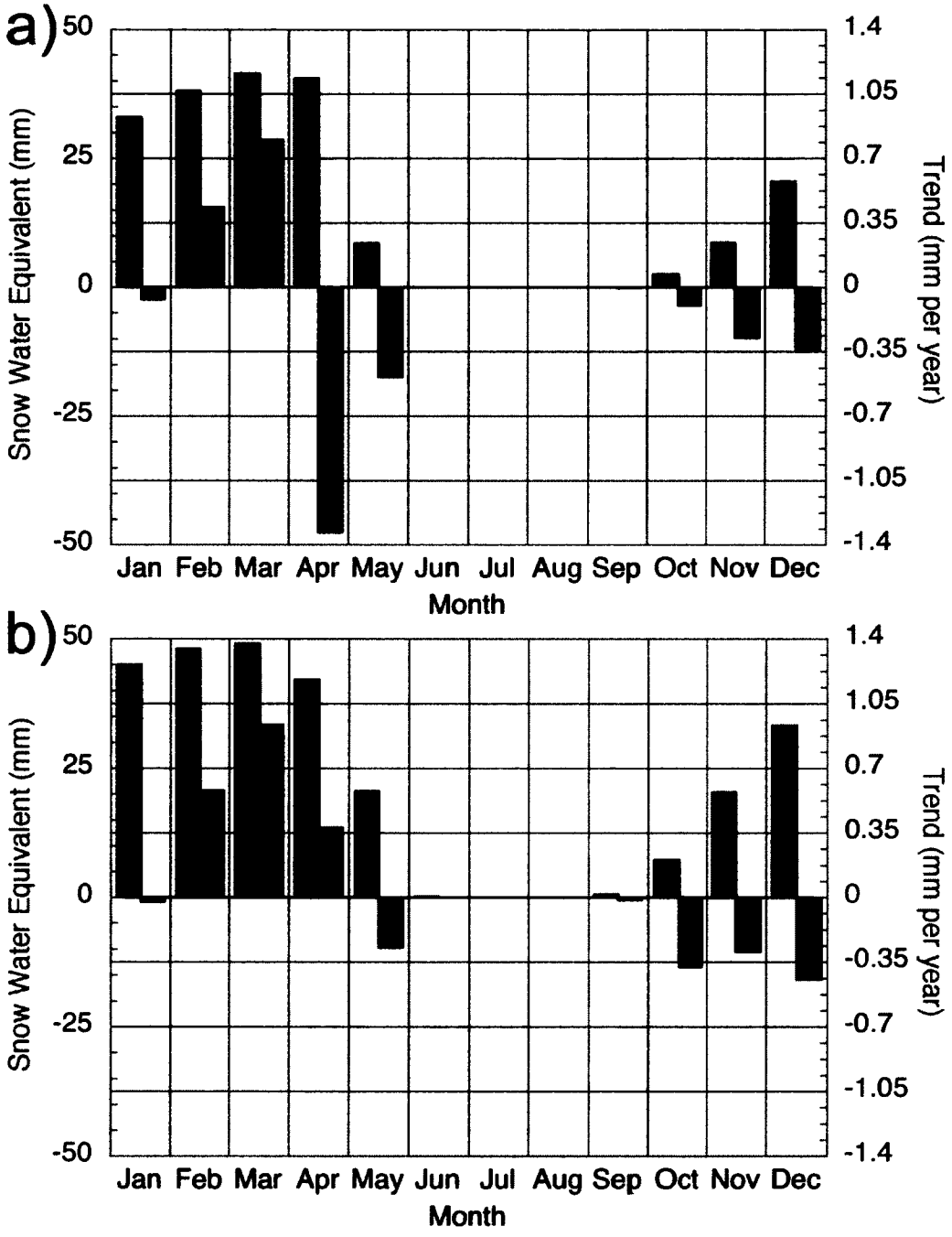

Figure 3.13. Monthly trends in SSM/I SWE (1987-2007) for the (a) lowlands/Yukon Delta and (b) Seward Peninsula sub-regions of the East Bering tundra region. The Seward Peninsula has greater SWE on average than the lowlands, however the spring trends are weaker in comparison and have opposite sign in April. SWE has declined in October-January in both sub-regions.

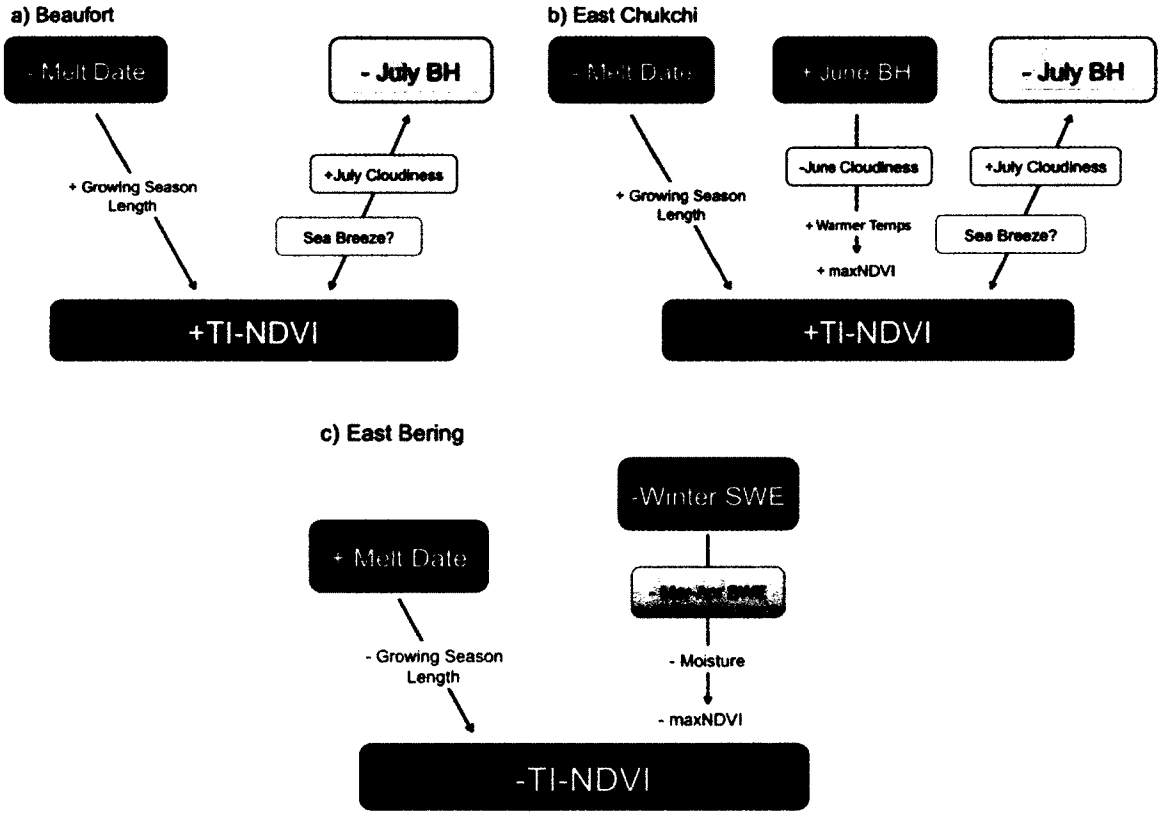

Figure 3.14 Summary of the key climate drivers of TI-NDVI for (a) Beaufort, (b) East Chukchi and (c) East Bering coastal tundra regions. In all three regions earlier snowmelt results in increased TI-NDVI, especially in the early season. In the Beaufort and East Chuckhi a weaker Beaufort High (BH) is linked with reduced cloudiness and there is also a complex linkage with the sea breeze the circulation. The sea breeze circulation is also influenced by the land-sea temperature contrast, and so changes in the surface temperature can feedback on the strength of the BH. Reduced winter snow water equivalent (SWE) is linked with reduced maxNDVI in the East Bering.

Table 3.1. Correlations between station snow melt date and full tundra time series of Beaufort, Chukchi and Bering TI-NDVI (TI) and May-June (MJ) NDVI. Correlations significant at the 95% or greater based on the student's t test shown in bold.

	Bethel	Kotzebue	Kuparuk	Umiat	Barrow
Beaufort TI	0.06	-0.04	-0.17	**-0.49**	-0.25
Chukchi TI	-0.10	-0.19	-0.24	**-0.56**	**-0.44**
Bering TI	**-0.51**	-0.25	-0.18	**-0.53**	-0.23
Beaufort MJ	-0.10	-0.03	**-0.49**	**-0.77**	**-0.44**
Chukchi MJ	-0.25	**-0.38**	**-0.38**	**-0.66**	**-0.60**
Bering MJ	**-0.48**	**-0.38**	-0.06	-0.35	-0.23

Table 3.2 Correlations between summer season and monthly Beaufort High MSLP index and time series of Treshnikov full tundra region TI-NDVI (TI) and maxNDVI (max) and monthly station cloud cover. Correlations significant at the 95% (90%) or greater based on the student's t test shown in bold (italics). The strongest correlations are with the July Beaufort High and indicate that a weaker high results in higher NDVI in the Beaufort and Chukchi region. Bering TI-NDVI is reduced with a stronger Jun-Aug Beaufort High.

	Jun-Aug	June	July	August
Beaufort max	0.00	0.19	**-0.47**	0.28
Beaufort TI	-0.21	0.10	**-0.53**	0.03
Chukchi max	0.19	**0.46**	*-0.32*	0.24
Chukchi TI	-0.15	0.09	**-0.42**	0.04
Bering max	0.08	-0.15	0.19	0.10
Bering TI	**-0.38**	*-0.34*	-0.18	-0.23
Bethel June Clouds	**0.43**	0.31	0.18	*0.35*
Bethel July Clouds	-0.03	-0.04	-0.06	0.05
Bethel Aug Clouds	-0.29	-0.18	-0.07	-0.31
Barrow June Clouds	*-0.34*	-0.31	0.12	**-0.48**
Barrow July Clouds	-0.31	-0.30	**-0.43**	0.10
Barrow Aug Clouds	-0.17	-0.02	-0.03	-0.27

Chapter 4 Climate Divisions For Alaska Based On Objective Methods[1]

Abstract

Alaska encompasses several climate types, due to its vast size, high latitude location, proximity to oceans and complex topography. There is a great need to understand how climate varies regionally for climate research and forecasting applications. While climate type zones have been established for Alaska based on seasonal climatologies, there has been little attempt to construct climate divisions, which identify regions with consistently homogeneous climate variability. In this study, cluster analysis was applied to monthly average temperature data from 1977-2010 at a robust set of weather stations to develop climate divisions for the state. Mean-adjusted AVHRR surface temperature estimates were employed to fill in missing temperature data when possible. Thirteen climate divisions were identified based on the cluster analysis and subsequently refined using local expert knowledge. Division boundary lines were drawn encompassing the grouped stations following major surrounding topographic boundaries. Correlation analysis between station and gridded downscaled temperature and precipitation data supported the division placement and boundaries. The new divisions north of the Alaska Range were the North Slope, West Coast, and Central, Northeast and Northwest Interior. Divisions south of the Alaska Range were Cook Inlet, Bristol Bay, Aleutians, Northeast and Northwest Gulf, and North, Central, and South Panhandle. Correlations with various Pacific and Arctic climate teleconnection indices showed

[1]Bieniek, P., U. Bhatt, R. Thoman, H. Angeloff, J. Partain, J. Papineau, F. Fritsch, E. Holloway, J. Walsh, C. Daly, M. Shulski, G. Hufford, D. Hill, S. Calos, and R. Gens, 2012: Climate divisions for Alaska based on objective methods. *J. Appl. Meteor. Climatol.* **51**, 1276-1289.

numerous significant relationships between seasonal division average temperature and the Arctic Oscillation, Pacific-North American Pattern, North Pacific Index, and Pacific Decadal Oscillation.

4.1 Introduction

The climate of a geographic location is strongly linked to its latitude, elevation, and proximity to oceans. There has long been a great need to understand how the climate varies by region for climate research and forecasting applications. Climate-classification techniques have often been employed to account for regional variability; the most well known being the Koeppen Scheme (Koeppen 1923) which broadly classifies regions by their mean temperature and precipitation. The Contiguous United States (CONUS) was first subdivided into broad climate regions in 1909 (Guttman and Quayle 1996). Initially these regions were based solely on river drainage basins but by as early as 1912 more robust measures dividing the regions using mean temperature were employed (Guttman and Quayle 1996). The National Climatic Data Center (NCDC) currently maintains the set of official climate divisions for the United States.

Due to Alaska's large geographical extent, complex terrain, and proximity to oceans and sea ice its climate is highly regionalized. Zones of homogeneous climate type were first outlined in the 1920s by general examination of the mean temperature of the few weather observation stations available at the time (Fitton 1930; red dashed line in Figure 4.1). While some of these initial boundaries intersected major terrain barriers, most notably the Brooks Range, Fitton (1930) noted the critical role of terrain boundaries in defining regional climate zones in Alaska. Later, a new set of boundaries were developed essentially based on drainage basin regions (Searby 1968), and are currently considered as the official climate divisions for Alaska by NCDC (green dashed line in Figure 4.1; National Climatic Data Center 2002). The most recent update is by Shulski

and Wendler (2007), who considered the NCDC climate divisions while updating the Alaska climate zones on the basis of annual mean temperature and precipitation (blue solid line in Figure 4.1). Overall, 10-11 general climate zones have been traditionally identified with disagreements in the exact locations of the boundaries, some of which bisect major terrain barriers. Studies have also identified zones of similar surface characteristics (i.e. ecoregions) in Alaska (Gallant 1995; Simpson et al. 2007). Previous Alaska climate regions were all based on seasonal climatologies or annual means in temperature and precipitation. In this study, we employ cluster analysis on observed station temperature as an objective method to independently develop climate divisions for Alaska based on climate variability, not long-term seasonal climatologies.

There is a pressing need to define official climate divisions for Alaska. The past climate zones defined for Alaska were based on short records of sparse station data and were meant to provide climate type zones, thus they do not necessarily coincide with regions of homogenous climate variability. While climate type zones give valuable information about the general characteristics of the average season, they are not as useful for seasonal climate forecasting and research applications as they do not give any information on year-to-year variability. There is now available a relatively long time length of station and remotely sensed data as well as robust objective methods to properly identify climate divisions for Alaska that fill this need.

Climate divisions have a wide variety of applications beyond simply identifying regions with similar climate types and variability. In the CONUS, studies have shown the influence of climate teleconnection indices in each division (Wolter et al. 1999; Budikova

2005), which is highly valuable for seasonal climate forecasting. The CONUS climate divisions are currently used as the zones for the seasonal climate predictions made by the Climate Prediction Center (CPC). Climate divisions are also widely used for hydrological applications such as drought monitoring in the CONUS. As a result, climate divisions not only give useful information on the spatial extent of regional climate variability in Alaska; they can also be used in the evaluation of diverse climate related problems.

A wide range of large-scale climate teleconnections affects Alaska in all seasons. One of the strongest links is between winter temperatures and the El Niño Southern Oscillation (ENSO) where the positive phase of ENSO results in above normal temperatures (Papineau 2001). ENSO has also been shown to influence spring temperatures and consequently Interior Alaska river ice breakup (Bieniek et al. 2011). North Pacific teleconnections such as the North Pacific Oscillation/West Pacific Pattern (Linkin and Nigam 2008), shifts in the Pacific Decadal Oscillation (PDO; Hartmann and Wendler 2005) and other climate indices (Bourne et al. 2010) have all been linked with the climate of Alaska in some way. Sea ice also plays an important role and has been linked with summer land temperatures and tundra vegetation along the Arctic and western Alaska coastlines (Bhatt et al. 2010). In all of these studies it is apparent that climate teleconnections impact different parts of Alaska in diverse ways. Therefore, regions with relatively homogeneous climate variability forced by a variety of different climate teleconnections must exist for Alaska.

Cluster analysis is a method that is commonly used to group data based on the degree of similarity in variability and was first applied to the atmospheric sciences by

Wolter (1987). Cluster analysis has been employed to determine climate zones in the CONUS based on station data (Fovell and Fovell 1993) and has also been applied to diverse climates such as Turkey (Unal et al. 2003) and Saudi Arabia (Ahmed 1997). Cluster analysis has also been applied regionally in the United States to identify climate zones in the northern plains (Bunkers et al. 1996), the northeast (DeGaetano 1996) and the Carolinas (Rhee et al. 2008). Wolter and Allured (2007) developed climate divisions for the CONUS using an approach that is based on cluster analysis (e.g. Fovell and Fovell 1993), but using a simplified method to process the data and correlation analysis for verification. In our study we will draw on elements from all of these studies to form an objective basis for climate divisions in Alaska. While our analysis relied heavily on objective methods, Alaska's vast size and relatively sparse station network, local expert knowledge was necessary to refine the final division boundaries. Local expert knowledge has been demonstrated to benefit scientific understanding of weather systems in Samoa (Lefale 2010) as well as land-cover changes in South Africa (Chalmers and Fabricius 2007).

The novel aspects of this study include: identifying regions of homogeneous climate variability to develop climate divisions in Alaska based on monthly station temperature, testing the division boundaries using gridded downscaled temperature and precipitation data, determining key seasonal climate teleconnection linkages with temperature in each climate divisions, and using AVHRR surface air temperature to fill gaps in station temperature data.

4.2 Data and methods

4.2.1 Meteorological data

Meteorological data were obtained for stations throughout Alaska and neighboring Canada (Figure 4.1). Monthly average temperature and accumulated precipitation were obtained from the National Climatic Data Center (NCDC), the Global Summary of the Day (GSOD) database at NCDC, Environment Canada (EC), the Alaska Climate Research Center (ACRC), and the National Weather Service (NWS). The location and source for each station are given in Table 4.1 (locations are plotted in Figure 4.1). The overall goal for the selection of stations for the analysis was to maximize the spatial coverage while minimizing the amount of missing data. Stations were also selected to achieve a relatively even distribution of stations throughout the state to reduce analysis bias. This required selecting a single station from groups of stations that were in close proximity to each other and was especially important in the Anchorage area and Southeast Alaska. Unfortunately, few stations located at high elevation locations had sufficient record length to be included in our analysis and the underrepresentation of high altitude locations is an ongoing concern in studies like this. The period of analysis was selected to be 1977-2010 since evaluation of the station data inventories revealed that the data coverage is quite sparse prior the mid 1970s. Canadian stations were included in the cluster analysis as a buffer to reduce the impact of the artificial boundary at the U.S.-Canadian boarder. The Canadian stations were not used beyond the cluster analysis nor assigned climate divisions.

Satellite based monthly land surface temperature from the Advanced Very High Resolution Radiometer (AVHRR) is available for the period 1982-2010 on a 25km square grid. The surface temperature data, based on the infrared channel, were enhanced using an improved cloud masking dataset and were calibrated using in situ surface air temperature (Comiso 2003). While the AVHRR data have been calibrated using in situ data, they add an independent perspective to the analysis of station data and provide a source to fill in station data gaps.

Gridded downscaled temperature and precipitation data for Alaska (Hill and Calos 2011) were used to validate the climate division boundaries. These data were derived from 1961-2009 station data. The complete list of available stations was filtered based on a minimum record length criterion, yielding 322 and 261 stations for temperature and precipitation respectively. Monthly anomalies were created by comparing station data to a 1971-2000 climate normal, obtained from the Parameter-elevation Regressions on Independent Slopes Model (PRISM; Simpson et al. 2005). These scattered anomalies were then interpolated onto a 2km x 2km grid, using the splines with tension interpolation method. Finally, synthesis of the anomaly and normal grids produced the gridded monthly precipitation and temperature fields.

Values of various climate indices for the period 1977-2010 were used in this analysis to identify possible seasonal large-scale climate teleconnection linkages with temperature within each division. Indices of West Pacific Pattern (WP), East Pacific/North Pacific Pattern (EP/NP), and Pacific-North American Pattern (PNA) were obtained from the CPC (online at: http://www.cpc.ncep.noaa.gov/data/teledoc/pna.shtml).

Also retrieved from CPC were the Arctic Oscillation (AO; online at: http://www.cpc.ncep.noaa.gov/products/precip/CWlink/daily_ao_index/ao.shtml), Southern Oscillation Index (SOI), and Niño region 3.4 (NINO3.4) sea surface temperature (SST) anomalies (online at: http://www.cpc.ncep.noaa.gov/data/indices/). The North Pacific Index (NPI; online at: http://www.cgd.ucar.edu/cas/jhurrell/npindex.html) and the PDO (online at: http://jisao.washington.edu/pdo/) were also used in this analysis.

4.2.2 Analysis methods

Our analysis followed this basic workflow: (1) the data were normalized; (2) cluster analysis was performed to group the stations; (3) the appropriate number of clusters was determined; (4) clustering method results were compared to determine the optimal groupings; (5) the final divisions were validated with correlation analysis and refined by manual inspection of regional climate characteristics using the local expert knowledge of experienced weather forecasters. Unfortunately, station precipitation was found to be too sparse to be suitable for cluster analysis, therefore temperature alone was used. However, precipitation data were used along side temperature in the validation when possible.

Three clustering methods were selected to group the stations to identify regions with consistently homogeneous climate anomalies: Wards, average linkage, and *k*-means Methods (Wilks 2006). Using multiple methods allowed for the comparison results, as each method uses different clustering assumptions and thus has a unique bias. In this case, the results were similar among the three methods allowing us to focus on the Wards

method for simplicity. The Wards method looks for the minimum variance or error sum of squares (ESS) among potential groups of stations to find the appropriate cluster configuration at each iteration. The ESS, or minimum variance distance measure is given as:

$$W = \sum_{g=1}^{G} \sum_{i=1}^{n_g} \sum_{k=1}^{K} (x_{i,k} - \bar{x}_{g,k})^2 \quad (1)$$

Where $\bar{x}$ is the cluster mean, G is the number of clusters, n_g is the number of stations and K is the number of time steps (Wilks 2006). Essentially, the difference between each station and the cluster average to which it was joined is squared then summed. To determine the optimal number of clusters, the ESS was visually checked for sudden jumps associated with a decreasing number of clusters. In other words, as the number of clusters decreases, the stations become increasing dissimilar to the clusters to which they are being joined. The results from all three methods were then compared to determine possible uncertainties or problems with the groupings of the stations.

In the ESS, relatively large station-cluster average differences would be amplified because the difference is squared and relatively large monthly and seasonal means would quickly dominate over the smaller magnitudes of climate variability in the formation of clusters (Wilks 2006). Consequently, the data were processed prior to clustering since mean temperature and precipitation varies greatly by season and geographic location in Alaska. While complex methods have been engaged such as Principal Component Analysis in previous studies (e.g. Fovell and Fovell 1993), our study employed a simple method to normalize the data. Following Wolter and Allured (2007), a three-month

moving mean was applied to the monthly station data. The resulting smoothed data were normalized by subtracting their corresponding three-month average and dividing by the standard deviation. Normalizing by the individual three-month period has the effect of equalizing the seasonal variance of the data. The smoothing also reduces the impact of isolated extreme monthly anomalies on the clustering results. Using a simplified method was preferred given the sparse number of stations available in Alaska.

Cluster analysis cannot operate with missing data, therefore gaps must either be filled in or the entire record removed. AVHRR monthly average land surface temperature is available for Alaska from 1982-2010. Correlation analysis comparing the station temperature with the AVHRR pixel nearest the station revealed correlation coefficients greater than 0.9 at all stations north of the Alaska Range (Table 4.1), with lower values south of the mountains. Missing values were filled using AVHRR for many station temperature time series and was guided by the correlation coefficients and visual comparison between the station and AVHRR data Where AVHRR was used it was first bias-corrected for the slight differences in monthly means. Unfortunately the AVHRR was not suitable for filling missing station values in coastal areas south of the Alaska Range, as the means were too dissimilar. This was likely due to interference from mixed ocean and land pixels, coupled with the complex topography and ground cover of the region. When AVHRR could not be used missing periods were filled with the long-term monthly mean for that station. The percent of missing data filled with AVHRR at each station is shown in Table 4.1.

Correlation analysis was applied to the station temperature and precipitation data to validate the final divisional memberships. Division average temperature and precipitation values were calculated based on the stations within each division. Annual and seasonal cross-correlations were carried out between the individual stations and the division averages.

4.3 Results

4.3.1 Constructing the divisions

Inspection of the ESS (Figure 4.2) showed that the distance between clusters and their members began to increase relatively rapidly after 13 clusters. The result of the Wards method is shown in Figure 4.3 for the 13-cluster solution (11 clusters were in Alaska and 2 entirely in Canada). In this case, missing station data were filled using the mean-adjusted AVHRR land surface temperature when possible and others were filled using the long-term monthly mean. All three methods yielded quite consistent results when using a corresponding 13 or 14-cluster solution, but the Wards method is presented for simplicity. The clustering result served as a starting point for the analysis based on local expert knowledge that follows.

For comparison, cluster analysis was also carried out when the missing station temperature was exclusively filled with the long-term monthly means. The result (not shown) yielded a similar set of 13 clusters, as in Figure 4.3, with minor differences. Therefore, while there was some sensitivity in the clustering results to how the missing data were filled, the overall number of clusters and general locations of the divisions did

not appear to strongly influence the final outcome. This was expected as only those stations with minimal missing data were used in our analysis. Furthermore, in spite of the problems encountered with the southern coastal data, the AVHRR captures the variability in areas north of the Alaska Range and was found to be useful in filling gaps in station temperature.

The station data and AVHRR were also clustered in different configurations as an additional test. Cluster analysis conducted on the full gridded AVHRR surface temperature (not shown) revealed boundaries that broadly resembled the Alaska ecodivisions (Gallant 1995) when using the Wards Method. It is not surprising that the AVHRR clusters resembled the ecodivisions, given that both are sensitive to surface characteristics (e.g. vegetation), many of which strongly influence or are influenced by the climate. However, possibly due to AVHRR data quality issues in the southern coastal regions, conflicting results among the different clustering methods indicated that the AVHRR could not be used solely to construct the divisions. In the data sparse areas of northern Alaska, proxy "station" values were estimated from the AVHRR data and added to the observed station dataset to test their usefulness. However, they did not appear to add useful information to the analysis, as they tended to cluster together.

The Climate Research Unit (CRU) TS 3.0 (Mitchell and Jones 2005) and the North American Regional Reanalysis (NARR; Mesinger et al. 2006) gridded temperature and precipitation datasets were also evaluated as potential candidates for determining the climate divisions (not shown). As the CRU data were interpolated using a simple method on a relatively sparse station network, the clusters unrealistically crossed major terrain

boundaries such as the Brooks and Alaska Ranges. The NARR precipitation data appeared to cluster around an artificial north-south boundary centered along the longitude of Fairbanks. While the NARR precipitation was problematic, the NARR temperature clusters appeared to be much more physically realistic, but an optimal number of clusters based on the ESS could not be identified. While the cluster analyses of the NARR and CRU gridded datasets were unsuitable in themselves for determining the climate divisions, their 13-cluster solutions were broadly similar to the locations of the divisions based on the station data and appear to support our findings.

Based on the clustering result of the Alaska stations in Figure 4.3, preliminary climate division boundaries were drawn by visually identifying major terrain features that surrounded the groups of stations. Given the spatial distribution of the clusters of stations, major terrain features appeared to be natural barriers between regions. Local expert knowledge of experienced National Weather Service forecasters was then used to improve and refine the division boundaries (Figure 4.4). At this step it was decided that Juneau and Haines should be grouped independently from each other to form North and Central Panhandle divisions respectively because of their seasonal climate differences. Annette and Ketchikan remained grouped together in the South Panhandle division. In southwest Alaska, two divisions were created encompassing areas along and inland from Bristol Bay and the south-central coast including Kodiak (Northwest Gulf) also based on seasonal differences in climate. Having these two divisions divided was also consistent with the historical climate type regions in Figure 4.1, which were divided by the Aleutian Range, a formidable mountain barrier. The reasons for deviating from the cluster results

will be discussed further when the climate characteristics of the individual divisions are presented in section 4.3.3.

4.3.2 Sensitivity analysis

Cross-correlation of station data with the division averages (not shown) yielded no case where a station was correlated higher with a different division for annual temperature and precipitation. Even when evaluated seasonally (not shown) very few stations had a higher correlation with another division average than their own. The few cases of stations correlating higher with another division tended to occur in the southern coastal areas. There were no cases were the correlation was consistently higher with another division throughout multiple seasons that might have warranted changing the station to another division.

To validate the division lines, the station division average temperature and precipitation were correlated with the 2km downscaled temperature and precipitation data for the entire state. The division membership of each point in the downscaled data was identified based on our lines. The time series for each grid point was then correlated with all 13 division averages for both temperature and precipitation. Each time a point had a higher correlation with another division other than its own the sum for that point was increased by 1. Ideally every point should have a count of zero, implying that it was best correlated with its own division. For both temperature and precipitation there were only a few areas with higher correlation with other division average time series than their own (Figure 4.5). Most areas with elevated counts were located in the Northeast Interior

division, which was based on a single station (Fort Yukon). The highest counts, and subsequently the highest uncertainty, occurred with precipitation (Figure 4.5b) with the highest counts along the boundary between the Southeast Interior and the Northeast Gulf divisions. With the exception of the Northeast Interior, every division was regularly correlated best with the division average temperature and precipitation from the stations assigned to that division. Overall, the positions of the division boundaries appear to be quite reasonable by this validation method.

4.3.3 Characteristics of the divisions

The long-term monthly average temperature and precipitation for each station and the average for all stations within each division are shown in Figure 4.6. The overall climate regimes of the individual stations within any division were generally consistent in seasonality and magnitude. The divisions with the highest precipitation amounts are along the southern coastal areas of Alaska, where the annual temperature ranges also tend to be the smallest in the state. The most extreme temperature ranges occur in the Interior where precipitation amounts are also the lowest in the state. Most divisions have the highest precipitation amounts in late summer or fall.

In section 4.3.1 the Bristol Bay stations were separated from Kodiak and Homer. Bristol Bay then became its own division (Figure 4.6k), Homer was added to the Cook Inlet division (Figure 4.6f), and Kodiak became part of the Northwest Gulf division (Figure 4.6m). When comparing the seasonal climates of the individual stations with their divisions (Figure 4.6k,f,m) it can be seen that the Bristol Bay stations tend to have

different seasonalities in precipitation and temperature than Kodiak and Homer. This was a case where, while these stations tended to share the same year-to-year climate anomalies, differences in their seasonal climate regimes suggest they were best grouped separately. This distribution of the stations was also consistent with the historical climate type regions (see Figure 4.1). A similar situation occurred when Haines and Juneau were grouped together with Dease Lake in Canada by the cluster analysis. Haines (North Panhandle, Figure 4.6h) tends to get less precipitation than Juneau (Central Panhandle, Figure 4.6j) from late spring through summer. Haines is also rain shadowed by the coastal mountains and therefore tends to be less cloudy than Juneau. The geographical and seasonal characteristics of each climate division are described next.

The North Slope division is shown as cluster 3 in Figure 4.3 and includes the stations at Barrow, Umiat, Barter Island and Prudhoe Bay. This division is the northernmost in Alaska and encompasses the arctic tundra portion of Alaska north of the Brooks Range. The division is bounded by the Arctic Ocean on the north and west and the Brooks Range on the south. The Arctic Ocean is covered by sea ice in winter, but has variable sea ice in summer. The climate of the region (Figure 4.6a) is among the driest with a maximum precipitation of less than 5 cm in the wettest summer month and seasonal average temperatures ranging from below -25°C in winter to above 10°C in summer.

The Central Interior division is shown as cluster 5 in Figure 4.3 and includes the stations at Bettles, Tanana, Galena and McGrath. The region is bounded by the Brooks Range to the north and the Alaska Range to the south. It is relatively far from ocean

influences and has a continental climate (Figure 4.6b) with relatively low precipitation compared with the coastal regions.

The Northeast Interior division is shown as cluster 11 in Figure 4.3 and includes the station at Fort Yukon. Since this division is far from the ocean, it has a very continental climate with the largest seasonal mean temperature range in Alaska (Figure 4.6c). This region is bounded to the north by the Brooks Range and to the south and west by the Yukon-Tanana Uplands. Precipitation here is amongst the lowest in the state.

The Southeast Interior division is shown as cluster 8 in Figure 4.3 and includes the stations at Fairbanks, McKinley Park, Big Delta, Eagle, Northway and Gulkana. This region is bounded to the north by the Yukon-Tanana Uplands and to the south by the Chugach Mountains, which block southerly maritime influence. The seasonal ranges in temperature (Figure 4.6d) are similar to those of the Central and Northeast Interior divisions and can be characterized as continental. This division has a summer maximum in precipitation.

The West Coast division is shown as cluster 4 in Figure 4.3 and includes the stations at Kotzebue, Nome and Bethel. This division is bounded to the west by the Bering and Chukchi Seas, to the east by the Kuskokwim Mountains, and to the north by the Brooks Range. The seasonal temperature range (Figure 4.6e) is more moderate than that of the Interior divisions. Precipitation is higher than Interior divisions but much lower than the southeast coastal regions of Alaska and this division has a summer maximum similar to the Interior.

The Cook Inlet division is shown as cluster 1 and part of 10 in Figure 4.3 and includes the stations at Talkeetna, Anchorage, Kenai and Homer. This is a coastal division that straddles Cook Inlet and is bounded by the Alaska Range and the Chugach Mountains. The seasonal temperature range (Figure 4.6f) is maritime with similar precipitation seasonality (although less in amount) to that of the Interior and West Coast divisions.

The Northeast Gulf division is shown as cluster 7 and part of 1 in Figure 4.3 and includes the stations at Valdez, Cordova, Yakutat, Elfin Cove, and Sitka. This division is situated along the northeast Gulf of Alaska with the Chugach Mountains to the north. It has a relatively small annual temperature range (Figure 4.6g) and receives amongst the highest seasonal average precipitation, with maximum values in fall.

The North Panhandle division is shown as cluster 9 in Figure 4.3 and contains the station at Haines. This division is in the interior of the Southeast Panhandle of Alaska and is bounded on all sides by mountains. The annual temperature range (Figure 4.6h) is also moderate like its neighboring division, Northeast Gulf. However it receives less precipitation in all seasons than the Northeast Gulf division. This region has its maximum precipitation in the fall.

The South Panhandle division is shown as cluster 2 in Figure 4.3 and contains the stations at Ketchikan and Annette. This division includes the southernmost coastal areas of Alaska and is bounded to the east by the Coast Mountains. Average monthly temperatures (Figure 4.6i) have small variability throughout the year and average precipitation is among the highest in the state with the maximum occurring in the fall.

The Central Panhandle division is shown as cluster 9 in Figure 4.3 and includes the station at Juneau. This division is located in the Interior of the southeast with mountains to the east and west. Monthly average temperatures (Figure 4.6j) are quite moderate and this division receives less precipitation than the Northeast Gulf and South Panhandle on average.

The Bristol Bay division is shown as cluster 10 in Figure 4.3 and includes the stations at Iliamna and King Salmon. This division is located along the southwest coast of Alaska along Bristol Bay and extends north to the Kuskokwim Mountains and east and south to the Aleutian Range. Monthly average temperatures (Figure 4.6k) are relatively moderate. Precipitation values are much lower than in the Northwest Gulf division and are maximum during late summer.

The Aleutians division is shown as cluster 12 in Figure 4.3 and includes the stations at Cold Bay and St. Paul. This division included the entire Aleutian Island chain and St. Paul Island. This division is bounded by the Pacific Ocean to the south and Bering Sea to the north. Monthly average temperatures (Figure 4.6l) have the smallest range of any of the divisions and have relatively low precipitation compared to the Northeast and Northwest Gulf divisions. Maximum precipitation occurs from late summer through fall.

The Northwest Gulf division is shown as the southern portion of cluster 10 in Figure 4.3 and includes the station at Kodiak. This division, located along the northwestern part of the Gulf of Alaska, includes Kodiak Island, coastal areas south of the Aleutian Range on the Alaska Peninsula and the southernmost portion of the Kenai Peninsula. Monthly average temperatures (Figure 4.6m) are moderate and precipitation

amounts are lower than the Panhandle divisions with the maximum generally occurring in late fall and winter.

4.3.4 Teleconnections

An example of the usefulness of these climate divisions can be found when the division average temperatures were correlated with climate indices. A set of climate teleconnection indices from the Pacific/arctic region were correlated, after being linearly detrended, with each division average temperature to demonstrate the individual links with the large-scale climate in each season for 1977-2010. Table 4.2 shows the teleconnection indices that were significantly correlated at the 95% or greater level based on a t-test with the division average temperatures each season.

Many of the climate divisions were significantly correlated with the Arctic Oscillation (AO) throughout much of the year. The AO (Thompson and Wallace 1998) is a leading mode of northern hemisphere sea level pressure variability and effects the large-scale circulation. Table 4.2 shows that the AO is significantly negatively correlated with temperature, or the negative phase results in warm temperature anomalies, in multiple climate divisions in each season. Note that most of Eurasia and the continental US are colder than normal during the negative phase of the AO (See graphical analysis online at: http://jisao.washington.edu/analyses0500/tempprecipao.1deg.gif).

ENSO has been shown to be a key driver in the climate of Alaska (Papineau 2001; Bieniek et al. 2011). Evaluation of tropical Pacific, or ENSO-related, climate indices showed a substantial and widespread relationship with significant correlations

occurring in each division in at least one season of the year. The ENSO-specific indices evaluated were the SOI and the Nino 3.4 SST anomaly. The PNA and is a natural mode of atmospheric variability that extends into the Alaska region (Wallace and Gutzler 1981). The PNA has been shown to be linked with ENSO (Horel and Wallace 1981) as well as purely midlatitude processes (Dole 1983). Of the ENSO related indices, the PNA had by far the most significant correlations. This seems to indicate that the PNA may be the primary pathway for the linkage between ENSO and the seasonal average temperature in most of the climate divisions. In all cases the PNA was positively correlated with temperature, which means that the positive phase of the PNA (which corresponds to the positive phase of ENSO) tends to result in above average temperatures in those divisions where the correlations were significant. Interestingly, the only time that ENSO had an opposite sign relationship from the rest of the divisions was for the North Slope division in winter (Table 4.2), where there was a positive correlation with the SOI. Our findings are in general agreement with the aforementioned studies.

In the North Pacific, several teleconnection indices were correlated with the division average temperatures. The NPI, a measure of the strength of the Aleutian Low (Trenberth and Hurrell 1994), was negatively correlated with multiple divisions and was correlated in all seasons. A negative correlation indicates that when the Aleutian Low was stronger, temperatures were warmer in Alaska. This is intuitive, since a stronger Aleutian Low will tend to advect warm air and moisture from the Pacific into Alaska. Also positively correlated with the divisions were the EP/NP and WP circulation indices, which are primarily winter modes of variability in the tropospheric circulation over the

north Pacific (Barnston and Livezey 1987). The EP/NP has widespread correlations throughout the year, but the WP was limited to the summer, which is perplexing because the WP is entirely a winter phenomena.

The PDO is a leading mode of variability of the north Pacific SSTs (Mantua et al. 1997). In every case the PDO had positive and significant correlations, meaning that the positive phase resulted in warmer temperatures. In winter and fall (Table 4.2), the PDO was correlated with divisions in the Interior and southern coastal regions. In spring and summer, the PDO was related only to divisions along the south-central coast and the Aleutians. The PDO was never significantly correlated with the North Slope division. These correlation results are consistent with the findings of Papineau (2001), Hartmann and Wendler (2005), and Bourne et al. (2010).

The correlations of Pacific and Arctic climate teleconnections with the division averages temperatures revealed several relationships. One is that the NPI, AO, PNA and PDO all had a strong influence on the variability of temperatures in all seasons throughout Alaska. No divisions, however, had consistently the same relationships with the same set of teleconnection indices. The exact mechanisms for these correlations are beyond the scope of this paper and are a fruitful area for future investigation.

4.4 Conclusions

A combination of objective analysis and local expert knowledge identified 13 regions of homogeneous climate variability, or climate divisions, for Alaska based on observed station temperature. The cluster analysis was limited to temperature because

precipitation data were too sparse for the cluster analysis. However, the available station precipitation correlated well within each division in the validation. Analysis of alternate gridded datasets, while not useful in determining the divisions on their own, tended to support the final clustering of the stations. The AVHRR was also shown to be invaluable in filling gaps in the station data north of the Alaska Range. Due to the vast geographical extent of Alaska, coupled with a relatively sparse station network, drawing the division boundaries relied heavily on following the major terrain features surrounding the grouped stations. A broad cross-correlation analysis using both station temperature and precipitation also supported the groupings of the stations. While the lines of the division boundaries could not be drawn completely objectively, correlation analysis using the division averages and downscaled gridded temperature and precipitation supported the final placement of the division boundaries.

Evaluation of the climates of the divisions revealed that the stations in each division have similar annual cycles in temperature and precipitation. Our divisions were determined using cluster analysis and the similar climate cycles also served to support our division choices. An evaluation of a diverse set of teleconnection indices with the division average temperature showed possible links between multiple indexes throughout the arctic and Pacific regions. The most prevalent significantly correlated indices were the AO, PNA, NPI and PDO, which all had significant correlations in all seasons. There were also numerous instances of the EP/NP throughout the year and the WP in summer. The relative importance and interactions between the various indices in controlling

temperature and in each division, which is highly relevant for seasonal climate prediction, is an area of potential future work.

There are a few major differences between the new climate divisions (Figure 4.4) and original historical climate zones (Figure 4.1). There were several new divisions identified through our analysis in both the Interior and the Panhandle of Alaska. Since our analysis was focused on identifying regions of homogenous variability and not climate type, differences between the climate divisions and the historical zones were expected. Novel to this analysis, the exact climate divisions boundaries were also evaluated. While there is still some uncertainty in the final boundaries, our analysis has confirmed that boundaries following terrain are quite reasonable.

The practical value of Alaska climate division is high across disciplines. An example of this can be seen when comparing Figure 4.4 with a map of Alaska native languages (Krauss et al. 2011). While there are differences between the exact locations of the lines, many of the language families have similarly located regions as the climate divisions, especially for the Yupik and Athabascan languages. The numerous potential relationships with other disciplines are also an area for future research related to climate divisions.

Acknowledgements

The authors would like to thank J. Talbot, D. Dammann, D. Atkinson, J. Mayfield, D. Walker, M. Raynolds and M. Murray for their comments and discussions that helped to improve this study. The authors would also like to thank the editor, J. Shepherd, the two anonymous reviewers, and P. Olsson for their thoughtful comments that improved this manuscript. This research was supported with funds from NOAA "Social Vulnerability to Climate Change and Extreme Weather of Alaska Coastal Communities" grant NA06OAR4600179, National Science Foundation award ARC-0652838, a University of Alaska Fairbanks graduate fellowship and the Geophysical Institute. The project described in this publication was supported by the Alaska Climate Science Center, funded by Cooperative Agreement Number G10AC00588 from the United States Geological Survey. Its contents are solely the responsibility of the authors and do not necessarily represent the official views of USGS.

References

Ahmed, B. Y. M., 1997: Climatic classification of Saudi Arabia: An application of factor-cluster analysis. *GeoJournal*, **41**, 69-84.

Barnston, A. G., and R. E. Livezey, 1987: Classification, Seasonality and Persistence of Low-Frequency Atmospheric Circulation Patterns. *Mon. Weather. Rev.*, **115**, 1083-1126.

Bhatt, U. S., and Coauthors, 2010: Circumpolar Arctic Tundra Vegetation Change Is Linked to Sea Ice Decline. *Earth Interact.*, **14**. [Available online at http://EarthInteractions.org.]

Bieniek, P. A., U. S. Bhatt, L. A. Rundquist, S. D. Lindsey, and X. D. Zhang, 2011: Large-Scale Climate Controls of Interior Alaska River Ice Breakup. *J. Climate*, **24**, 286-297.

Bourne, S. M., U. S. Bhatt, J. Zhang, and R. Thoman, 2010: Surface-based temperature inversions in Alaska from a climate perspective. *Atmos. Res.*, **95**, 353-366.

Budikova, D., 2005: Impact of the Pacific Decadal Oscillation on relationships between temperature and the Arctic Oscillation in the USA in winter. *Climate Res.*, **29**, 199-208.

Bunkers, M. J., J. R. Miller, and A. T. DeGaetano, 1996: Definition of climate regions in the Northern Plains using an objective cluster modification technique. *J. Climate*, **9**, 130-146.

Chalmers, N., and C. Fabricius, 2007. Expert and generalist local knowledge about land-cover change on South Africa's Wild Coast: can local ecological knowledge add value to science? *Ecol. Soc.*, **12** (1), [available online at: http://www.ecologyandsociety.org/vol12/iss1/art10/.]

Comiso, J. C., 2003: Warming trends in the Arctic from clear sky satellite observations. *J. Climate*, **16**, 3498-3510.

DeGaetano, A. T., 1996: Delineation of mesoscale climate zones in the northeastern United States using a novel approach to cluster analysis. *J. Climate*, **9**, 1765-1782.

Dole, R. M., 1983: Persistent anomalies of the extratropical Northern Hemisphere wintertime circulation. In: Hoskins B. J., Pearce R. P. (eds) Large-scale dynamical processes in the atmosphere. Academic Press.

Fitton, E. M., 1930: The climates of Alaska. *Mon. Wea. Rev.*, **58**, 85-103.

Fovell, R. G., and M. Y. C. Fovell, 1993: Climate Zones of the Conterminous United-States Defined Using Cluster-Analysis. *J. Climate*, **6,** 2103-2135.

Gallant, A. L., 1995: *Ecoregions of Alaska.* U.S. Government Printing Office. 73 pp.

Guttman, N. B., and R. G. Quayle, 1996: A historical perspective of US climate divisions. *Bull. Amer. Meteor. Soc.*, **77,** 293-303.

Hartmann, B., and G. Wendler, 2005: The significance of the 1976 Pacific climate shift in the climatology of Alaska. *J. Climate*, **18,** 4824-4839.

Hill, D. F., and S. Calos, 2011: High resolution gridded monthly precipitation and temperature data for Alaska. *J. Hydro.l*, submitted.

Horel, J. D., and J. M. Wallace, 1981: Planetary-Scale Atmospheric Phenomena Associated with the Southern Oscillation. *Mon. Wea. Rev.*, **109,** 813-829.

Koeppen, W., 1923: *Die klimate der Erde: Grundriss der Klimakunde (The Earth's Climate: Climatological Compendium).* Walter de Gruyter, 369 pp.

Krauss, M. E., G. Holton, J. Kerr, and C. T. West, 2011: Indigenous peoples and languages of Alaska. Alaska Native Language Center and Institute of Social and Economic Research Map. [Available online at http://www.uaf.edu/anla/collections/ search/resultDetail.xml?id5G961K2010.]

Lefale, P., 2010: Stormy weather today: traditional ecological knowledge of weather and climate. The Samoa experience. *Climatic Change*, DOI:10.1007/s10584-009 9722-z.

Linkin, M. E., and S. Nigam, 2008: The north pacific oscillation-west Pacific teleconnection pattern: Mature-phase structure and winter impacts. *J. Climate*, **21,** 1979-1997.

Mantua, N. J., S. R. Hare, Y. Zhang, J. M. Wallace, and R. C. Francis, 1997: A Pacific interdecadal climate oscillation with impacts on salmon production. *B Am Meteorol Soc*, **78,** 1069-1079.

Mesinger, F., and Coauthors, 2006: North American regional reanalysis. *Bull. Amer. Meteor. Soc.*, **87,** 343-360.

Mitchell, T. D., and P. D. Jones, 2005: An improved method of constructing a database of monthly climate observations and associated high-resolution grids. *Int. J. Climatol.*, **25,** 693-712.

National Climatic Data Center, 2002: Divisional normals and standard deviations of temperature, precipitation, and heating and cooling degree days 1971–2000 (and previous normals periods). National Climatic Data Center Climatography of the United States No. 85, 278 pp. [Available online at http://cdo.ncdc.noaa.gov/cgi-bin/climatenormals/climatenormals.pl?directive5prod_select2&prodtype5CLIM85&subrnum5.]

Papineau, J. M., 2001: Wintertime temperature anomalies in Alaska correlated with ENSO and PDO. *Int. J. Climatol.*, **21,** 1577-1592.

Rhee, J., J. Im, G. J. Carbone, and J. R. Jensen, 2008: Delineation of climate regions using in-situ and remotely-sensed data for the Carolinas. *Remote Sens. Environ.*, **112,** 3099-3111.

Searby, H. W., 1968: Climates of the states: Alaska, ESSA, Climatology of the United States. No. 60-49, U.S. Government Printing Office, 23 pp.

Shulski, M., and G. Wendler, 2007: *The Climate of Alaska.* University of Alaska Press, 216 pp.

Simpson, J. J., M. C. Stuart, and C. Daly, 2007: A discriminant analysis model of Alaskan biomes based on spatial climatic and environmental data. *Arctic*, **60,** 341-369.

Simpson, J. J., G. L. Hufford, C. Daly, J. S. Berg, and M. D. Fleming, 2005: Comparing maps of mean monthly surface temperature and precipitation for Alaska and adjacent areas of Canada produced by two different methods. *Arctic*, **58,** 137-161.

Thompson, D. W. J., and J. M. Wallace, 1998: The Arctic Oscillation signature in the wintertime geopotential height and temperature fields. *Geophys. Res. Lett.*, **25,** 1297-1300.

Trenberth, K. E., and J. W. Hurrell, 1994: Decadal Atmosphere-Ocean Variations in the Pacific. *Climate Dyn.*, **9,** 303-319.

Unal, Y., T. Kindap, and M. Karaca, 2003: Redefining the climate zones of Turkey using cluster analysis. *Int. J. Climatol.*, **23,** 1045-1055.

Wallace, J. M. and D. S., Gutzler, 1981: Teleconnections in the geopotential height field during the Northern Hemisphere winter. *Mon. Wea. Rev.*, **109**, 784-812.

Wilks, D. S., 2006: *Statistical Methods in the Atmospheric Sciences.* 2nd ed. Academic Press, 627 pp.

Wolter, K., 1987: The Southern Oscillation in Surface Circulation and Climate over the Tropical Atlantic, Eastern Pacific, and Indian Oceans as Captured by Cluster-Analysis. *J. of Climate Appl. Meteor.*, **26,** 540-558.

Wolter, K., and D. Allured, 2007: New climate divisions for monitoring and predicting climate in the U.S. *Intermountain West Climate Summary*, Vol. 3, Issue 5, 2–6. [Available online at http://www.colorado.edu/IWCS/archive/IWCS_2007_Jun.pdf.]

Wolter, K., R. M. Dole, and C. A. Smith, 1999: Short-term climate extremes over the continental united states and ENSO. Part I: Seasonal temperatures. *J. Climate*, **12,** 3255-3272.

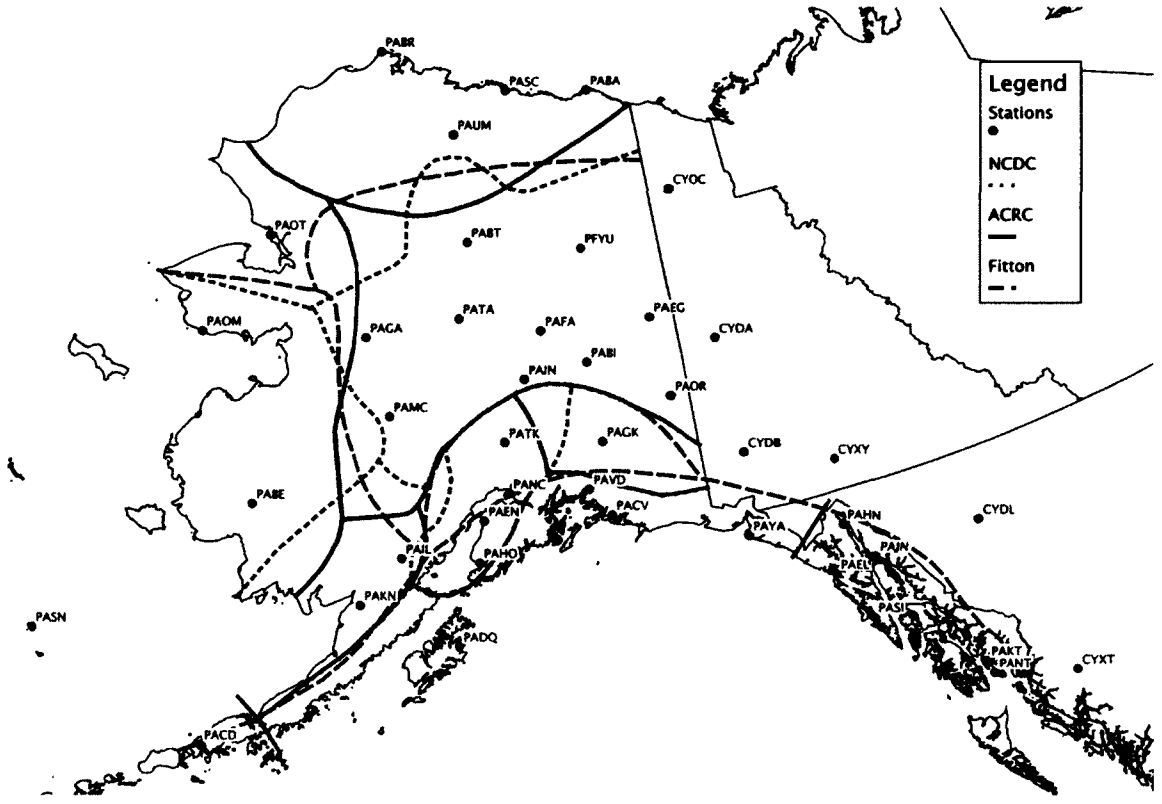

Figure 4.1. Map of historical climate zones for Alaska. Fitton (1930) zones outlined by red dashed, National Climate Data Center (NCDC) climate divisions green dashed, and the Alaska Climate Research Center (ACRC) climate regions solid blue lines, respectively. The stations used in the cluster analysis are shown by red dots with their airport codes (station list in Table 4.1). The climate zones have undergone only minor revisions since their inception, and were drawn based on mean station temperature and precipitation and/or following major terrain features and river basins.

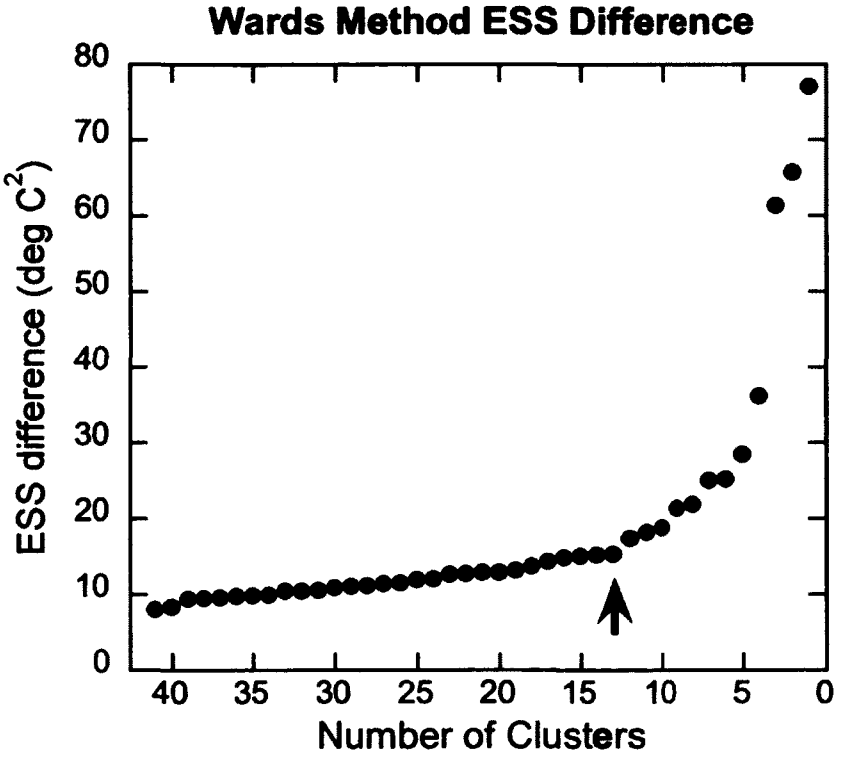

Figure 4.2. Error Sum of Squares (ESS) difference from step to step for the Wards method cluster analysis of station temperature for 1977-2010. An arrow marks where the optimal number of clusters was selected for our data (13 clusters).

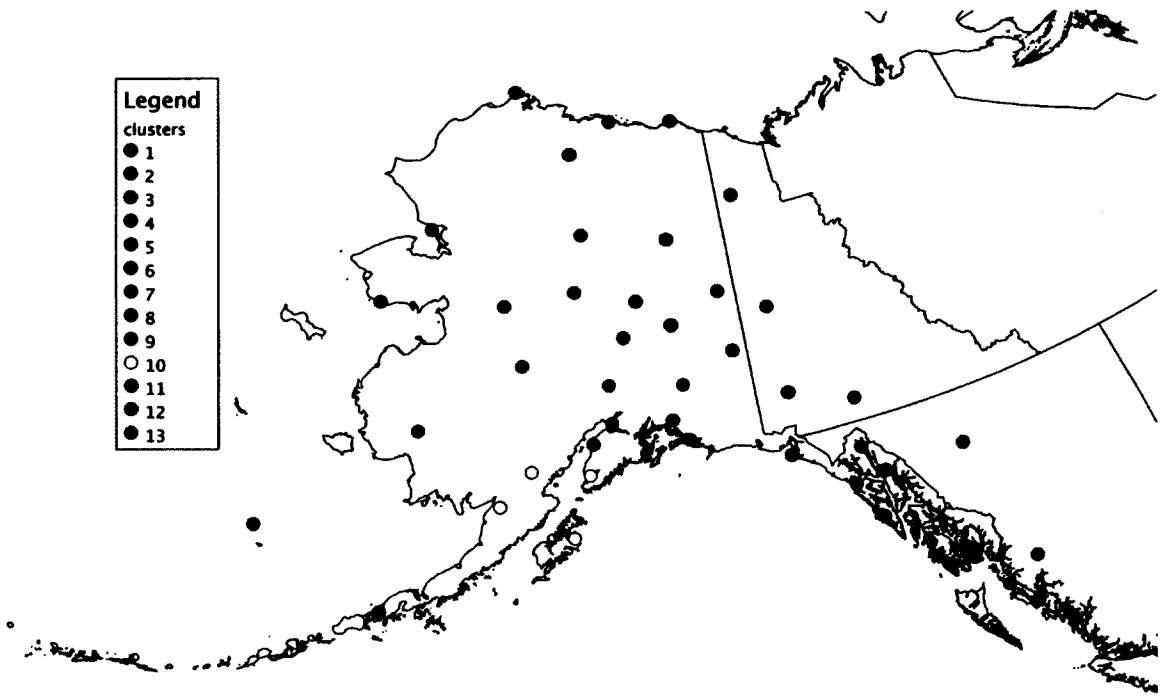

Figure 4.3. The 13-cluster solution from the Ward's method cluster analysis of station temperature. Dots are color-coded by their cluster membership. There are 11 clusters in Alaska with 2 entirely in Canada. The stations appear to group around major terrain features (terrain can be seen in Figure 4.4).

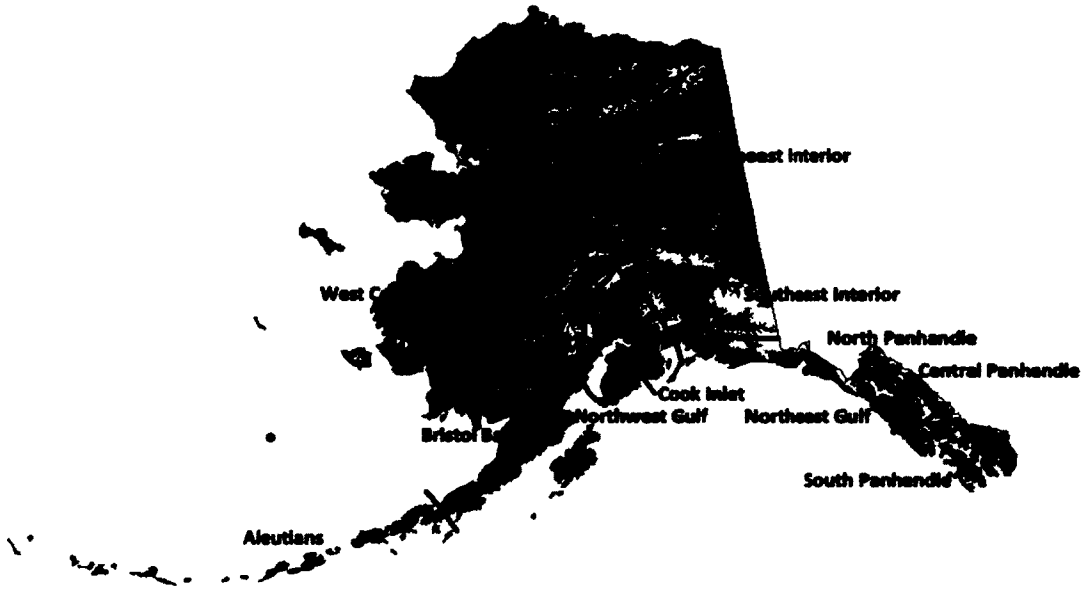

Figure 4.4. Climate division boundaries are shown over Alaska topography with the division names. Black dots indicate the locations of the Alaska stations used in the cluster analysis. Local expert knowledge from experienced weather forecasters in Alaska was employed to draw the final lines.

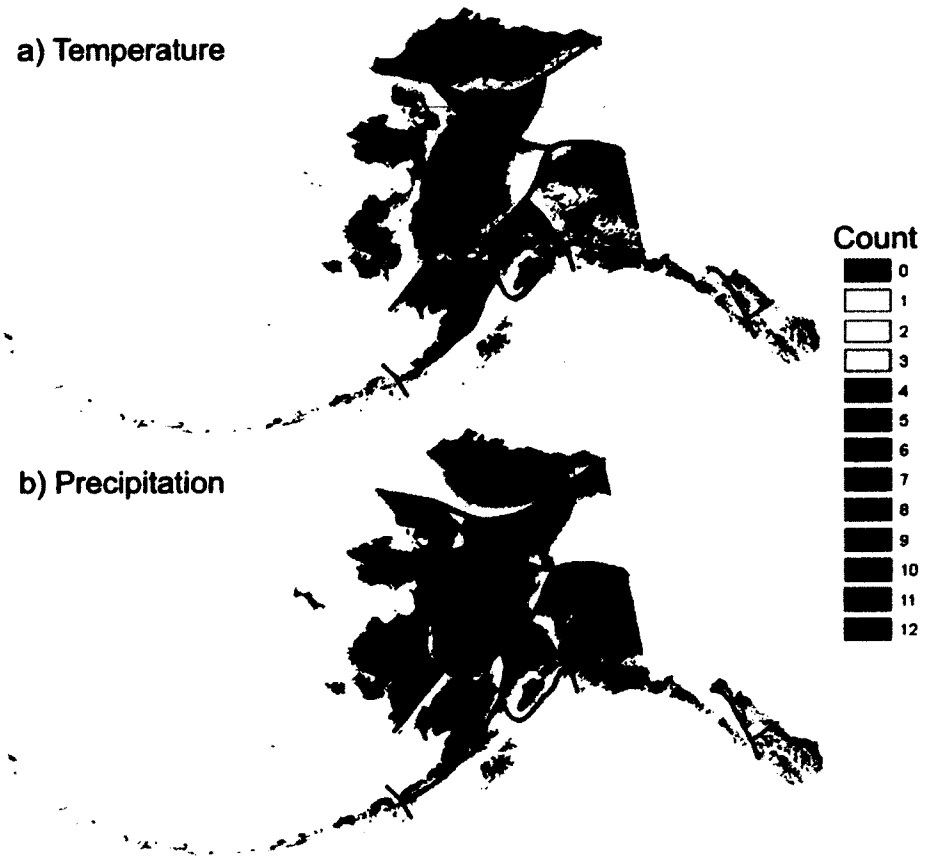

Figure 4.5. Each division average time series based on station data was correlated with every grid point of the Hill and Calos (2011) data set. This plot displays the number of times each grid point had a higher correlation with another division average time series than with its own division. This is shown for (a) temperature and (b) precipitation. Most areas have counts of zero and therefore correlate best with their own division average time series demonstrating that the climate division boundaries drawn aided by local expert knowledge were quite robust.

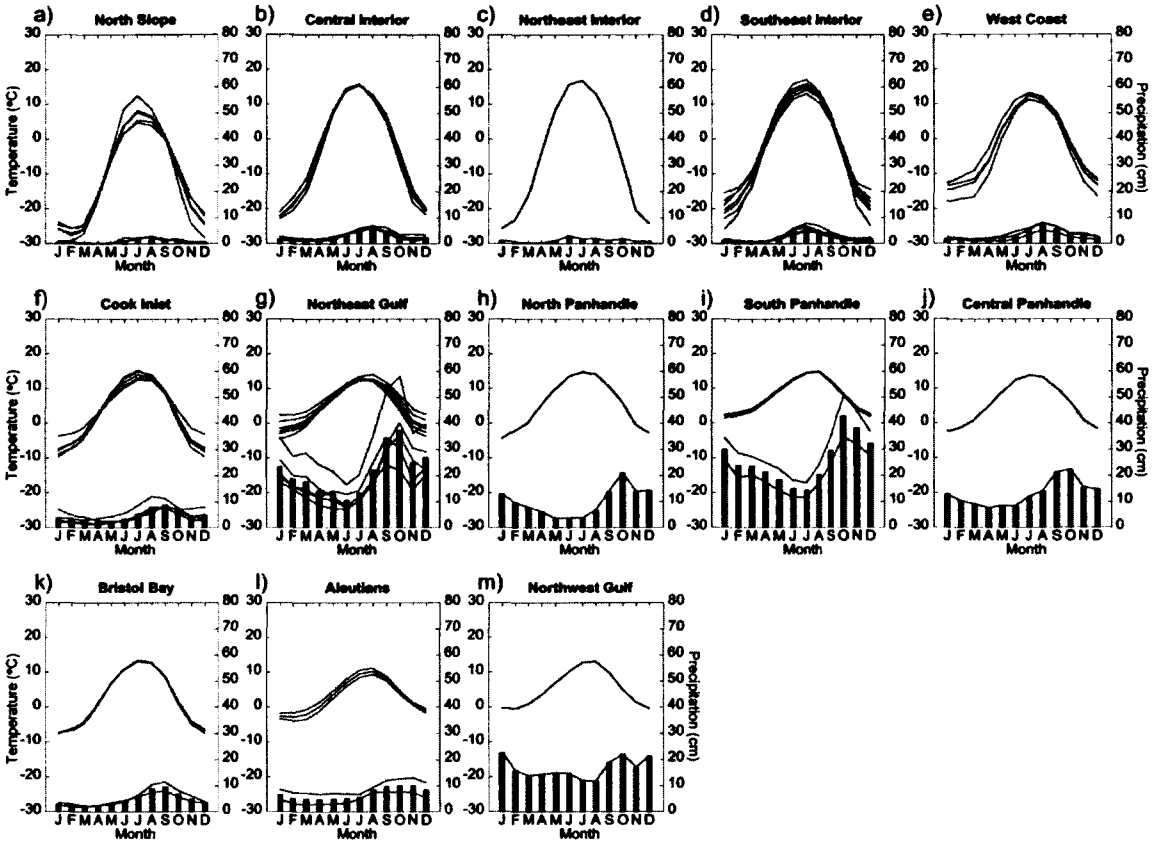

Figure 4.6. Annual cycle of long-term monthly mean temperature (lines) and precipitation (columns). Black lines/columns show the division average and the grey lines show the individual station long-term means. Within each division there is little spread and the annual cycles are similar. The Northeast Interior has the largest annual temperature range while the Northeast Gulf and South Panhandle are the wettest divisions in Alaska.

Table 4.1. List of stations with their airport code, data source, latitude/longitude, correlation with the nearest AVHRR pixel, percent missing temperature at the station 1977-2010 and the percent of the missing replaced with mean adjusted AVHRR when applicable.

Code	Name	Source	Lat °N	Lon °W	Correlation	% Missing	% AVHRR
PANC	Anchorage	NCDC	61.17	150.02	0.92	0.25	
PANT	Annette	NCDC	55.03	131.57	0.92	0.00	NA
PABR	Barrow	NCDC	71.28	156.77	0.98	5.81	100.00
PABA	Barter Island	GSOD	70.13	143.58	0.97	18.18	100.00
PABE	Bethel	NCDC	60.78	161.82	0.97	0.51	100.00
PABT	Bettles	NCDC	66.9	151.50	0.98	0.25	100.00
PABI	Big Delta	NCDC	63.98	145.72	0.98	0.00	
CYDB	Burwash	NWS	61.37	139.05	0.95	11.62	100.00
PACD	Cold Bay	NCDC	55.22	162.72	0.82	0.00	NA
PACV	Cordova	NCDC	60.48	145.45	0.91	0.51	
CYDA	Dawson City	EC	64.04	139.13	0.97	10.35	100.00
CYDL	Dease Lake	EC	58.43	130.01	0.93	8.84	
PAEG	Eagle	NWS	64.79	142.20	0.97	0.00	NA
PAEL	Elfin Cove	NCDC	58.18	136.33	0.82	1.77	
PAFA	Fairbanks	ACRC	64.8	147.87	0.98	0.00	NA
PFYU	Fort Yukon	GSOD	66.57	145.25	0.98	7.07	64.29
PAGA	Galena	NWS	64.73	156.93	0.98	12.12	81.25
PAGK	Gulkana	NCDC	62.15	145.45	0.97	0.00	NA
PAHN	Haines	NCDC	59.23	135.50	0.88	5.30	
PAHO	Homer	NCDC	59.63	151.48	0.88	0.00	
PAIL	Iliamna	NCDC	59.75	154.90	0.95	4.04	
PAJN	Juneau	NCDC	58.35	134.55	0.89	2.27	
PAEN	Kenai	NCDC	60.57	151.23	0.94	0.00	
PAKT	Ketchikan	NCDC	55.35	131.70	0.88	17.93	
PAKN	King Salmon	NCDC	58.67	156.65	0.93	0.51	
PADQ	Kodiak	NCDC	57.75	152.48	0.87	0.00	NA
PAOT	Kotzebue	NCDC	66.88	162.58	0.94	3.28	
PAMC	McGrath	ACRC	62.95	155.60	0.97	0.00	NA
PAIN	McKinley Park	NWS	63.73	148.91	0.95	0.25	100.00
PAOM	Nome	NCDC	64.5	165.43	0.96	1.01	
PAOR	Northway	NCDC	62.95	141.92	0.98	3.28	100.00
CYOC	Old Crow	EC	67.57	139.84	0.98	19.44	66.23
PASC	Prudhoe Bay	NWS	70.32	148.71	0.98	32.07	100.00
PASI	Sitka	NCDC	57.03	135.35	0.88	6.82	
PASN	St. Paul	NCDC	57.15	170.22	0.81	0.00	NA
PATK	Talkeetna	NCDC	62.32	150.08	0.96	0.51	100.00
PATA	Tanana	NCDC	65.17	152.10	0.98	1.01	50.00
CYXT	Terrace	EC	54.47	128.58	0.89	0.25	
PAUM	Umiat	NWS	69.37	152.14	0.98	31.57	98.40
PAVD	Valdez	NCDC	61.12	146.35	0.90	0.00	NA
CYXY	Whitehorse	EC	60.71	135.07	0.95	15.91	100.00
PAYA	Yakutat	NCDC	59.5	139.67	0.82	0.00	NA

Table 4.2. Correlations significant at the 95% or greater level between climate indices and division average station temperature for each season.

Division	Index	DJF	MAM	JJA	SON
North Slope	PNA				0.39
	EP/NP	0.53	0.51		
	WP			0.50	
	AO				-0.37
	SOI	0.40			
Central Interior	PNA	0.53	0.38	0.45	0.44
	EP/NP		0.39	0.46	
	WP			0.41	
	AO	-0.54		-0.34	-0.38
	SOI			-0.36	
	NPI	-0.47	-0.60	-0.54	-0.44
	PDO	0.45			0.35
Northeast Interior	PNA		0.38		
	EP/NP			0.44	
	WP			0.59	
	NINO3.4				0.41
	NPI		-0.48		
Southeast Interior	PNA	0.70	0.54	0.35	0.53
	EP/NP			0.44	
	WP			0.50	
	AO	-0.45	-0.38		-0.39
	SOI			-0.34	
	NPI	-0.59	-0.62	-0.37	-0.59
	PDO	0.52			0.43
Bering Sea Coast	PNA			0.46	
	EP/NP		0.54	0.41	0.41
	AO			-0.49	-0.36
	NINO3.4		0.40		
	NPI		-0.61	-0.59	
	PDO				0.40
Cook Inlet	PNA	0.64	0.62		0.57
	EP/NP				0.37
	AO	-0.53	-0.46		
	NINO3.4	0.37			
	NPI	-0.60	-0.75	-0.38	-0.66
	PDO	0.60	0.52	0.43	0.48
Northeast Gulf	PNA	0.82	0.65		0.60
	EP/NP		0.35		0.36
	AO	-0.42	-0.39		
	SOI	-0.39			
	NINO3.4	0.44			
	NPI	-0.73	-0.72		-0.64
	PDO	0.60	0.54	0.41	0.40

Table 4.2. Continued...

Division	Index	DJF	MAM	JJA	SON
North Panhandle	PNA	0.74	0.39		0.47
	EP/NP			0.41	
	SOI			-0.43	
	NINO3.4			0.37	
	NPI	-0.62			-0.52
	PDO	0.46		0.45	0.38
South Panhandle	PNA	0.77	0.62		0.43
	EP/NP			0.49	
	WP			0.39	
	SOI	-0.54	-0.40		
	NINO3.4	0.54	0.40	0.36	
	NPI	-0.68	-0.67		-0.46
	PDO	0.63	0.66	0.41	0.46
Central Panhandle	PNA	0.80	0.65		0.37
	EP/NP			0.41	
	WP			0.45	
	SOI	-0.34			
	NINO3.4	0.37			
	NPI	-0.67	-0.60		-0.53
	PDO	0.48	0.40		
Bristol Bay	PNA	0.39	0.47		
	EP/NP		0.52		0.44
	AO	-0.50	-0.37		
	NINO3.4		0.36		
	NPI	-0.37	-0.75		-0.48
	PDO	0.46	0.47	0.52	0.41
Aleutians	EP/NP		0.51		0.49
	AO	-0.50			
	NPI		-0.37		
	PDO	0.41		0.37	
Northwest Gulf	PNA	0.46	0.38		0.39
	EP/NP		0.52		0.45
	AO	-0.65	-0.40		
	NINO3.4		0.35		
	NPI	-0.51	-0.62		-0.59
	PDO	0.67	0.44	0.38	0.52

Chapter 5 Conclusions

5.1 Summary

The climate of Alaska is varied and is experiencing change in multiple parts of the biophysical system. Due to the economic, environmental and health impacts of climate on the people living in Alaska, it is imperative to understand the basic function of the regional climate. There exist many gaps in knowledge and this study aimed to address this problem by studying relevant components of the climate system.

River ice breakup poses a hazard to travel and can pose a threat to human life when it causes flooding. As a result, improving the prediction of breakup is of a great benefit to Alaska. River ice breakup date and the large-scale climate are linked. Analysis of gridded reanalysis and station data revealed that the El Niño Southern Oscillation (ENSO) is a key driver of breakup date. The mechanism is as follows: when ENSO is in its positive phase (El Niño), sea surface temperatures in the Equatorial Pacific are above normal, fewer storms track into the Gulf of Alaska, reducing cloudiness over Interior Alaska in March-April. The reduction of cloud cover results in increased solar insolation, earlier snow and ice melt and earlier breakup date. This mechanism primarily requires the prediction of April-May temperatures and the presence of a positive (negative) ENSO will generally predict an earlier (later) breakup date in Alaska. However correlations with ENSO, while significant, were not strong enough to predict breakup with great certainty each year with much lead-time.

Through an evaluation of the Normalized Difference Vegetation Index (NDVI) it was found that the increase in NDVI in the Beaufort and Chukchi Sea coastal tundra

zones was driven by changes in climate at multiple scales. Monthly temperatures in the Beaufort and East Chukchi regions are generally influenced by the strength of the Beaufort High at the large scale and changes in the sea breeze at smaller scales in summer. In the Bering coastal tundra region, NDVI is declining in contrast to northern Alaska. The decline in NDVI has been driven by a decrease in winter snow water equivalent (SWE) due to less moisture availability for the plants. In the Bering the snow is remaining on the ground later due to late season snowfall and reducing the length of the growing season and is in turn reducing NDVI in the early part of the growing season.

Climate divisions delineate regions of homogeneous climate variability and were identified for Alaska using cluster analysis of monthly station temperature. Climate divisions are needed to enhance seasonal forecasting and climate research. For example, climate divisions can be used as a basis to parse study areas or even a way to divide gridded reanalysis data for comparison with station data. They also greatly improve the basic understanding of how climate variability differs in the various regions of Alaska and objectively identifies these regions. This analysis revealed 13 individual climate divisions in Alaska. Average seasonal temperatures in each climate division were significantly correlated with multiple teleconnection indices including the Pacific Decadal Oscillation, Arctic Oscillation, and the Pacific North American Pattern.

5.2 Conclusions

These analyses have shown the many complexities of the climate of Alaska, while demonstrating that there are mechanisms that drive the Alaskan climate at many different scales. While many gaps in knowledge of Alaska climate processes still exist, these studies have each helped to bridge a few of these gaps. Climate divisions showed that the climate does not vary uniformly across the state, even at seasonal and annual scales. This better allows for the targeted evaluation of regional climate impacts within the vast geographic extent of Alaska. The climate division boundaries can now aid future climate researchers by helping them better understand how the climate variability of their geographic study area relates to that of another in Alaska.

Both the evaluation of river ice breakup date and tundra NDVI has shown that there are physical links between climate processes in Alaska and the earth climate system acting at many different scales. Understanding these mechanisms allows for improved seasonal forecasting of temperatures in spring and the timing of river ice breakup. Future climate related changes associated with tundra vegetation could also be better understood if the key processes of variability are identified. These studies have both demonstrated that processes at multiple scales could drive trends in Alaska. Breakup date was found to be linked with the large-scale climate, therefore changes in the global climate system will propagate down the pathway and result in changes in the timing of river ice breakup. NDVI change was found to have a more complex relationship with climate at multiple scales as changes in landscape have a feedback on the local and regional climate; therefore local and large-scale climate processes are driving changes in NDVI.

The studies of breakup date and tundra NDVI change have both demonstrated that the differences in regional climate processes within Alaska. Based on the results of these studies it can be concluded that the climate of Alaska is extensively linked with the global climate system, but local climate processes can play a role depending on the season and location. These regional differences in processes demonstrate that Alaska local climate regions have, often seasonally, independent relationships with the climate system.

These conclusions provide possibilities to improve the view of Alaska climate for the broader community of climate stakeholders. The first deliverable is that there are teleconnections, such as ENSO, that can be applied as predictors for some applications. Understanding the physical mechanisms that relate these teleconnections with what is being predicted will help to evaluate uncertainty in any seasonal forecasting applications. Second is that the function of climate in Alaska varies by region and season, therefore how climate analysis is conducted regionally should be evaluated. Careful analysis based on the regional nature of climate will provide a clearer picture of what processes are important and at what scale. It is important to always be aware that the climate processes change from season to season in Alaska.

5.3 Future outlook

There is a great need to maintain the current network of Alaska weather observation stations into the future. This is critical to continue to improve our understanding of climate variability and change in Alaska. There is also a great need to expand the current station network into remote locations of the North Slope to develop a long-term data set of climate parameters such as temperature, precipitation and wind to enhance future studies of Alaska climate. Robust station networks are critical to many climate applications such as the evaluation of gridded reanalysis and satellite data, and the verification and validation of future climate projections. Even with the inclusion of satellite-derived data, none of the analysis presented in this study would have been possible without the few, long-term observational records that exist for Alaska. The loss of existing stations with long records would be a tragedy and would have a negative impact on climate science in Alaska.

Due to the sparse station network in Alaska and the Arctic, there is also a great need to enhance and extend the current suite of satellite-derived data sets. Such data sets need to have long, consistent records to be most valuable for climate analysis. These data will be needed long into the future to understand climate, especially in remote areas of Alaska.

Many critical gaps in knowledge remain concerning the mechanisms that drive the climate of Alaska. Future analysis should be conducted to understand the differing role of cyclones on temperature and precipitation in the different regions of Alaska. This includes understanding if the location where cyclones form and how they approach

Alaska play a significant role in regional temperature and precipitation variability throughout the year.

It is important to continue to investigate the basic mechanisms that drive the climate of Alaska. This will be increasingly important as the Arctic climate continues to change. The people who live in Alaska and the Arctic face great challenges due to its extreme climate conditions. Change results in an increasingly uncertain future for them. Improving our understanding of how the climate functions helps to reduce some of this uncertainty and improves the human condition.

Finally, communication between the climate science and stakeholder/user/public communities needs to continue to be developed and enhanced. Doing so will maximize the practical nature of climate science to society. Communication between these groups will help climate scientists better understand the needs of the stakeholders, and at the same time, stakeholders will better understand climate science. This will also result in better decision making in response to current and future changes in weather and climate. This is especially important in Alaska where weather and climate directly impacts nearly every person and industry in some way. Climate scientists should therefore work to reach out to those stakeholders. Armed with an improved understanding of the climate data/information needs of society, scientists should then endeavor to meet theses needs.